Technische Universität München
Institut für Physikalische und Theoretische Chemie
- Lehrstuhl II für Physikalische Chemie -

FT-ICR Studies of Solvated Ions

Brigitte S. Fox

Vollständiger Abdruck der von der Fakultät für Chemie der Technischen Universität München zur Erlangung des akademischen Grades eines

Doktors der Naturwissenschaften

genehmigten Dissertation.

Vorsitzender: Univ.-Prof. (Komm.) Dr. W. Nitsch, em.

Prüfer der Dissertation:

1. Univ.-Prof. V. E. Bondybey, Ph.D. (Univ. of California, Berkeley, USA)
2. apl.-Prof. Dr. F. R. Kreißl
3. Univ.-Prof. Dr. E. Nolte

Die Dissertation wurde am 12.12.2001 bei der Technischen Universität München eingereicht und durch die Fakultät für Chemie am 23.1.2002 angenommen.

für Martin

Die Neugier steht immer an erster Stelle eines Problems,
das gelöst werden will.

GALILEO GALILEI

Contents

1 Introduction

The understanding of solvation phenomena is of considerable importance for many applications in chemistry, industry, and biology. The presence of the solvent has a significant influence upon the properties of the reactants, and upon the course of chemical reactions. Firstly, the temperature at the reaction site remains well defined because of the contact and the collisions of the reactants with the solvent, which acts as a heat bath. The collisions remove energy resulting from exothermic reactions or can supply the energy needed for endothermic reactions. Secondly, the solvent itself may through its interactions with the reactants and products change their reactivity or other chemical properties and thus have a strong influence on the energetics of the reaction. In fact, one can in many cases steer the course of the reaction by choosing a suitable solvent.

Solvated ions are ideal model systems for understanding solution chemistry and they were thus extensively studied in the last years.[1-9] High-pressure mass spectrometry and collision induced dissociation studies can yield information about binding energies[2,10-12] whereas insight into the structure and stepwise formation of solvation shells can be obtained from spectroscopic[13-17] and computational studies.[8,18-23] More recently, it has been demonstrated that hydrated ions and ionized water clusters can serve as model systems for direct studies of condensed phase reactions.[24-36]

Fourier transform ion cyclotron resonance (FT-ICR) mass spectrometry is particularly useful to investigate reactions of solvated ions.[6] The FT-ICR has the advantage of a very high resolution which allows the unambigous identification of the elemental composition of reactants and products. Furthermore, unlike in many other

experiments, one does not have to work with a whole distribution of cluster sizes, but can mass select a cluster of any desired size and composition if unambigous interpretaion requires it. In addition, it has been shown that clusters which are exposed to the room temperature background infrared radiation in the ion trap of the FT-ICR gradually fragment.[37-43] In this way, one can remove the solvent molecules one by one, and investigate thus the effect of the solvation upon chemical reactions. It has been established that reactions of water clusters proceed under these conditions comparable to bulk aqueous solutions,[31-34,44] and macroscopic concepts like pH[36] or solubility[35] can be transferred to the molecular level.

The laser vaporization source used for the experiments presented in this work can also produce hydrated metal cations in unusual oxidation states and offers thus the unique possibility to study their chemistry. Chapter 3 deals with a study of hydrated first-row transition metal cations in oxidation state +I, $M^+(H_2O)_n$, n≈40, M=Ti, V, Cr, Mn, Fe, Ni, Co, Cu, Zn. Strictly speaking, Zn is not counted to the transition metals because the metal and its ions have completely filled d-shells. However, Zn was included in the presented study to investigate the influence of a completely filled d-shell upon the reactivity of the half filled s orbital. With the exception of Cu, the aqueous chemistry of the above named metals in oxidation state +I is virtually unknown since the singly charged ions are unstable in aqeous media.[45] In order to investigate possible blackbody radiation induced intracluster reactions which might lead to hydrogen evaporation and oxidation of the metal, hydrated transition metal cations of the type $M^+(H_2O)_n$, n≈40, were produced and stored in the FT-ICR cell for several seconds. Reactions of these hydrated ions with HCl have been studied to get additional insight into their chemistry.

Another important polar solvent which like water efficiently stabilizes ionic species is ammonia. To compare the properties of clusters composed of one of those

important solvents, the first systematic investigation of the blackbody radiation induced fragmentation of ammoniated silver cations, $Ag^+(NH_3)_n$, n=4-21, and protonated ammonia clusters, $H^+(NH_3)_n$, n=5-30, was carried out, and the results were compared to the respective water analogues, $Ag^+(H_2O)_n$, n=4-45, and $H^+(H_2O)_n$, n=5-65. Accompanying DFT calculations of the cluster structures and of their harmonic frequencies and intensities were performed to facilitate the interpretation of the interpretation of the experimental observations. The results of this study are presented in chapter 4.

Ammonia is not only an important solvent but also the most important nitrogen-containing donor ligand in aqueous chemistry, especially important in the aqueous chemistry of silver. If NH_3 is added to an aqueous solution of a silver salt, the extremely stable linearly coordinated $[Ag(NH_3)_2]^+$ ion is formed. It is well-known that silver(I) prefers in general linear coordination which is often explained by its electronic structure. In aqueous solution and liquid NH_3, however, the tetrahedral $Ag(solv)_4^+$ ions are formed, which seems to be contradictory. In order to examine the coordination with mixed ligands, the reaction of hydrated silver cations $Ag^+(H_2O)_n$ with NH_3 and the complementary process, the reaction of ammoniated silver cations $Ag^+(NH_3)_n$ with H_2O, were investigated. Again, DFT calculations have been performed to get a more detailed insight into the structure and energetics of small clusters. The results of this combined FT-ICR/DFT study are documented in chapter 5.

At the end of the summary section, an outlook will be given on future studies of solvated ions based on the results of this work.

References

(1) Duncan, M. A. *Annu. Rev. Phys. Chem.* **1997**, *48*, 69.

(2) Freiser, B. S. *J. Mass Spectrometry* **1996**, *31*, 703.

(3) Yourshaw, I.; Zhao, Y. X.; Neumark, D. M. *J. Chem. Phys.* **1996**, *105*, 351.

(4) Dedonder-Lardeux, C.; Gregoire, G.; Jouvet, C.; Martenchard, S.; Solgadi, D. *Chem. Rev.* **2000**, *100*, 4023.

(5) Fuke, K.; Hashimoto, K.; Iwata, S. In Structures, Spectroscopies, and Reactions of Atomic Ions with Water Clusters; Advance in Chemical Physics, Vol. 110; Prigogine, I., Rice, S. A., Eds.; John Wiley &Sons: New York, 1999; pp 431-523.

(6) Niedner-Schatteburg, G.; Bondybey, V. E. *Chem. Rev.* **2000**, *100*, 4059.

(7) Zhong, Q.; Castleman, A. W. *Chem. Rev.* **2000**, *100*, 4039.

(8) Dykstra, C. E.; Lisy, J. M. *J. Mol. Struc.-Theochem.* **2000**, *500*, 375.

(9) Fahey, D. W.; Böhringer, H.; Fehsenfeld, F. C.; Ferguson, E. E. *J. Chem. Phys.* **1982**, *76*, 1799.

(10) Keesee ,R. G.; Castleman, A. W. *J. Phys. Chem. Ref. Data* **1986**, *15*, 1011.

(11) Rodgers, M. T.; Armentrout, P. B. *Mass Spectrom. Rev.* **2000**, *19*, 215.

(12) Kebarle, P. *Int. J. Mass Spectrom.* **2000**, *200*, 313.

(13) Lisy, J. M. *Int. Rev. Phys. Chem.* **1997**, *16*, 267.

(14) Cao, Y.; Choi, J.-H.; Haas, B.-M.; Okumura, M. *J. Phys. Chem.* **1994**, *98*, 12177.

(15) Choi, J.-H.; Kuwata, K. T.; Haas, B.-M.; Cao, Y.; Johnson, M. S.; Okumura, M. *J. Chem. Phys.* **1994**, *100*, 7153.

(16) Dessent, C. E. H.; Kim, J.; Johnson, M. A. *Account. Chem. Res.* **1998**, *31*, 527.

(17) Weber, J. M.; Kelley, J. A.; Nielsen, S. B.; Ayotte, P.; Johnson, M. A. *Science* **2000**, *287*, 2461.

(18) Feller, D.; Glendening, E. D.; de Jong, W. A. *J. Chem. Phys.* **1999**, *110*, 1475.

(19) Ricca, A.; Bauschlicher, C. W. *J. Phys. Chem.* **1995**, *99*, 9003.

(20) Beyer, M.; Lammers, A.; Savchenko, E. V.; Niedner-Schatteburg, G.; Bondybey V. E. *Phys. Chem. Chem. Phys.* **1999**, *1*, 2213.

(21) Beyer, M.; Savchenko, E. V.; Niedner-Schatteburg, G.; Bondybey V. E. *J. Chem. Phys.* **1999**, *110*, 11950.

(22) Watanabe, H.; Iwata, S. *J. Phys. Chem.* **1996**, *100*, 3377.

(23) Agmon, N. *J. Phys. Chem. A* **1998**, *102*, 192.

(24) Peschke, M.; Blades A. T.; Kebarle, P. *Int. J. Mass Spectrom.* **1999**, *187*, 685.

(25) Plastridge, B.; Cohen, M. H.; Cowen, K. A.; Wood, D. A.; Coe, J. V. *J. Phys. Chem.* **1995**, *99*, 118.

(26) Squires, R. R. *Int. J. Mass Spectrom. Ion Proc.* **1992**, *117*, 565.

(27) Gilligan, J. J.; Castleman, A. W. *J. Phys. Chem. A* **2001**, *105*, 5601.

(28) Viggiano, A. A.; Morris, R. A.; Deakyne, C. A.; Dale, F.; Paulson, J. F. *J. Phys. Chem.* **1991**, *95*, 3644.

(29) Van Dorren, J. M.; Viggiano, A. A.; Morris, R. A. *J. Am .Chem. Soc.* **1994**, *116*, 6957.

(30) Schindler ,T.; Berg, C.; Niedner-Schatteburg, G.; Bondybey, V.E. *J. Chem. Phys.* **1996**, *104*, 3998.

(31) Berg, C.; Achatz U.; Beyer M.; Joos, S.; Albert, G.; Schindler, T.; Niedner-Schatteburg, G.; Bondybey, V.E. *Int. J. Mass Spectrom. Ion Proc.* **1997**, *167/168* 723-734.

(32) Berg, C.; Beyer, M.; Achatz, U.; Joos, S.; Niedner-Schatteburg, G.; Bondybey, V.E. *Chem. Phys.* **1998**, *239*, 379.

(33) Achatz, U.; Joos, S.; Berg, C.; Schindler, T.; Beyer ,M.; Albert, G.; Niedner-Schatteburg, G.; Bondybey, V.E. *J. Am. Chem. Soc.* **1998**, *120*, 1876.

(34) Beyer, M.; Achatz, U.; Berg, C.; Joos, S.; Niedner-Schatteburg, G.; Bondybey, V.E. *J. Phys. Chem. A* **1999**, *103*, 671.

(35) Fox, B.S.; Beyer, M.K.; Achatz, U.; Joos, S.; Niedner-Schatteburg, G.; Bondybey, V.E. *J. Phys. Chem. A* **2000**, *104*, 1147-1151.

(36) Achatz, U.; Fox, B. S.; Beyer, M. K.; Bondybey, V. E. *J. Am. Chem. Soc.* **2001**, *123*, 6151.

(37) Thölmann, D.; Tonner, D. S.; McMahon, T. B. *J. Phys. Chem.* **1994**, *98*, 2002.

(38) Dunbar, R. C.; McMahon, T. B. *Science* **1998**, *279*, 194.

(39) Sena, M.; Riveros, J. M. *Chem. Eur. J.* **2000**, *6*, 785.

(40) Rodriguez-Cruz, S. E.; Jockusch, R. A.; Williams, E. R. *J. Am. Chem. Soc.* **1999**, *121*, 8898.

(41) Schindler, T.; Berg, C.; Niedner-Schatteburg, G.; Bondybey, V. E *Chem. Phys. Lett.* **1996**, *250*, 301.

(42) Beyer, M. K.; Fox, B. S.; Reinhard, B. M.; Bondybey, V. E. *J. Chem. Phys.* **2001**, *115*, 9288.

(43) Rodriguez-Cruz, S. E.; Jockusch, R. A.; Williams, E. R. *J. Am. Chem. Soc.* **1998**, *120*, 5842.

(44) Fox, B. S.; Balteanu, I.; Balaj, O.-P.; Liu, H.; Beyer, M. K.; Bondybey, V. E., *J. Am. Chem. Soc.*, in print.

(45) Hollemann, A.F.; Wiberg, E. *Lehrbuch der Anorganischen Chemie*, Walter de Gruyter: Berlin, 1995.

2 Experimental and Theoretical Methods

2.1 Fourier Transform Ion Cyclotron Resonance Mass Spectrometry (FT-ICR MS)

2.1.1 General

Ion Cyclotron Resonance Mass Spectrometry (ICR-MS) uses the possibility to determine the mass of an ion with charge q by measuring its cyclotron frequency ν_c in a magnetic field B_0:

$$\nu_c = \frac{qB_0}{2\pi m} \qquad (1)$$

The time and thus also the frequency can be measured with very high accuracy.[1] Therefore, ICR-MS allows to determine masses with an accuracy of $\Delta m/m=10^{-6}$ or better.[2] Accordingly, the composition of ions with the same nominal mass can be determined by their mass defect. For example, N_2^+ with a mass of 28.0056 amu and CO^+ with a mass of 27.9944 amu are represented by two separate peaks.[2] The introduction of Fourier Transformation into ICR-MS by A.G. Marshall and M.B. Comisarow[3] allows the acquisition of mass spectra over a continuous mass range. Thus, Fourier Transform Ion Cyclotron Resonance Mass Spectrometry (FT-ICR MS) became an universal tool for chemical analysis and pure research.

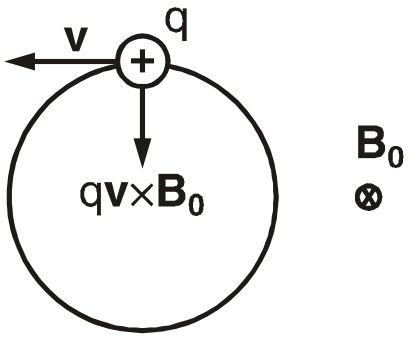

Figure 2.1: Origin of the cyclotron motion: A particle with charge q and velocity v perpendicular to the magnetic field B_0 is forced to move on a circular path by the Lorentz force.

To transform the cyclotron motion shown in Fig. 2.1 into a detectable electronic signal the ions are trapped in a cell by applying an electrostatic potential of the order of <5V, applying the storage scheme of a Penning trap. Some popular cell geometries are shown in Fig. 2.2. For detection, the ions are excited on larger radii by a broadband high frequency signal which contains all the frequencies in the desired mass range. The excitation results in formation of coherent ion packages. This process is shown schematically in Fig. 2.3. The ion packages induce a small electric potential between the detection plates which oscillates with the cyclotron frequency ν_c. This signal is amplified, recorded with an analog-digital converter and stored as the digitized transient. Fourier transformation of the transient yields a frequency spectrum, which is converted to a mass spectrum by applying Equation 1, as is shown schematically in Fig. 2.4.

Collisions with the background gas and coulomb repulsion among the ions destroy the coherence of the ion packages and result in an exponential decay of the signal. This leads to peak broadening limiting the mass resolution. Ultra high vacuum, with pressures lower than 10^{-8} mbar, can minimize the collisional broadening.

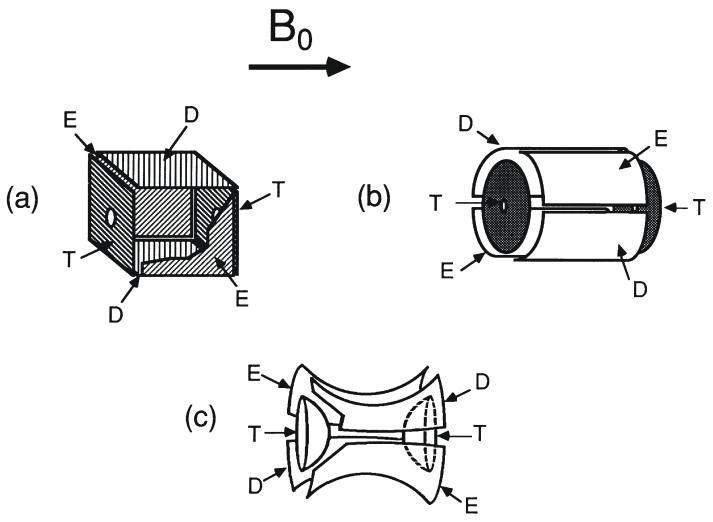

Figure 2.2: Customary ICR cell geometries: (a) cubic cell, (b) cylindric cell, (c) hyperbolic cell. T indicates the trapping electrodes, D the detection electrodes and E the excitation electrodes.[8]

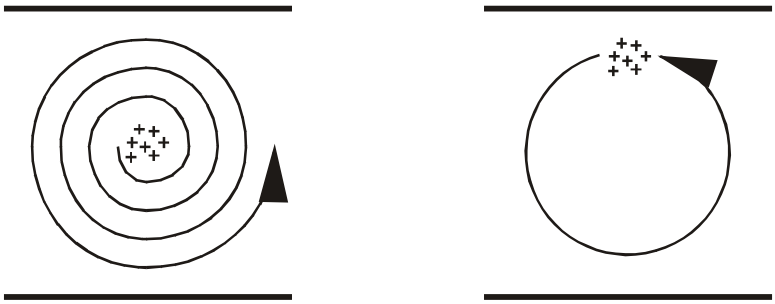

Figure 2.3: The initially incoherent cyclotron motion of the ions is transformed into a coherent and thus detectable motion upon irradiation of radio frequency.[8]

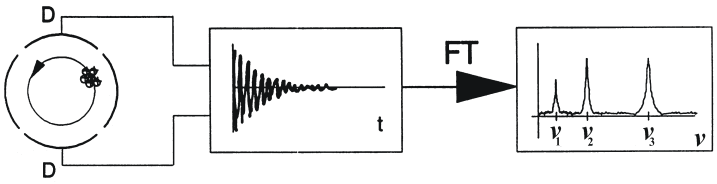

Figure 2.4: The coherent ion package induces a potential difference between the detection plates which oscillates with the cyclotron frequency ν_c. Coulomb repulsion among the ions and collisions with the background gas lead to an exponential decay of the transient. Fourier transformation of the transient yields a frequency spectrum.

The quadrupol potential which is necessary to trap the ions leads to additional oscillations of the ions, these are the magnetron motion and trapping oscillations.[2]

Ions of a defined mass can be accelerated by application of a resonant radio frequency signal which is utilized to perform energy resolved studies,[4] or to eject unwanted ions from the cell. This is done under software control. Highly sophisticated multiple mass spectrometry schemes MS^n can be devised, limited only by the capabilities of the electronics and by the trapping characteristics of the ICR-cell.

2.1.2 The Garching FT-ICR

The Garching FT-ICR[5-7] which is displayed schematically in Fig. 2.5 is a modified Bruker/Spectrospin CMS47X. It is equipped with a 4.7 T supraconducting magnet with cylindrical room temperature bore, a cylindrical 60 mm x 60 mm infinity cell[9] and a differentially pumped ultra high vacuum system with external ion transfer optics. The experiment is controlled by an ASPECT3000 minicomputer. The instrument was modified by adding a source chamber with an additional differential pumping stage which allows the application of molecular beam ion sources with a high gas load.[7,10]

Ions are produced in the source chamber with a molecular beam ion source. The molecular beam is skimmed and an ion beam is formed by the subsequent ion optics. The 0.8 mm skimmer acts as the first flow constraint which separates the source chamber from the next differential pumping stage. To guide the ion beam against the magnetic mirror effect[11] into the homogenous high field region of the magnet it is accelerated to 3 keV kinetic energy. The beam is passing two additional flow constraints, separating stages of differential pumping, and stepwisely decelerated below the trapping potentials. The ions can be trapped by using the Caravatti method.[12] In this method, a small potential gradient

is applied perpendicular to the velocity of the ions. In this way, part of the kinetic energy of the ions is converted from translational energy along the axis of the magnetic field into cyclotron and magnetron motion perpendicular to it.

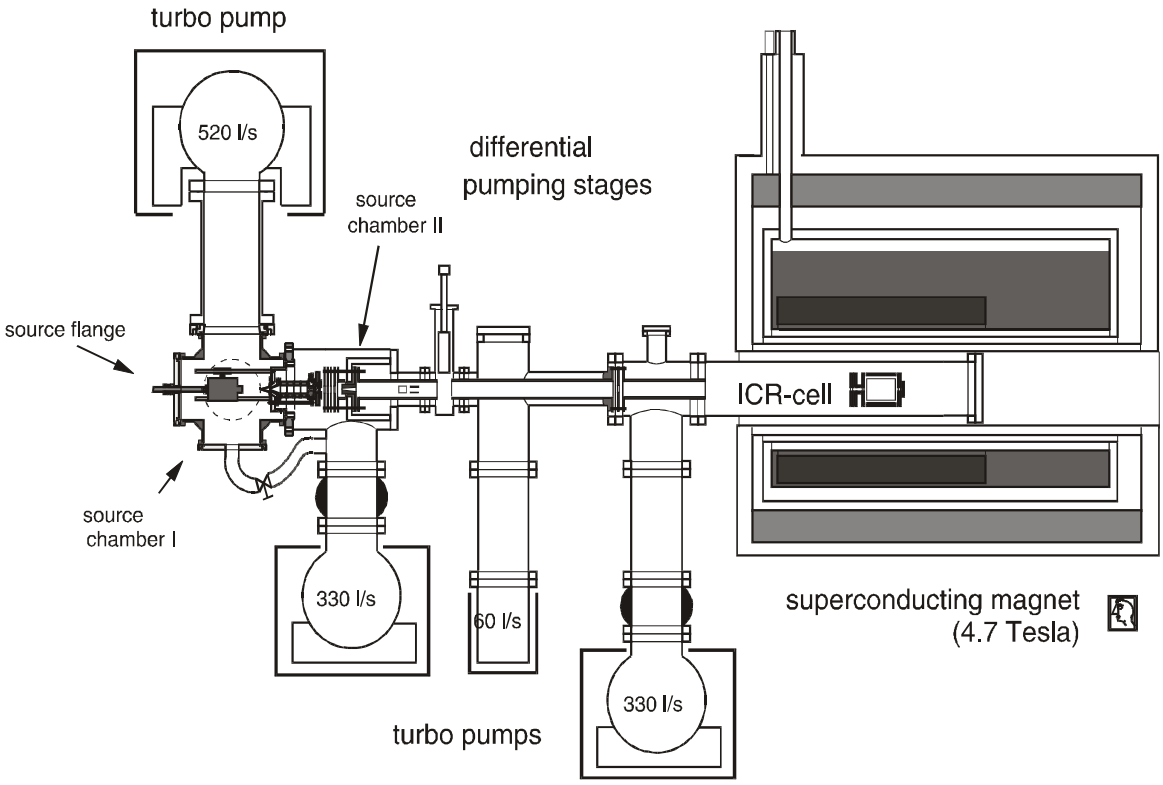

Figure 2.5: Side-view of the Garching FT-ICR. Ions are produced in the source chamber and transferred to the ICR-cell inside the magnet by a system of electrostatic lenses. Four differential pumping stages allow the application of molecular beam ion sources with a high gas load.

The turbomolecular pumps are shielded against the high magnetic stray field with soft iron, the rotary roughing pumps are operated without shielding. Pumping speeds are, for turbomolecular pumps and rotary pumps, respectively, 550 l/s and 30 m^3/s in the source region, 330 l/s and 8 m^3/s in the second stage of differential pumping, and 60 l/s, 330 l/s and 16 m^3/h in the ultra high vacuum region.The turbomolecular pumps are from Pfeiffer, the roughing pumps from Pfeiffer, Edwards, and Alcatel. Typical pressures

without gas load are 5×10^{-6} mbar, 5×10^{-7} mbar, and 1×10^{-10} mbar in the first, second and fourth stage of differential pumping, respectively. Reaction gas can be introduced into the UHV region by two sapphire-gold sealed needle valves, type Balzers UHD40. The gas inlet system can be evacuated by a rotary pump, type Edwards RV8, for cleaning purposes. The UHV region, the needle valves, and the UHV turbo molecular pumps are routinely baked out.

Pressure is measured by Penning ionization gauges, type Balzers IKR 020, in the source chamber, the second region and the ultra high vacuum. The Penning gauge in the UHV region is placed 80 cm away from the ICR cell directly on top of the turbomolecular pump. Upon introduction of a collision gas into the cell, a constant backing pressure is obtained as a stationary state between gas flowing into the cell, atoms or molecules sticking on the apparatus walls and desorbing again, and pumping. These processes are highly dependent on the specific gas, and the actual pressure in the cell is different from the pressure above the pump where the Penning ionization gauge is placed. The pressure reading is therefore corrected by an empirical geometry factor G and the sensitivity of the ion gauge R_x according to the following equation:[13]

$$p_x^{cell} = \frac{G p_x^{IG}}{R_x} \tag{2}$$

In a good approximation, G is independent of the specific gas and the pressure range. The experimentally obtained value for G is 3.7±1.0.[13] R_x values are collected in several tables.[14,15]

A Bruker ASPECT3000 minicomputer is used for experiment control and data processing. The processor has limited multitasking capabilities. It is equipped with 768 kB

RAM and a 400 MB hard disk. Data are stored in 24 bit words. Two ADC analog-digital converters are integrated for transient recording. A fast ADC with 20 MHz sampling rate and 9 bit resolution is used for broad band detection, a slow ADC with 50 kHz sampling rate and 12 bit resolution is used for high resolution heterodyne[16] detection. The lowest detectable mass, i.e. the highest detectable frequency, is limited by the sampling rate of the fast ADC to 11.5 amu. Transients up to 128 kWords can be recorded. An FFT fast fourier transform processor undertakes the computationally demanding fourier transformation of the transient. It is fast enough to allow for an online display of a nonlinearized mass spectrum for transients up to 32 kWords, which is very useful for signal optimization purposes.

The I89 FT-ICR operating system allows software control of the experiment by automation routines, which are programmed in a very limited, non-standard programming language. Up to ten different pulses can be applied for a variety of purposes, like ion excitation, gating of the ion trap, or triggering of external hardware, such as lasers or pulsed valves. Puls lengths may be integer multiples of 1 μs, delays between pulses are integer multiples of 10 μs.

Mass spectra are transferred with the Bruker software package NMRLINK[17] to a PC, which is linked to the local UNIX workstation cluster, transformed to ASCII format with the program BRUKER,[18] and displayed with the public domain graphics package XMGR.[19] In addition, the mass-intensity information can be transfered from the ASPECT to the PC via an RS232 serial port, and further processed under UNIX, to enable e.g. fits of reaction kinetics. A set of programs including LLCRUNCH,[20] LLCORR,[21] C2N,[22] NNORM,[21] and FIT,[22] have been developed for these purposes.

2.1.3 The Laser Vaporization Molecular Beam Ion Source

In the experiments of chapters 3-5, a laser vaporization source[23-25] with a rotable target disk is used, illustrated in Fig. 2.6. Ions are produced without post-ionization by laser ablation of a small amount of the target material by a focused laser pulse, at a typical pulse length of 5 ns and an energy of 2-20 mJ. The plasma is entrained into a precisely timed carrier gas pulse, e.g. helium, and cooled by supersonic expansion into the high vacuum of the source chamber. Cations as well as anions can be extracted from the source,[26] depending on the polarity of the electrostatic ion transfer optics. By seeding the carrier gas with water, metal ions solvated in water clusters with up to 100 water molecules can be produced.[27-29] By using a mixture of Helium and NH_3 it is also possible to generate large ammoniated ions.[30,31]

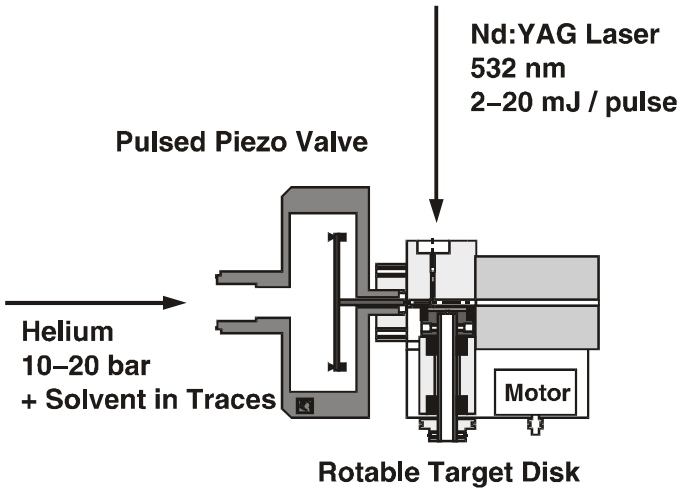

Figure 2.6: Laser vaporization molecular beam ion source. Material is vaporized with a 5 ns laser pulse from a rotating target disk. Together with an accurately timed, ~50 µs short gas pulse, the hot plasma is expanded via a confining channel into high vacuum. The plasma is collisionally cooled, and clusters are formed in the supersonic expansion. Solvated ions are produced by adding traces of the desired solvent to the carrier gas.

The homebuilt piezoelectric valve[7] is the sophisticated outcome of an ongoing development that goes back to an initial design by Proch and Trickl.[32] It is driven with a typically 50 µs long and up to 1 kV high pulse from a homebuilt pulsing circuit.[33] As a vaporization laser, a Nd:YAG laser Continuum Surelite II is used, operated frequency doubled at 532 nm, with 5 ns pulse length and up to 20 mJ pulse energy.

Fig. 2.7 shows schematically wiring and control of the laser vaporization unit. Piezo valve, laser Q-switch and flash lamps are operated by the TTL pulses labelled U, V and W as supplied by the ASPECT 3000. The inverter unit makes sure that the piezo valve is triggered by the falling edges of the pulse, which allows to adjust the timing within 1 µs accuracy. The piezo driver pulse box allows tuning of the pulse within 0-200 µs pulse length and 0-1000 V pulse height.

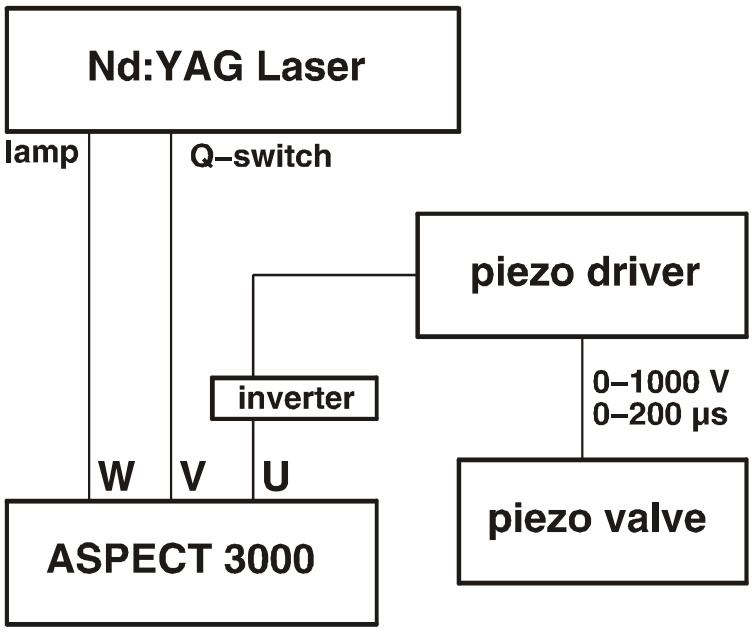

Figure 2.7: Schematic wiring diagram for operating the laser vaporization source. The ASPECT 3000 minicomputer triggers lamp and Q-switch of the Nd:YAG laser and the driver of the piezo valve via the external TTL-pulses U, V, W.

The laser vaporization unit is integrated into the ICR duty cycle by a small control program, a so-called AU routine. The pulse scheme of a typical experiment is shown in Fig. 2.8. The duty cycle starts with a quench pulse P1, which cleans the ICR cell from ions that might be accidentally trapped at the start of the experiment. The cell is subsequently filled with typically 20 cycles of ion generation and trapping, which consist of the firing of the flash lamps, opening of the piezo valve, and laser Q-switch trigger. The so-called gate-pulse P2 lowers the trapping voltage of the first trapping plate to 0 V, which allows the ions to enter the cell. Shifting D5 and P2, one can utilize time of flight-effects to preselect ions of certain mass and stoichiometry. The amount of ions produced, as well as their composition, are critically dependent on the relative timing between the gas pulse and the laser pulse. In the case of the solvated metal ions, this timing has to be accurate to 1 µs to ensure a maximum yield of the desired species. Ion generation is typically followed by optional mass selection, by a variable reaction delay, and by detection of the mass spectrum.

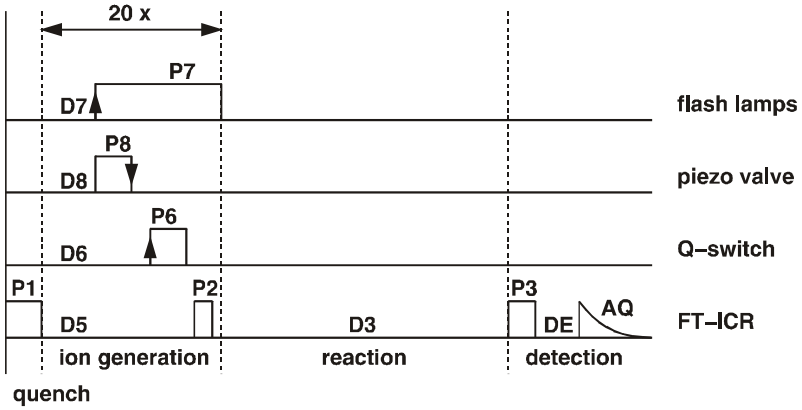

Figure 2.8: Pulse sequence of a typical ICR-experiment with the laser vaporization source. The quench pulse P1 ejects all charged particles from the cell, which is subsequently filled in typically 20 ion generation cycles. The piezo valve is triggered with the falling edge of the pulse, which allows 1 µs accuracy. After a reaction delay, the ions in the cell are accelerated by the broad-band pulse P3, and the transient is recorded during AQ. The short delay DE ensures that the transient is not affected by the pulse P3.

2.2 Quantum Chemical Methods

2.2.1 Density Functional Theory and Hybrid Methods

Density functional theory (DFT) is primarily a theory of ground state electronic structure, expressed in terms of the electronic density distribution $\rho(\vec{r})$. Since its birth about thirty years ago, it has become increasingly useful for the understanding and calculation of the ground state density and energy of molecules, clusters, and solids with or without applied static perturbations. It is an alternative and complementary approach to the traditional methods of quantum chemistry which are formulated in terms of the many-electron wave function $\Psi(\vec{r}_1,\vec{r}_2,...,\vec{r}_n)$.[34]

Hohenberg and Kohn[35,36] have shown that, without explicit knowledge of the electronic wave function, the total energy E of an *n* electron system can be expressed as a functional of its electron density $\rho(\vec{r})$. Usually, the total energy is partitioned in the following form:[37]

$$E(\rho) = E^T(\rho) + E^V(\rho) + E^J(\rho) + E^{XC}(\rho) \qquad (2)$$

where E^T is the kinetic energy of the electrons, E^V the sum of the Coulombic repulsion energy between the atomic nuclei and the attractive Coulombic interaction of the positive nuclei with the negative electron density, E^J the Coulombic repulsion energy between the electrons, also called Coulombic self-interaction of the electron density, and E^{XC} the exchange-correlation term. $E^T + E^V + E^J$ is the classical, i.e. non-quantum mechanical contribution to the energy, and each contribution can be expressed

analytically. However, no analytical expression exists for the exchange-correlation term E^{XC}. Hohenberg and Kohn[35] state that the energy is determined by the electron density of the system. If $E(\rho)$ is taken as the exact total energy, Equation 2 can be regarded as a definition of E^{XC}. The difficulty in the application of density functional theory to chemical problems lies in finding a physically reasonable analytic expression, which is a good approximation for E^{XC}, the exact exchange.

A common approach, incorporated in commercial quantum chemical program packages such as Gaussian98,[38] is to approximate E^{XC} as an integral of the spin densities and gradients:[37]

$$E^{XC}(\rho) = \int f(\rho_\alpha(\vec{r}),\rho_\beta(\vec{r}),\nabla\rho_\alpha(\vec{r}),\nabla\rho_\beta(\vec{r}))d^3\vec{r} \qquad (3)$$

Here, $\rho = \rho_\alpha + \rho_\beta$ denotes the total electron density composed of the α (spin up) and β (spin down) spin densities. E^{XC} is then further split up into contributions of same-spin and mixed-spin interactions, which define the terms exchange functional E^X and correlation functional E^C, respectively:

$$E^{XC}(\rho) = E^X(\rho) + E^C(\rho) \qquad (4)$$

Functionals which only depend on the electron density ρ are called *local*, while functionals of the electron density ρ and of its gradient $\nabla\rho$ are called *non-local* or *gradient-corrected*.

In the development of density funtionals for the calculation of isolated molecules, gradually more refined functionals emerged. The basic local exchange funtional called

E^X_{LDA} is defined as:

$$E^X_{LDA} = -\frac{3}{2}\left(\frac{3}{4\pi}\right)^{\frac{1}{3}} \int \rho^{\frac{4}{3}} d^3\vec{r} \tag{5}$$

This functional was developed as the exchange energy of a uniform electron gas.[36] Application to molecules and molecular systems, however, leads to significant errors. Therefore, gradient-corrections were introduced, of which the most widely used is the one developed by Becke in 1988.[39] The gradient corrected exchange functional is known as the Becke88 functional, and as "B" part of the method acronyms in Gaussian98:

$$E^X_{Becke88} = E^X_{LDA} - \gamma \int \frac{\rho^4 \left|\nabla\rho\right|^2}{1 + 6\gamma \sinh^{-1}\left(\rho^{\frac{4}{3}} \left|\nabla\rho\right|\right)} d^3\vec{r} \tag{6}$$

γ is a parameter fitted to the exchange energies of rare gas atoms, and amounts to 0.0042 Hartrees according to Becke.

Similarly, various local and gradient-corrected correlation functionals are in use, of which the VWN3[40] local correlation functional and the Perdew-Wang PW91[41] and Lee-Yang-Parr LYP[42] gradient corrections are among the most popular.

For chemical purposes, density-functional methods are sufficiently accurate for certain kinds of molecules, but may lead to significant errors for others, for which Hartree-Fock based methods sometimes seem to be superior. To find density functionals that are reliably applicable to a large variety of, i.e. ideally all, chemical species, Becke introduced a Hartree-Fock admixture into his exchange functional, and applied a fit procedure in order to derive the ideal contribution of several exchange and correlation functionals. The

result is the by now widely used B3LYP[43] functional, which is of the form:

$$E_{B3LYP}^{XC} = (1-c_0)E_{LDA}^{X} + c_0 E_{HF}^{X} + c_X \Delta E_{B88}^{X} + (1-c_C)E_{VWN3}^{C} + c_C E_{LYP}^{C} \qquad (7)$$

The parameter c_0 allows any combination of LDA and Hartree-Fock local exchange, with the gradient correction part of the Becke88 functional, ΔE_{B88}^{X}, scaled by c_X. As correlation functional, a mixture of the local VWN3 and the gradient-corrected LYP functional are used, determined by the parameter c_C. The constants c_0, c_X, and c_C are those determined by Becke by fitting to the 56 atomization energies, 42 ionization potentials, 8 proton affinities, and 10 first-row atomic energies in the G1 molecule set,[43-45] obtaining values of $c_0 = 0.20$, c_X=0.72, and c_C=0.81. However, Becke used the PW91 functional instead of VWN3 and LYP. The applicability of the same fit parameters to different functionals illustrates that this approach is physically justified.

2.2.2 Basis Functions and Basis Sets

To calculate the energy $E[\rho(\vec{r})]$ of a given molecule, a self-consistent field approach is used. Starting with a reasonable guess for the electron density $\rho(\vec{r})$, the energy is calculated. According to the variation principle, the lowest energy is obtained from the physically correct function $\rho(\vec{r})$. In every iteration step, $\rho(\vec{r})$ is modified to lower the energy, until a stationary state is reached. This is determined by the convergence criterion, which is fulfilled when the energy difference between two subsequent iterations is smaller than a pre-chosen cutoff value. To make the formalism of electron density capable for computers, it is useful to express $\rho(\vec{r})$ by a set of molecular orbital wave

functions $\phi_i(\vec{r})$, which are linear combinations of a set of N fixed functions $\chi_\mu(\vec{r})$, the *basis functions*:[37]

$$\phi_i(\vec{r}) = \sum_{\mu=1}^{N} c_{\mu i}\chi_\mu(\vec{r}) \tag{8}$$

In a closed-shell n electron system, the total wavefunction $\Psi(\vec{r})$ can be constructed from the n/2 molecular orbitals $\phi_i(\vec{r})$ and α and β spin functions. With $\rho(\vec{r}) = \left|\Psi(\vec{r})\right|^2$, the functional $E[\rho(\vec{r})]$ becomes a function of the (N×n/2) parameters $c_{\mu i}$, $E[\rho(\vec{r})] = E(c_{\mu i})$.

Introducing the functions $\chi_\mu(\vec{r})$ makes evaluation of the density functionals feasible. It introduces, however, constraints on the electron density $\rho(\vec{r})$, as the total wavefunction $\Psi(\vec{r})$ is composed of the fixed functions $\chi_\mu(\vec{r})$. This is a significant source of error in the calculated energies. It can, however, be minimized by choosing physically reasonable functions $\chi_\mu(\vec{r})$, and by providing a large enough number N of these functions, which gives back to the electron density $\rho(\vec{r})$ some of its initial flexibility.

Gaussian98, as well as most other quantum chemical packages, employ atom-centered gaussian-type atomic functions $g(\alpha,\vec{r})$, the *primitive gaussians*:[37]

$$g(\alpha,\vec{r}) = cx^n y^m z^l e^{-\alpha\vec{r}^2} \tag{9}$$

The radial extent of the function is determined by α, and the powers of *x*, *y*, *z* determine the spatial symmetry of *g*. The constant *c* ensures normalization:

An actual basis function is composed of several primitive gaussians, leading to *contracted gaussians* χ_μ:

$$\chi_\mu = \sum_p d_{\mu p} g_p \tag{11}$$

$d_{\mu p}$ are fixed constants within a given basis fuction. A set of basis functions that describes the orbitals of an atom is called basis set. Standard basis sets for most elements are available via the basis set library of Gaussian98. Alternatively, the coefficients $d_{\mu p}$ and exponents α_p can be defined by the user.

2.2.3. Calculating Enthalpies of Reaction

All frequency calculations carried out with Gaussian98 include thermochemical analysis of the system. By default, this analysis is carried out at 298.15 K and 1 atm of pressure, using the principle isotope for each element type. Gaussian predicts various important thermodynamic quantities at the specified temperature and pressure, including the thermal energy correction, heat capacity and entropy. It also provides the sum of electronic and thermal enthalpies which is defined as follows:

$$H = E + RT \tag{12}$$

where $E = E_0 + E_{vib} + E_{rot} + E_{trans}$ and $E_0 = +E_{elec} +$ zero-point correction[37]

The usual way to calculate enthalpies of reactions is to calculate heats of formation, and take the appropriate sums and differences. However, since Gaussian

provides the sum of electronic and thermal enthalpies, enthalpies of reaction can simply be calculated by taking the difference of the sums of these values for the reactants and the products. This way is correct since the number of atoms of each element is the same on both sides of the reaction.[46]

2.3. References

(1) Wineland, D. J. *Science* **1984**, *226*, 395.
(2) Marshall, A. G.; Grosshans, P. B. *Anal. Chem.* **1991**, *63*, 215A.
(3) Comisarow, M. B.; Marshall, A. G. *Chem. Phys. Lett.* **1974**, *25*, 282.
(4) Beyer, M.; Bondybey, V. E. *Rapid Commun. Mass Spectrom.* **1997**, *11*, 1588.
(5) Berg, C.; Schindler, T.; Niedner-Schatteburg, G.; Bondybey, V. E. *J. Chem. Phys.* **1995**, *102*, 4870.
(6) Schindler, T. *Dissertation.* Fakultät für Chemie, Biologie und Geowissenschaften, Technische Universität München, Garching, 1996.
(7) Berg, C. *Dissertation.* Fakultät für Chemie, Biologie und Geowissenschaften, Technische Universität München, Garching, 1995.
(8) Marshall, A. G.; Verdun, F. R. *Fourier Transforms in NMR, Optical, and Mass Spectrometry*; Elsevier: Amsterdam, 1990.
(9) Caravatti, P.; Allemann, M. *Org. Mass Spectrom.* **1991**, *26*, 514.
(10) Berg, C. *Diplomarbeit.* Physik Department, Technische Universität München, Garching, 1992.
(11) Jackson, J. D. *Klassische Elektrodynamik;* de Gruyter: Berlin, New York, 1983.
(12) Caravatti, P. USA Patent Nr. 4 924 089, May 8, 1990.
(13) Schindler, T. *Diplomarbeit.* Physik Department, Technische Universität München, Garching, 1992.
(14) Summers, R.L. NASA Technical Note TN D-5285, 1969.
(15) Bartmess, J.E.; Georgiadis, R.M. *Vacuum* **1969**, *33*, 149.
(16) Horowitz, P.; Hill, W. *The Art of Electronics*; Cambridge University Press: Cambridge, 1989.
(17) Bruker Spectrospin, Nancy, 1992.

(18) Lammers, A. Garching, 1994.

(19) Turner, P. J. Beaverton, 1994; Thoma, A.; Schallmoser, G.; Lammers, A. Garching, 1995; Lammers, A. Garching, 1996.

(20) Beyer, M. Garching, 1996.

(21) Schindler, T. Garching, 1994; Beyer, M. Garching, 1996.

(22)Schindler, T. Garching, 1994.

(23) Bondybey, V. E.; English, J. H. *J. Chem. Phys.* **1981**, *74*, 6978.

(24) Bondybey, V. E. *Science* **1985**, *227*, 4683.

(25) Dietz, T. G.; Duncan, M. A.; Powers, D. E.; Smalley, R. E. *J. Chem. Phys.* **1981**, *74*, 6511.

(26) Berg, C.; Beyer, M.; Achatz, U.; Joos, S.; Niedner-Schatteburg, G.; Bondybey, V. E. *J. Chem. Phys.* **1998**, *108*, 5398.

(27) Beyer, M.; Berg, C.; Görlitzer, H.W.; Schindler, T.; Achatz, U.; Albert, G.; Niedner-Schatteburg, G.; Bondybey, V.E. *J. Am. Chem. Soc.* **1996**, *118*, 7386-7389.

(28) Berg, C.; Achatz, U.; Beyer, M.; Joos, S.; Albert, G.; Schindler, T.; Niedner-Schatteburg, G.; Bondybey, V.E. *Int. J. Mass Spectrom. Ion Processes* **1997**, *176/168*, 723-734.

(29) Berg, C.; Beyer, M.; Achatz, U.; Joos, S.; Niedner-Schatteburg, G.; Bondybey, V.E. *Chem. Phys.* **1998** ,*239*, 379-392.

(30) Fox, B.S.; Beyer, M.K.; Bondybey, V.E. *J. Phys. Chem. A* **2001**, *105*, 6386-6392.

(31) Fox, B.S.; Beyer, M. K.; Bondybey, V. E., submitted to *J. Am. Chem Soc.*

(32) Proch, D.; Trickl ,T. *Rev. Sci. Instrum.* **1989**, *60*, 713.

(33) Sell, M. Garching, 1996.

(34) Kohn, W. ; Becke, A.D.; Parr, R.G. *J. Phys. Chem.* **1996**, *100*, 12974.

(35) Hohenberg, P.; Kohn, W. *Phys. Rev. A* **1964**, *136*, 864.

(36) Ziegler, T. *Chem. Rev.* **1991**, *91*, 651.

(37) Foresman, J. B.; Frisch, A. *Exploring Chemistry with Electronic Structure Methods* Gaussian Inc.: Pittsburgh, 1996.

(38) Gaussian 98, Revision A.7, Frisch, M. J.; Trucks, G. W.; Schlegel, H. B.; Scuseria, G. E.; Robb, M. A.; Cheeseman, J. R.; Zakrzewski, V. G.; Montgomery,J. A Jr., Stratmann, R. E.; Burant, R. E.; Dapprich, S.; Millam, J. M.; Daniels, A. D.; Kudin, K. N.; Strain, M. C.; Farkas, O.; Tomasi, J.; Barone, V.; Cossi, M.; Cammi, R.; Mennucci, B; Pomelli, C.; Adamo, C.; Clifford, S.; Ochterski, J.; Petersson, G. A.; Ayala, P. Y.; Cui, Q.; Morokuma,

K.; Malick, D. K.; Rabuck, A. D.; Raghavachari, K.; Foresman, J. B.; Cioslowski, J.; Ortiz, J. V.; Baboul, A. G.; Stefanov, B. B.; Liu, G.; Liashenko, A.; Piskorz, P.; Komaromi, I.; Gomperts, R.; Martin, R. L.; Fox, D. J.; Keith, T.; Al-Laham, M. A.; Peng, C. Y.; Nanayakkara, A.; Gonzalez, C.; Challacombe, M.; Gill, P. M. W.; Johnson, B.; Chen, W.; Wong, M. W.; Andres, J. L.; Gonzalez, C.; Head-Gordon, M.; Replogle, E. S.; Pople, J. A. Gaussian, Inc., Pittsburgh PA, 1998.

(39) Becke, A. D. *Phys. Rev. A* **1988**, *38*, 3098.

(40) Vosko, S. H.; Wilk, L.; Nusair, M. *Canadian J. Phys.* **1980**, *58*, 1200.

(41) Burke, K.; Perdew, J. P.; Wang, Y. *Electronic Density Functional Theory: Recent Progress and New Directions*, J. F. Dobson, G. Vignale and M. P. Das (Eds.), Plenum, 1998.

(42) Lee, C.; Yang, W.; Parr, R. G. *Phys. Rev. B* **1988**, *37*, 785.

(43) Becke, A. D. *J. Chem. Phys.* **1993**, *98*, 5648.

(44) Pople, J. A.; Head-Gordon, M.; Fox, D. J.; Raghavachari, K.; Curtiss, L. A. *J. Chem. Phys.* **1989**, *90*, 5622.

(45) Curtiss, L. A.; Jones, C.; Trucks, G. W.; Raghavachari, K.; Pople, J. A. *J. Chem. Phys.* **1990**, *93*, 2537.

(46) Ochterski, J. W. Thermochemistry in Gaussian, Gaussian White Papers, http://www.gaussian.com/thermo.htm

3 Reactions of Hydrated Transition Metals in Oxidation State I

3.1 Introduction

Ionic water clusters provide an interesting medium for investigating aqueous chemistry on a microscopic scale. Recent studies have demonstrated, that most reactions in such clusters proceed in a manner quite analogous a bulk aqueous solution, and that one can transfer many macroscopic concepts such as concentration, acidity or solubility to species dissolved in finite clusters.[1-4]

A convenient, versatile method for generating solvated ions is laser vaporization of metals in the presence of a carrier gas seeded with the desired solvent. Interestingly, but perhaps understandably, regardless of the preferred oxidation state of the element in question, the laser vaporization usually produces solvated monovalent ions, and for most metals examined thus far, ion clusters of the type $M^+(H_2O)_n$ were formed, regardless of whether the monovalent ions of the metal are known in bulk aqueous chemistry or not.[5-12] The solvated ions formed in this way and stored in an ICR trap can then survive for the many second duration of the experiment, which allows their chemistry to be studied. The clusters gradually absorb photons from the room temperature black body radiation background, and lose the solvent, one molecule at a time.[13-18]

In a number of cases, redox reactions take place in the cluster, oxidizing the ion to its favored valence state. For example as the solvent is removed from the Mg^+ or Ca^+ cations,[5,6,9-11] formation of atomic hydrogen is observed, and the metal oxidized to the corresponding dication. On the other hand, the stable oxidation state of aluminum is +III,

and accordingly, black body fragmentation of $Al^+(H_2O)_n$ cations results in an oxidation of the metal to Al^{3+}, yielding $Al(OH)_2^+(H_2O)_n$ complex cations, accompanied by the loss of molecular hydrogen, H_2.[7,8] These processes can be accelerated by reaction of the clusters with acids, e.g. HCl.[5,6,8] Similar reactions which lead to formation of hydrogen have recently also been observed for solvated sodium dimers.[19-21]

Unlike main group metals like Mg or Al, which exhibit a clear preference for forming Mg^{2+} and Al^{3+} ions respectively, transition metals occur in a number of oxidation states and are also able to easily change their oxidation state which is the reason for their wide use as catalysts.[22] In order to get insight into possible redox reactions which might lead to more than one product the black body radiation induced fragmentation of the monovalent first-row transition metal cations Ti^+ to Zn^+ and their reactions with HCl were studied. Except for Cu^+, all these monovalent ions are unknown in aqueous chemistry. Hence, this study is the first investigation of the aqueous chemistry of these ions. Strictly speaking, Zn^+ is not counted to the transition metals because the metal and its ions have completely filled d-shells. However, Zn^+ was included in this study to investigate the influence of a completely filled d-shell upon the reactivity of the half filled s orbital.

3.2 Experimental Details

The experiments were performed on a modified Spectrospin CMS47X mass spectrometer described in detail elsewhere.[7,23] Hydrated transition metal cations were produced by laser vaporization of a solid disk of the respective metal (Ti: Alfa, 99.5%, V: Aldrich, 99.7%+, Cr: Alfa, 99.996%, Mn: Alfa, 99.95%, Fe: Alfa, 99.995%, Co: Aldrich, 99.95%, Ni: Alfa, 99.994%, Cu: Alfa, 99.999%, Zn: Alfa, 99.98%). The helium carrier gas (Messer Griesheim 4.6) at 10 bar backing pressure was seeded with 30 mbar of water

vapor. The metal plasma was entrained in a pulse of the carrier gas, cooled by flowing through a confining channel and by subsequent supersonic expansion into high vacuum, resulting in formation of hydrated metal cations. The ions were transferred through several stages of differential pumping into the high-field region of the superconducting magnet and stored inside the ICR cell at a background pressure of 4×10^{-10} mbar. The reactant gas HCl was introduced into the ultrahigh vacuum region via a needle valve at a pressure of typically 6×10^{-8} mbar. After varying delays, the ions remaining in the cell were excited, and the mass spectra of the reaction products identified.

3.3 Computational Details

The calculations were carried out on a Pentium III based Linux system using the Gaussian98[24] program package, employing the three-parameter hybrid Hartree-Fock/Density functional (B3LYP) method described by Becke[25-27] with the Lee-Yang-Parr correlation functional[28] as incorporated in Gaussian98. For magnesium, oxygen, and hydrogen, the 6-311++(3df,3pd) basis set, treating explicitly all electrons with two diffuse and four polarization functions, was employed. For zinc, the quasi-relativistic effective core potential basis set of the Stuttgart/Dresden group[29] as implemented in Gaussian98 was used. All geometries were fully optimized and verified to be local minima on the potential energy surface by frequency calculations. Thermal corrections were evaluated in harmonic approximation.

3.4 Black Body Radiation Induced Fragmentation of Hydrated Transition Metal Cations $M^+(H_2O)_n$, M = Ti, V, Cr, Mn, Fe, Co, Ni, Cu, Zn

3.4.1 Titanium

Several attempts to generate hydrated titanium cations $Ti^+(H_2O)_n$ failed. Only clusters with mass 2 amu lower could be produced, either being $TiO^+(H_2O)_n$ or $Ti(OH)_2^+(H_2O)_{n-1}$. Similar problems of generating hydrated Ti cations have been reported by Deng et al.[30] who used laser induced plasma reactions of Ti and water to produce the cluster ions. Dalleska et al.[31] finally succeeded to produce $Ti^+(D_2O)_n$, n=1-4, by adding CH_4 to their flow tube prior to D_2O. In the absence of CH_4, Ti^+ reacted with D_2O to form $TiO^+(D_2O)_n$ clusters. They suggested initial ligation with CH_4 followed by ligand exchange with D_2O as production mechanism.

3.4.2 Vanadium

In contrast to titanium, hydrated vanadium cations $V^+(H_2O)_n$ could be produced without any difficulties. In a typical experiment presented in Fig. 1, the initial distribution at a nominal t=0 contains clusters $V^+(H_2O)_n$, n=13-34, with the corresponding peaks connected by a dashed line. Besides the hydrated V^+ clusters, one can note much weaker peaks shifted two amu lower in mass, which are denoted by the dotted line. These correspond clearly to clusters with two hydrogen atoms less, which can be written as either $VO^+(H_2O)_{n-1}$ or as $V(OH)_2^+(H_2O)_{n-2}$, V(III) hydroxide. Panels b-d) in Fig. 1 show the effect of retaining the cluster ions in the ICR cell for 2, 10, and 50 s, prior to measuring

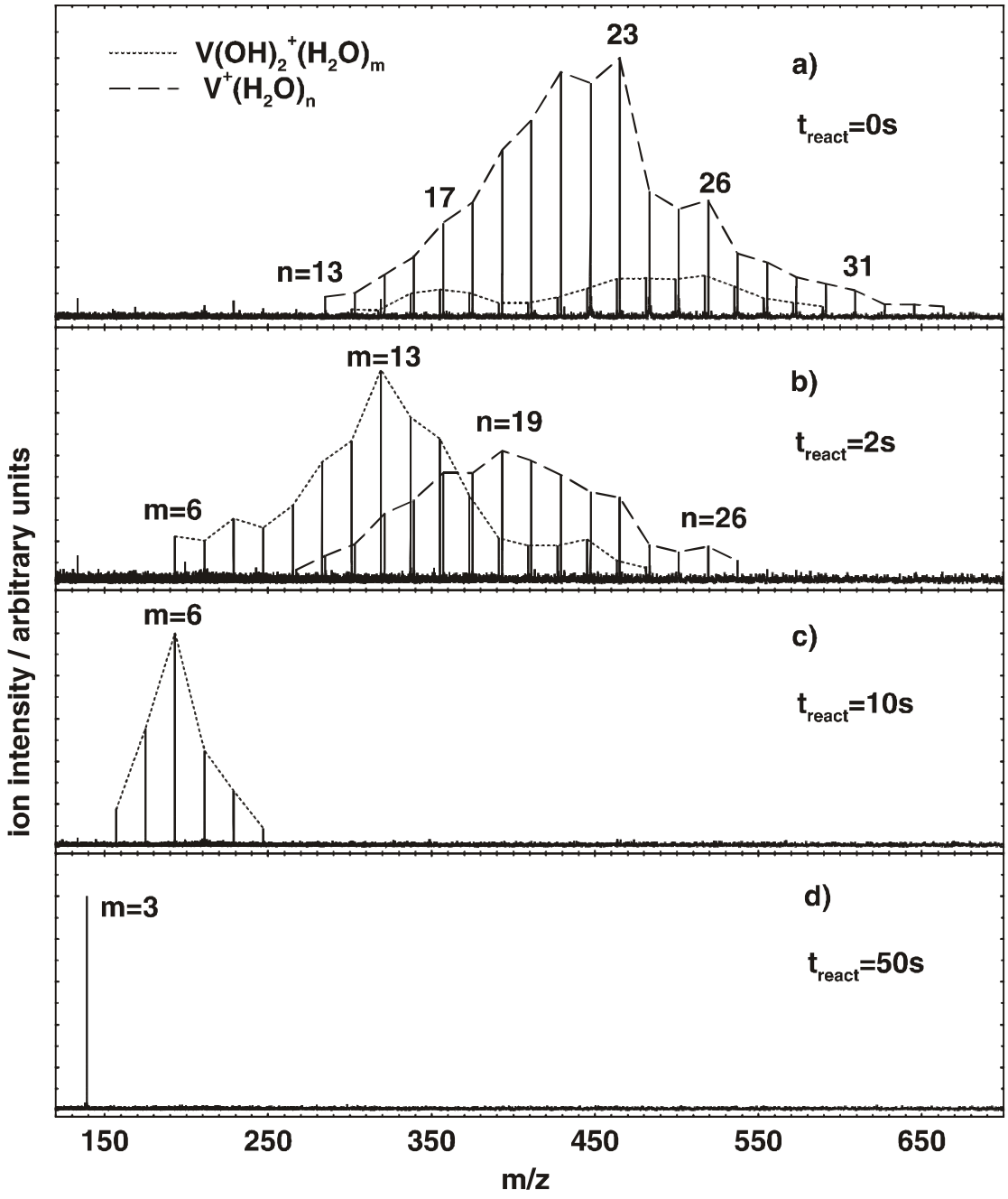

Figure 1: Mass spectra showing the fragmentation of $V^+(H_2O)_n$, n=13-34, after variable reaction delays. At a pressure of about $4x10^{-10}$ mbar in the cell region, the fragmentation is induced by the black-body background radiation. The initial cluster distribution which also contains $V(OH)_2^+(H_2O)_m$, m=12-28, is observed after accumulating the ions for 2 s in the cell (a). After a reaction delay of 2 s (b), the clusters shifted to lower masses. Moreover, a distinct shift in favor of the $V(OH)_2^+(H_2O)_m$ clusters can be observed. The $V^+(H_2O)_m$ have completely disappeared after 10 s (c), while the $V(OH)_2^+(H_2O)_m$ further evaporate water until the final product $V(OH)_2^+(H_2O)_3$ is reached (d).

the mass spectrum, thereby allowing them to absorb the infrared black body radiation and to fragment. One can clearly note not only a gradual loss of water ligands, but also a distinct shift of the distribution in favor of the hydroxide clusters, indicating that besides fragmentation, also an intracluster redox reaction takes place:

$$V^+(H_2O)_n \rightarrow V(OH)_2^+(H_2O)_{n-2-x} + H_2 + x\ H_2O \qquad (1)$$

Similar to the case of aluminum,[7,8] vanadium in the unusual +I state corresponding to a $3d^4$ electron configuration is oxidized to its much more common V(III) $3d^2$ state, with a concurrent reduction of water to form hydroxide and molecular hydrogen. The shift of the hydroxide cluster distribution to lower masses, with respect to that of the original hydrated ions suggests, that the heat of reaction liberated in this process probably also leads to an evaporation of one or several water ligands. As can be seen in Fig. 1d, after some 50 s the fragmentation process is completed, all the clusters have been oxidized, and as a final product only the $V(OH)_2^+(H_2O)_3$ ion remains. At a point where the clusters have reached thermal equilibrium with the apparatus walls, and their internal energy is no longer sufficient to evaporate a further ligand, the fragmentation ends.[8,32]

It is interesting to note that the reaction of bare V^+ ions with D_2O has previously been investigated both experimentally[33] and theoretically.[34] Although the formation of VO^+ and D_2 was predicted to be exothermic, for ground state V^+ the reaction was not observed. On the other hand, an excited triplet state of V^+ was found to dehydrogenate D_2O very efficiently. This reported lack of reactivity of bare V^+ ions, and their efficient oxidation observed here suggests, that the solvation shell has a pronounced effect upon the course of the reaction. In view of this, it surely appears interesting to probe more specifically the effect of the size of the solvation shell upon the V^+ reactivity.

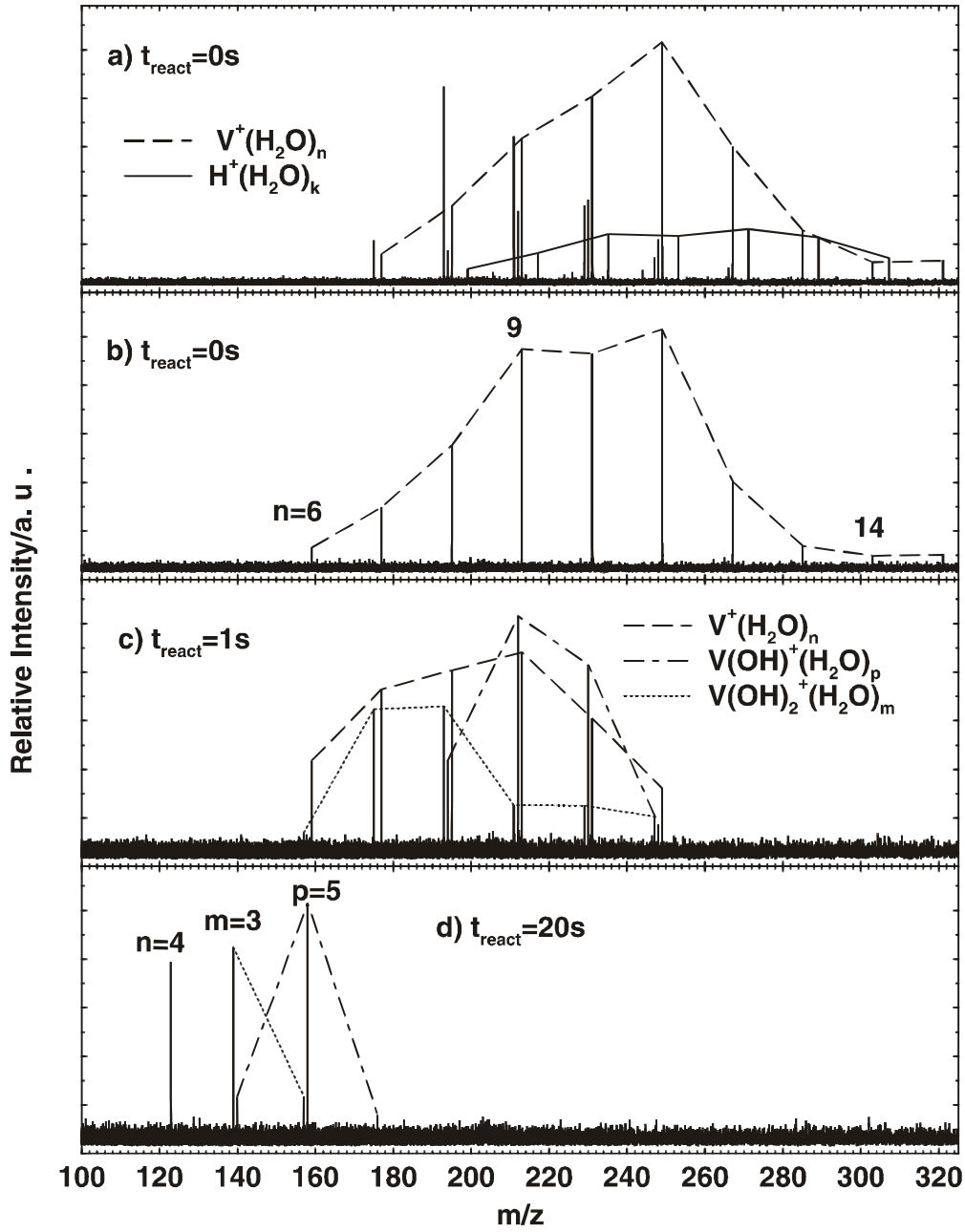

Figure 2:a) Mass spectrum showing a distribution of small hydrated vanadium cations, $V^+(H_2O)_n$, n=7-15. Almost every $V^+(H_2O)_n$ peak is accompanied by hydroxide containing cluster species, $V(OH)^+(H_2O)_{n-1}$ and $V(OH)_2^+(H_2O)_{n-2}$. In addition, protonated water clusters, $H^+(H_2O)_m$, m=11-21, have been produced in the cluster source. b) Clean distribution of $V^+(H_2O)_n$, n=6-15, generated by ejecting the unwanted species. After storing these clusters for 1s in the FT-ICR cell (c), hydrated vanadium hydroxide species, $V(OH)^+(H_2O)_p$ and $V(OH)_2^+(H_2O)_m$, have been formed due to absorption of black body radiation. The different cluster species further evaporate water. After 20 s (d), the most dominant products are $V(OH)^+(H_2O)_5$, $V(OH)_2^+(H_2O)_3$ and $V^+(H_2O)_4$.

To investigate if there is a lower limit n for reaction (1), the time of flight conditions were modified to favor smaller clusters. This resulted, however, in a relatively complex initial distribution, containing besides the desired $V^+(H_2O)_n$ clusters and the hydroxide $V(OH)_2^+(H_2O)_m$ species discussed above, also hydrated proton clusters, $H^+(H_2O)_k$, Fig. 2a. Somewhat unexpectedly, however, one can also see clusters with masses one amu lower than the hydrated vanadium clusters. Exact mass measurements clearly revealed that they possess a $V(OH)^+(H_2O)_p$ elemental composition, corresponding to a +II oxidation state of vanadium. Obviously under these conditions with a variety of products in the initial distribution it would be difficult to establish conclusively, if the V(II) species are already produced in the source, or form in an intracluster reaction in the ICR trap. Therefore, the ability of the ICR instrument to eject unwanted ions was used to produce a clean initial distribution of smaller $V^+(H_2O)_n$ ions which is displayed in Fig. 2b. Panels c) and d) in Fig. 2 present the effect of black body radiation absorption upon this clean initial n=6-14 distribution. Even though at t=0 in panel b) only $V^+(H_2O)_n$ clusters are present already after 1 s in panel c) two types of products can be seen: $V(OH)_2^+(H_2O)_m$ and $V(OH)^+(H_2O)_p$. Apparently, unlike in the case of the large hydrated vanadium clusters, for the smaller ones besides reaction (1) a second intracluster reaction channel opens up:

$$V^+(H_2O)_n \rightarrow V(OH)^+(H_2O)_{n-1-x} + H + x\,H_2O \qquad (2)$$

Clearly, vanadium V^+ is again oxidized but only to V^{2+} in this case, forming hydrated V(II) mono-hydroxide ion clusters, and the reduction of water yields a hydrogen atom, quite similar to the reactions previously reported for magnesium.[5,6,10,11] Fig. 2d shows that even when the reaction is allowed to proceed for quite a long time, 20 s in this

case, vanadium in three oxidation states, +I, +II and +III is still present. The final product distribution contains with comparable intensities three types of ions, $V^+(H_2O)_n$, $V(OH)^+(H_2O)_p$ and $V(OH)_2^+(H_2O)_m$, with clusters with n=4, p=5 and m=3 being dominant. Thus, in some of the clusters the vanadium is oxidized to the +III state, in others to +II, and in still others not at all.

To establish if the dihydroxide species $V(OH)_2^+(H_2O)_m$ in this experiment are formed in a single step with a loss of molecular H_2, or if a two step process with consecutive evaporation of two hydrogen atoms can also occur, we have generated an initial clean distribution of hydrated vanadium monohydroxide cations, $V(OH)^+(H_2O)_p$, p= 6-9, by first allowing the hydrated V^+ ions to react, and then ejecting the remaining $V^+(H_2O)_n$ ions as well as the $V(OH)_2^+(H_2O)_m$ products. The only reaction channel observed for these clusters was fragmentation, resulting again in a final $V(OH)^+(H_2O)_p$, p= 5, product.

The experiments described above have shown that a competition between three processes takes place: cluster fragmentation, oxidation to V^{2+} with evolution of hydrogen atoms, and to V^{3+} freeing molecular H_2. In order to obtain more detailed information about the size-dependence of these three reaction channels and about the corresponding branching ratios, the ability of the FT-ICR technique to mass select a single cluster of any desired size and composition was used. Data obtained in such an experiment are exemplified in Fig. 3 for $V^+(H_2O)_{10}$, which shows the mass spectrum immediately after the selection, and then 0.4 s and 0.6 s later. In addition to the simple loss of a water molecule, also a loss of an H atom resulting in $V(OH)^+(H_2O)_p$ with p=8, 9, as well as release of molecular hydrogen to form $V(OH)_2^+(H_2O)_6$ can be observed.

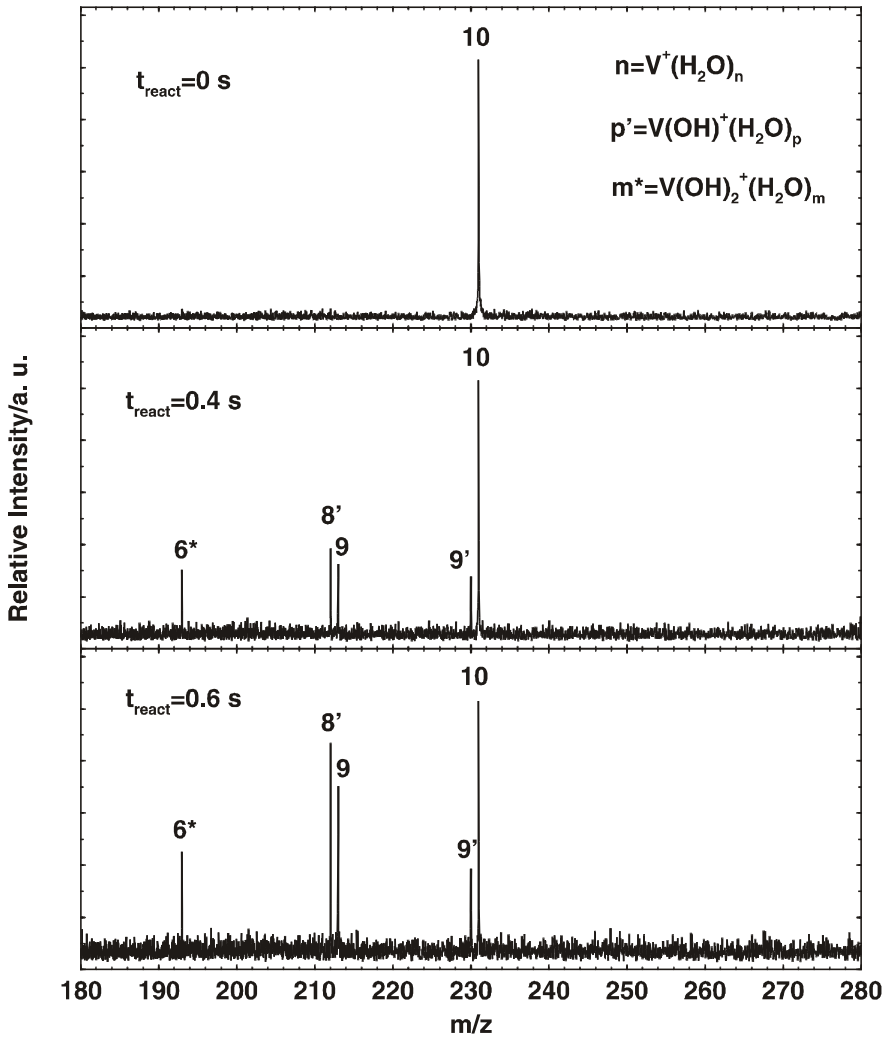

Figure 3: Mass spectra of the black body radiation induced unimolecular reactions of size-selected $V^+(H_2O)_{10}$ with a delay of (a) 0 s, (b) 0.4 s, (c) 0.6 s after trapping. The main fraction of the clusters undergoes an intracluster reaction to form $V(OH)^+(H_2O)_{8,9}$. Smaller fractions fragment to $V^+(H_2O)_9$ or undergo an intracluster reaction to form $V(OH)_2^+(H_2O)_6$.

Such size-selected measurements were carried out for all clusters from n=5-30. For each cluster, the decay of the selected reactant, and the growth of the observed primary products were fitted according to first order reaction kinetics to obtain the rate constants for each channel. The time profile together with the fitted rate constants for $V^+(H_2O)_{10}$ is displayed as an example in Fig. 4. The data obtained in this way for n=5-30 are summarized in Table 1, and presented graphically in Fig. 5.

Table 1: Measured fragmentation and reaction rates of individual size selected clusters, and the number of ligands lost in the observed oxidation reactions.

	k_{frag} [s^{-1}]	$k(H_2)$ [s^{-1}]	$x(H_2)$	$k(H)$ [s^{-1}]	x(H)
$V^+(H_2O)_5$	0.22	-	-	-	-
$V^+(H_2O)_6$	0.44	-	-	-	-
$V^+(H_2O)_7$	0.59	-	-	-	-
$V^+(H_2O)_8$	1.04	-	-	-	-
$V^+(H_2O)_9$	0.44	0.19	2	0.79	0;1
$V^+(H_2O)_{10}$	0.56	0.32	2	0.89	0;1
$V^+(H_2O)_{11}$	0.63	0.40	2; 3	0.92	0;1
$V^+(H_2O)_{12}$	1.20	1.53	2	0.36	0
$V^+(H_2O)_{13}$	0.77	2.00	2; 3	-	-
$V^+(H_2O)_{14}$	2.50	0.50	2	-	-
$V^+(H_2O)_{15}$	0.26	-	-	-	-
$V^+(H_2O)_{16}$	3.00	0.35	3	-	-
$V^+(H_2O)_{17}$	2.85	0.58	3	-	-
$V^+(H_2O)_{18}$	3.50	1.40	3	-	-
$V^+(H_2O)_{19}$	4.10	1.20	3	-	-
$V^+(H_2O)_{20}$	1.78	0.62	2	-	-
$V^+(H_2O)_{21}$	4.00	0.40	3	-	-
$V^+(H_2O)_{22}$	3.00	0.38	3	-	-
$V^+(H_2O)_{23}$	4.50	1.40	3	-	-
$V^+(H_2O)_{24}$	5.00	-	-	-	-
$V^+(H_2O)_{25}$	3.50	-	-	-	-
$V^+(H_2O)_{26}$	5.57	-	-	-	-
$V^+(H_2O)_{27}$	5.60	-	-	-	-
$V^+(H_2O)_{28}$	8.43	-	-	-	-
$V^+(H_2O)_{29}$	5.38	-	-	-	-
$V^+(H_2O)_{30}$	8.07	-	-	-	-

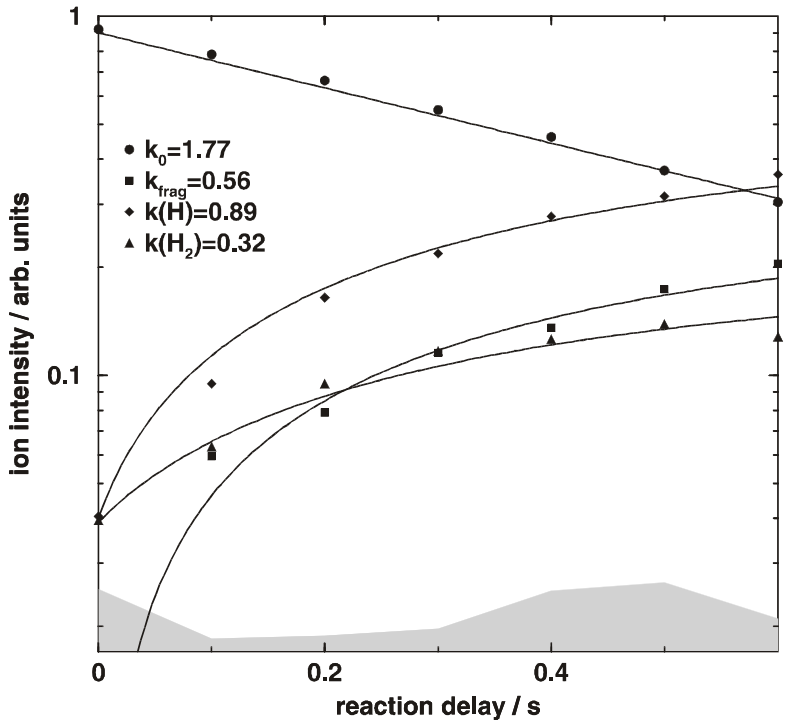

Figure 4: Time-intensity profile for the black body radiation induced fragmentation and reactions of $V^+(H_2O)_{10}$. The experimental data (solid points) are fitted assuming first-order kinetics (solid lines). Grey shaded areas denote the noise level.

Similar to previous observations for a number of other solvated clusters, the rates of fragmentation by the black body radiation scale overall linearly with the number of ligands n,[3,5-7,18,32] even though some specific clusters deviate from this dependence well outside the experimental error. Particularly interesting is the fragmentation of the n=20 cluster, which is about a factor of two slower than those of either n=19 or n=21. Essentially final product of the fragmentation is, as noted previously, the n=4 cluster, whose further fragmentation is at the ICR experiment time scale exceedingly slow.

Consistent with the previous observation that ground state V^+ does not react with water in the gas phase, the small $V^+(H_2O)_n$, n=4-8, do not react by reducing water. Similar to the earlier studies of Mg^+ and Al^+, an upper reactivity limit is also found for V^+, with n≥24 clusters only fragmenting. Interestingly, also for n=15 there is no observable

intracluster reaction. Other clusters between n=9 and n=23 reduce water with development of molecular hydrogen according to reaction (1), with variable reaction rates. It is interesting to note, that although only clusters up to n=23 reduce water and form hydroxides, as can be seen in Fig. 1, small amounts of $V(OH)_2^+(H_2O)_m$ clusters can be observed in the initial distribution even for n>23. This is probably due to reactions of electronically excited or translationally hot V^+ ions directly in the laser vaporization source. These clusters may also be due to hydration of VO^+ impurity ions formed by the vaporization in the supersonic expansion.

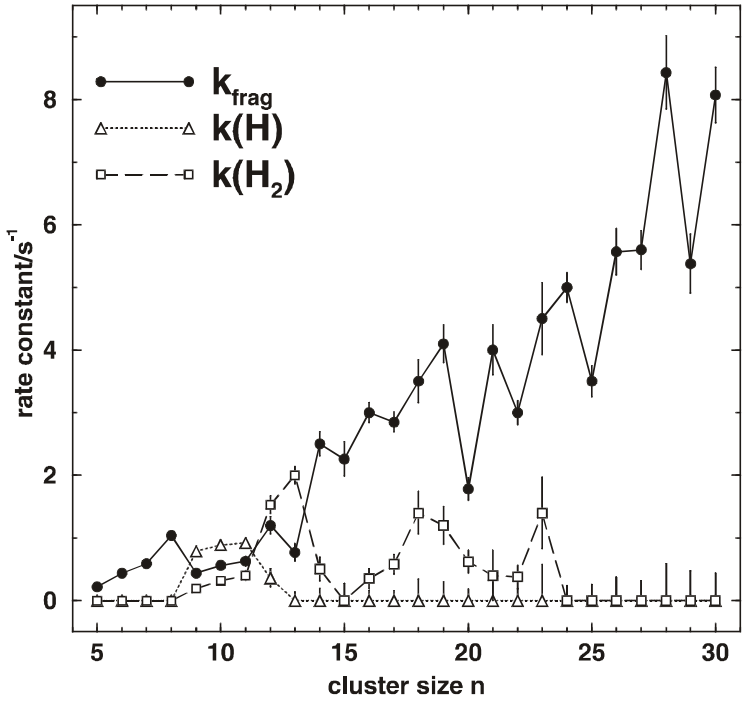

Figure 5: First-order rate constants of the black body radiation induced unimolecular reactions of size-selected $V^+(H_2O)_n$, n=5-30. Very small hydrated vanadium cations $V^+(H_2O)_n$, n=5-8, and very large clusters, n=24-30, only fragment by losing water molecules. Small clusters, n=9-11, preferentially decay by forming atomic hydrogen, but also water evaporation or formation of molecular hydrogen is possible. For n=12 and n=13, formation of molecular hydrogen is the most efficient reaction channel. Less efficient is the simple loss of a water molecule, and formation of atomic hydrogen is only observed for n=12 but to a very small extent. Clusters of size $14 \leq n \leq 23$ preferentially fragment, but also formation of molecular hydrogen is observed.

As can be seen in Fig. 3 and Table 1, the formation of molecular hydrogen is apparently exothermic enough to also cause a concurrent evaporation of two, and in some cases three water molecules, column x(H_2) in the table. The loss of the water molecules must be, on the timescale of the ICR experiment, almost instantaneous, i.e. faster than a few milliseconds, since e.g. in Fig. 3b) and c) no trace of the $V(OH)_2^+(H_2O)_7$ is observed. The evaporation of the water ligands places an upper limit for the enthalpy of the oxidation reaction in the range of about $\Delta H < -80$ kJ/mol. While for most of the larger species x(H_2)=3, it is 2 for the n=20 hydrate, suggesting again a higher thermodynamic stability of this cluster. It should be noted that the fact that for all clusters for which H_2 formation is observed x(H_2) $\geq$2 suggests that even for those which do not get oxidized the reaction is exothermic, but does not occur due to a high activation barrier or for entropic reasons.[18] As can be seen in Fig. 5, reaction (1) is most efficient for n=12 and 13, where it is in fact the dominant channel. Even though the values of x indicate that the redox reaction is more exothermic for the larger clusters, this is not reflected in the rate constants, which are in fact much smaller than the corresponding fragmentation rates. This indicates that the processes are not enthalpy driven, but kinetically controlled. In size regions which exhibit competing reactions, the activation energy for the evaporation of a water molecule, i.e. the vaporization enthalpy, $\approx$40 kJ/mol, is an upper limit for the barriers of the hydrogen formation processes. For cluster sizes which do not exhibit the intracluster reactions, either the activation energy is too high or the process is much more unlikely than fragmentation as has also been suggested for the decay channels of hydrated electrons,[18] presumably because of very tight transition states.

For small clusters, n=9-12, a third channel, reaction (2) with hydrogen atom formation appears and competes with the other processes. As can again be seen in Fig. 5 and in Table 1, for n=9-11 this becomes the dominant channel. As might, however, be

expected, the formation of atomic hydrogen is much less exothermic, since at most one, and sometimes no water molecule is evaporated (column x(H) in Table 1), which places its enthalpy in the range of $\Delta H > -50$ kJ/mol. In the case of Mg^+ which was previously studied,[5,6] the oxidation to Mg^{2+} was accompanied by a simultaneous loss of one or two water molecules, indicating that the process is more exothermic than the formation of V^{2+}. This is quite understandable considering that Mg^+ is an open shell radical with a half-filled s-shell and gains rare gas configuration in $MgOH^+$ while the ground state V^+ has an [Ar] $3d^4$ electron configuration. In the case of aluminum, the loss of molecular hydrogen is accompanied by the loss of two or three water molecules, similar to what is observed for vanadium.

3.4.3 Chromium, Manganese, Iron, Cobalt, Nickel, Copper, Zinc

Hydrated metal cations $M^+(H_2O)_n$ containing the heavier metals Cr, Mn, Fe, Co, Ni, Cu, and Zn could be produced without any traces of oxides or hydroxides in the initial distribution. In every case, the parameters were optimized to get an initial distribution with $n_{min}\approx12$ and $n_{max}\approx37$. These clusters were also stored in the ICR cell and exposed to the black body radiation. Their decay was observed for up to 50 s. Regardless of the metal ion, these clusters fragmented by a simple subsequent loss of water molecules similar to the previously investigated fragmentation of hydrated silver cations,[32] protonated water clusters,[17] and hydrated iodine species.[3] After 50 s, $M^+(H_2O)_3$ was obtained as final product for M=Cr, Fe, Co, Ni, Cu, Zn. However, the black body radiation induced fragmentation of hydrated Mn cations leads to $Mn^+(H_2O)_4$ as dominant product after 50s. $Mn^+(H_2O)_3$ can also be identified in this spectrum but only with very weak intensity. This indicates that $Mn^+(H_2O)_4$ fragments considerably more slowly than the other $M^+(H_2O)_4$

clusters. The fragmentation rate constant is basically dependent on the ratio of the rate of energy absorption and the binding energy. Accordingly, compared to the other investigated clusters, $Mn^+(H_2O)_4$ either has a very small rate of energy absorption or the fourth water molecule is more tightly bound if Mn^+ is the central ion. Dalleska et al. determined binding energies of $M^+(H_2O)_n$ (n=1-4, M=Ti to Cu).[31] Their results for the fourth water ligand are summarized in Table 2. The lowest binding energies for the fourth water ligand were found for Fe and Mn. Hence, a small energy uptake rate must be the reason for the small fragmentation rate constant of $Mn^+(H_2O)_4$. As discussed in detail previously,[3,5-7,17,18] the low frequency cluster modes of the hydrogen bonded ligand network are responsible for the efficient energy uptake from the black body background radiation. Thus, a possible explanation for the different behaviour of $Mn^+(H_2O)_4$ might be a different geometry: It is imaginable that in $Mn^+(H_2O)_4$ every water ligand is directly bound to the metal ion whereas the other clusters form structures with one or two water molecules already bound in the second solvation sphere. Unfortunately, only a small number of theory studies on hydrated monovalent transition metal cations exists to test this assumption. Ricca et al. computed structures for $Fe^+(H_2O)_n$, n=1-4, using DFT.[36] They obtained a C_2 structure as optimal structure for $Fe^+(H_2O)_4$ where all ligands are directly coordinated to Fe^+. However, it is not clear if they also used structures as initial geometries which contain at least one water molecule in the second solvation shell. The same problem appears for studies by El-Nahas et al.[37] and Schneider et al.[38] who found a tetrahedral and a planar structure, respectively, to be the optimum geometries for $Cu^+(H_2O)_4$. A recent MP2 study of $Cu^+(H_2O)_4$ by Feller et al.,[39] however, showed that a C_2(2+2) structure with 2 water ligands directly coordinated and 2 water ligands in the second solvation shell is favored with 11.8 kJ/mol compared to a C_1(3+1) structure and with 32.3 kJ/mol compared to a C_2(4+0) structure.

Table 2: Enthalpy changes at 298 K for the following dissociation reaction:[31]

$$M^+(H_2O)_4 \rightarrow M^+(H_2O)_3 + H_2O$$

M^+	ΔH (kJ/mol)
Ti^+	83.3
V^+	66.9
Cr^+	50.6
Mn^+	49.4
Fe^+	49.4
Co^+	57.3
Co^+	51.5
Ni^+	53.6

As noted above, no evidence for intracluster reactions could be observed for M=Cr to Zn which seems to be most surprising for Mn^+, Fe^+ and Zn^+ because the bare monocations have a singly filled s orbital like Mg^+ as can be seen in Table 3. The DFT calculations of Ricca et al.[36] showed, however, that a spin change takes place with increasing hydration in the case of $Fe^{+\cdot}$. $Fe^+(H_2O)$ has a sextet ground state like bare Fe^+ because 4s-4p polarization reduces the iron-ligand repulsion. In contrast to this, a quartet ground state is more favorable for $Fe^+(H_2O)_n$, $n\geq2$. The presence of two or more water ligands leads to the 4s→3d promotion overcoming the metal ligand repulsion due to the interaction between the H_2O orbitals and the iron 4s orbital. A similar septet-quintet change is imaginable for Mn^+. For Zn^+, however, a spin change is impossible because of the completely filled d-shell. Thus, it is still surprising why hydrated Zn^+ cations do not react similar to hydrated Mg^+ cations. The following reaction mechanism has been proposed for the intracluster reaction of hydrated Mg^+ cations:[5,6,10] If a sufficient amount of water is present, the rather unstable Mg^+ cation is further oxidized, leading to the formation of a Mg^{2+} cation and a hydrated electron. When the large clusters containing the

very stable Mg^{2+}_{aq} cation and e^{-}_{aq} lose successively solvent molecules, the amount of water is no longer sufficient to completely solvate both the Mg^{2+} and the electron, and the system is destabilized. Around n=21 a charge transfer and a subsequent chemical reaction takes place. Mg^{2+}_{aq} and e^{-}_{aq} recombine to form a highly reactive Mg^{+}_{aq} cation which reacts with one of the nearby water ligands to form a hydrated $MgOH^{+}_{aq}$ product and a hydrogen atom. Hence, a possible explanation for the different behavior of Zn^{+} and Mg^{+} can be found by comparing the ionization potentials of the bare ions: To form Mg^{2+} and an electron, 1451 kJ/mol are necessary, to form Zn^{2+} and an electron, 1733 kJ/mol.[40] Of course, solvation will change these values significantly, but the relative order should be similar.

Table 3: Electron configuration[42] and ionization potential[40] of the bare monocations Ti^{+} to Zn^{+}

M^{+}	Electron Configuration	2. Ionization Potential [kJ/mol]
Ti^{+}	[Ar] $3d^2\ 4s^1$	1310
V^{+}	[Ar] $3d^4$	1415
Cr^{+}	[Ar] $3d^5$	1591
Mn^{+}	[Ar] $3d^5\ 4s^1$	1509
Fe^{+}	[Ar] $3d^6\ 4s^1$	1562
Co^{+}	[Ar] $3d^8$	1648
Ni^{+}	[Ar] $3d^9$	1753
Cu^{+}	[Ar] $3d^{10}$	1958
Zn^{+}	[Ar] $3d^{10}\ 4s^1$	1733

A closer examination of the electron configurations noted in Table 3 shows that vanadium, the only monovalent cation which is oxidized due to a black body radiation induced intracluster reaction, is also the only one with a less than half-filled d shell. The d electrons are known to shield the charge of the nucleus insufficiently which is for example

reflected in the so-called d contraction. Due to this effect, the d-electrons of the heavier transition metals are more tightly bound, which is reflected in the monotonic increase of the second ionization potential for the metals which do not contain electrons in the 4s orbital, i.e. V, Cr, Co, Ni, Cu. These values are also displayed in Table 3. Comparison with the second ionization potential of Mg, 1451 kJ/mol, reveals that this value is considerably larger for the heavier transition metals which might be the reason for the lack of intracluster reactions in these cases.

3.5 Reactions of Hydrated Transition Metal Cations $M^+(H_2O)_n$ with HCl

3.5.1 Possible Reaction Pathways

So far, four possible reaction pathways of hydrated metal(I) cations with HCl have been observed. In every case, the HCl molecules collide with the ionic clusters, and about 10% of the collisions are reactive, with the hydrochloric acid being taken up and ionically dissolved in the cluster.[2,35] The enthalpy of this reaction is released and heats the cluster, which in turn leads to evaporative cooling by loss of two or three water molecules. Depending on the number of available water ligands, additional HCl molecules may be absorbed into the water cluster. Conversely, as the solvent molecules are continously removed from the clusters due to collisional and evaporative heating, finally the ionic solution becomes destabilized, and an HCl molecule may evaporate from the cluster.

Once the HCl molecule is dissolved in the water cluster, aqueous phase chemical reactions can take place. For instance, the metal ion may be oxidized according to the following equations with atomic or molecular hydrogen being released, as previously observed for hydrated Mg^+ or Al^+ ions, respectively.[5-8]

$$Mg^+(H_2O)_n + HCl \rightarrow MgCl^+(H_2O)_{n-x} + H + x\ H_2O \quad (3)$$

$$Al^+(H_2O)_n + HCl \rightarrow Al(OH)Cl^+(H_2O)_{n-y-1} + H_2 + y\ H_2O \quad (4)$$

$$Al(OH)Cl^+(H_2O)_n + HCl \rightarrow AlCl_2^+(H_2O)_{n-z+1} + z\ H_2O \quad (5)$$

Such chemical change and hydrogen loss is easily detected in the high-resolution mass spectrum provided by the FT-ICR instrument. An alternative possibility is the precipitation of a single molecule of the metal chloride in the cluster which does, of course, not leave an immediate signature in the mass spectrum. By monitoring the subsequent reactions and ligand evaporation as a function of time, however, one can unmistakably diagnose if the salt remains ionized, or forms a single molecule precipitate.[2]

In clusters containing a metal cation, which forms a highly soluble chloride such as sodium, three ions, i.e. Na^+, H^+ and Cl^-, have to be individually solvated. Similarly in a protonated water cluster containing dissolved HCl, three ions, $2H^+$ and Cl^-, are present. As the cluster is gradually heated and desolvated, finally the H^+ and Cl^- recombine to form HCl, and the covalent hydrogen chloride evaporates from the $M(HCl)(H_2O)_n^+$ cluster. This occurs around n=12.[2,35] A quite different situation was found for Ag^+ which forms an insoluble chloride. In this case, the last HCl is lost when only four molecules of water are left, surely too little solvent to hydrate three separate ions.[2] One can conclude from this observation that only a single H^+ ion is present, and the covalent AgCl formed as a precipitate in the cluster. Thus, the number of water molecules n at which HCl is eliminated from the $M(HCl)(H_2O)_n^+$ cluster can be viewed as a measure of the solubility of the corresponding chloride.

Similar minimum size values for HCl uptake by water clusters containing H^+ or Na^+ have recently been observed in flow reactor studies,[4] which indicates that the minimum size of the cluster is an intrinsic property of the reaction system, and not an

artefact of the experimental method and timescale.

3.5.2 Titanium

The reaction of $[TiO(H_2O)_n]^+$ was investigated to get information about the nature of the central ion since hydrated titanium oxide clusters are expected to behave differently than hydrated titanium dihydroxide clusters. In the case of hydrated titanium oxide cations, the clusters would take up a specific number of HCl molecules depending on their size. Due to collisions and black body radiaition the clusters would shrink and evaporate an HCl molecule if a certain number of water molecules is reached which is too less to stabilize the three ions, TiO^+, H^+, and Cl^-. In contrast to this, hydrated titanium hydroxide ions would react similar to hydrated aluminum dihydroxide cations by a substitution reaction:[9]

$$Ti(OH)_2^+(H_2O)_n + 2HCl \rightarrow TiCl_2^+(H_2O)_{n-x+2} + xH_2O \qquad (6)$$

For this purpose, a distribution of $[TiO(H_2O)_{12-32}]^+$ was reacted with HCl. Three products are observed after 20 s: $TiCl_2^+(H_2O)_{3-5}$. These clusters could also be written as $[TiO(HCl)_2(H_2O)_{2-4}]^+$ but this small number of water molecules is surely too low to stabilize the TiO^+ cation and two ionically dissolved HCl molecules. Accordingly, the ions in the initial distribution are of the hydrated hydroxide type, $Ti(OH)_2^+(H_2O)_n$. Chen et al.[41] studied the reaction of bare Ti^+ with D_2O and found the formation of TiO^+ and D_2 to be the dominant process. Thus, it is imaginable that Ti^+ reacts in the cluster source to TiO^+ and further solvation leads to proton transfer processes and formation of solvated $Ti(OH)_2^+$.

3.5.3 Vanadium

As described above, hydrated vanadium cations react to hydrated vanadium dihydroxide and monohydroxide clusters when exposed to black body radiation. But the small amount of clusters with 2 amu less in the initial distribution could still be oxides. To investigate the nature of the central ion also in this case, a similar distribution to the one shown in Fig. 1a was reacted with HCl. This reaction leads to formation of products with $V(OH)Cl^+(H_2O)_n$ composition. Consequently, the initially existing second cluster species are of the hydroxide type which might result of excited V^+ ions which then react similar to the Ti^+ ions or of hydrated VO^+ ions formed as an impurity in the cluster source. Both cluster types react according to the following equations with the upper size limit being removed in the case of $V^+(H_2O)_n$:

$$V(OH)_2^+(H_2O)_n + HCl \rightarrow V(OH)Cl^+(H_2O)_{n-x+2} + xH_2O \quad (7)$$

$$V^+(H_2O)_n + HCl \rightarrow V(OH)Cl^+(H_2O)_{n-x} + H_2 + (x-2)H_2O \quad (8)$$

Surprisingly, only one HCl molecule is taken up in this case. Only oxidation to V^{III} takes place in the case of $V^+(H_2O)_n$ because a distribution of large clusters was reacted with HCl. Since a minimum number of water molecules is necessary to take up and stabilize HCl the reaction of smaller clusters was not investigated.

3.5.4 Chromium, Manganese, Iron, Cobalt, Nickel, Copper, Zinc

The reactions of the heavier hydrated transition metal cations $M^+(H_2O)_n$ with HCl were also examined. For M=Cr to Cu, again, no hydrogen formation was observed. Only $Zn^+(H_2O)_n$ showed a redox reaction:

$$Zn^+(H_2O)_n + HCl \rightarrow ZnCl^+(H_2O)_{n-x} + H + xH_2O \qquad (9)$$

The mass spectrum of this reaction with a delay of 50 s can be seen in Fig. 6b. The initial distribution shown in Fig. 6a had a size range of n=17-35. The reaction products are $ZnCl^+(H_2O)_3$ and $ZnCl^+(H_2O)_4$. $Zn^+(H_2O)_3$ clusters can also be observed in the spectrum which have been produced by fragmentation of the cluster ions which were too small to dissolve HCl. This redox reaction is similar to the Mg case,[5,6] however, in contrast to Mg, in the case of Zn atomic hydrogen is only formed if a proton is present. Thus, the additional activation by a proton might be needed to lower the barrier for the oxidation reaction or the formation of $ZnOH^+$ is endothermic and only formation of $ZnCl^+$ is exothermic. To check the second suggestion the enthalpies of reactions (10)-(13) were calculated. Since experimental data are not available for all of the involved species, DFT calculations were performed at the B3LYP/6-311++(3df,3pd)/SECP level to obtain the relevant values.

$$Zn^+ + H_2O \rightarrow ZnOH^+ + H \qquad \Delta H_{10} = +267.5 \text{ kJ/mol} \qquad (10)$$

$$Zn^+ + HCl \rightarrow ZnCl^+ + H \qquad \Delta H_{11} = -13.6 \text{ kJ/mol} \qquad (11)$$

$$Mg^+ + H_2O \rightarrow MgOH^+ + H \qquad \Delta H_{12} = +183.3 \text{ kJ/mol} \qquad (12)$$

$$Mg^+ + HCl \rightarrow MgCl^+ + H \qquad \Delta H_{13} = -79.7 \text{ kJ/mol} \qquad (13)$$

The enthalpies clearly show that the reaction of Zn^+ with H_2O is much more endothermic than the corresponding reaction of Mg^+. Of course, hydration will decrease these values significantly, but in the case of Zn^+ the stabilization is obviously not enough to thermodynamically favor the reaction. The reaction of Zn^+ with HCl is exothermic even

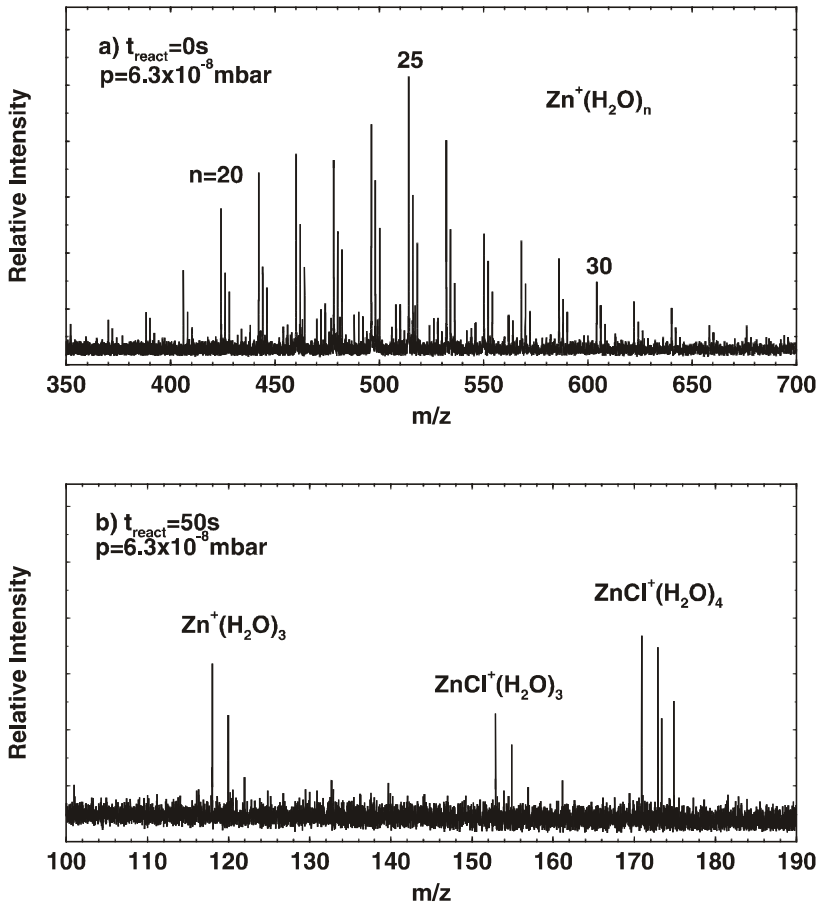

Figure 6: Mass spectrum of the reaction of hydrated Zn cations $Zn^+(H_2O)_n$, n=17-35, with HCl, taken with a reaction delay of a) 0s and b) 50 s at an HCl pressure of $6.3x10^{-8}$ mbar. Final products of the redox reaction are $ZnCl^+(H_2O)_n$, n=3, 4. The third cluster species $Zn^+(H_2O)_3$ was formed by fragmentation of clusters which were too small to take up any HCl.

without solvent. Thus, although less exothermic than the respective Mg^+ reaction, the oxidation reaction can take place in this case.

As already mentioned above, unlike the hydrated Mg^+, Al^+, V^+, and Zn^+ cations which are upon reaction with HCl readily oxidized, the ions of Cr, Mn, Fe, Co, Ni, and Cu do not change their oxidation state even in the presence of the strongly corrosive hydrochloric acid, but react, similar to silver monochloride, without changing their oxidation state. The resulting cluster containing the chloride precipitate and a proton then

gradually loses water ligands. When some specific number of water ligands n_{min}, which is characteristic of the particular metal, is reached, an HCl molecule is lost, and a hydrated monovalent cation $M^+(H_2O)_n$ remains. Typical data are displayed in Fig. 7 with Cu as an example. The initial distribution of $Cu^+(H_2O)_n$, n=11-33, was reacted with HCl for 10 s. After this relatively long reaction delay, aggregates of $Cu^+(H_2O)_n(HCl)_m$ composition have formed. It is immediately evident that the number of HCl molecules m in the cluster depends on the cluster size. Thus, clusters with n≤4 do apparently contain no HCl molecules at all, while at least five water molecules are necessary to stabilize one HCl molecule and at least six to stabilize two HCl molecules.

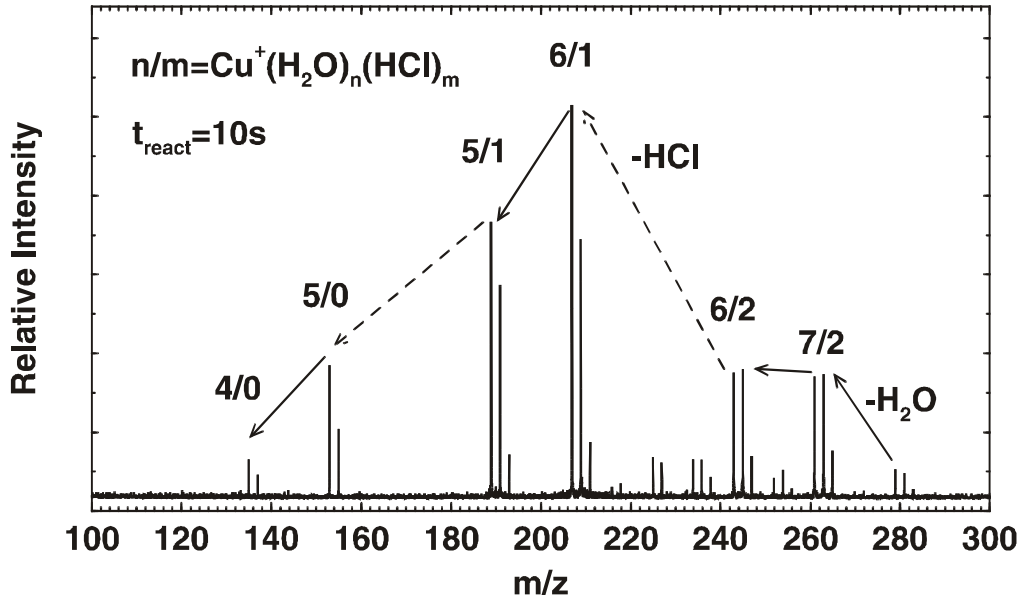

Figure 7: Typical part of a mass spectrum of the reaction of hydrated Cu cations $Cu^+(H_2O)_n$, n=11-35, with HCl, taken with a reaction delay of 10 s at an HCl pressure of $7.6x10^{-8}$ mbar. The clusters are basically saturated with HCl and can be written as $Cu^+(H_2O)_n(HCl)_m$. Collisionally and black body radiation induced dissociation are the dominant processes, leading to evaporation of either HCl or H_2O as indicated by the arrows. Loss of HCl preferentially occurs at n=5 and n=6 water molecules, as at this characteristic cluster sizes HCl recombines due to the lack of solvent molecules needed for ionic dissolution.

Table 4 gives the number n_{min} of solvent molecules remaining when the last HCl is eliminated for the precipitation reactions investigated in the present work, and compares it with cations studied previously. The table also gives the solubility constant of the salt in water, where available. It can clearly be seen that the solubilities correlate qualitatively with the values of n_{min}. If this correlation has some broader validity, one could predict an extremely low solubility for MnCl which does not eliminate HCl even when n=3 is reached, followed by FeCl, where the HCl loss at n=3 is only observable after t≈50 s. Conversely, it would suggest for NiCl and CoCl solubilities higher than that of CuCl.

Table 4: Cluster size limits for the reaction of $M^+(H_2O)_n$ with HX and available solubility constants[40] of compounds MX

MX	cluster size limit	solubility constant (mol^2l^{-2})
CrCl	4	-
MnCl	≤3	-
FeCl	3	-
CoCl	6	-
NiCl	7	-
CuCl	5	$1.7x10^{-7}$
AgCl[a]	4	$1.8x10^{-10}$
AgBr[b]	3	$5.4x10^{-13}$
NaCl[a]	12	$3.7x10^{1}$

[a]Reference 2; [b]Reference 43

It is interesting to consider the charge transfer between H^+ and the metal chloride occuring in the cluster when the last HCl molecule is lost:

$$H^+(H_2O)_n(MCl) \rightarrow H...MCl^+(H_2O)_n \rightarrow M^+(H_2O)_n + HCl \qquad (14)$$

This reaction is trongly exothermic in the gas phase (n=0), but in view of the enormous lowering of the H atom ionization potential due to solvation, endothermic in bulk solution (n=∞). Clearly, the thermochemistry of this reaction depends on the available solvent, and has to reverse sign as n is reduced, i.e. solvent is lost. The exact value of n_{min} where this will occur for a specific metal will depend on its ionization potential, the strength of the MCl bond, the preferred coordination of the metal cations, and on its hydration enthalpy.

Table 5: Electrochemical series of so far investigated metals[40] (pH=0)

Red → Ox	ε_0 [V]
$Mg \rightarrow Mg^{2+}$	-2.372
$Al \rightarrow Al^{3+}$	-1.662
$Mn \rightarrow Mn^{2+}$	-1.185
$V \rightarrow V^{2+}$	-1.175
$Cr \rightarrow Cr^{2+}$	-0.913
$Zn \rightarrow Zn^{2+}$	-0.7618
$Fe \rightarrow Fe^{2+}$	-0.447
$Co \rightarrow Co^{2+}$	-0.28
$Ni \rightarrow Ni^{2+}$	-0.257
$Fe \rightarrow Fe^{3+}$	-0.037
$Cu \rightarrow Cu^{+}$	0.153
$Cu \rightarrow Cu^{2+}$	0.3419

The low solubility of AgCl is usually explained by the strongly covalent character of the silver-chlorine interaction, and it is therefore quite reasonable that also other transition metals, with their partly filled d-shell should form relatively insoluble metal(I) chlorides. More surprising may appear the observation, that with the exception of vanadium and zinc, the singly ionized cations of the first row transition metals are not readily oxidized into their more favored oxidation state, even in the presence of hydrochloric acid. If one considers the standard electrochemical series in acidic solution, Table 5, and the potentials needed to oxidize the respective metals, one finds the order Mg < Al < Mn < V < Cr < Zn < Fe < Co < Ni < Cu. Except Cu, all the potentials are negative indicating that oxidation of the metal and reduction of water to molecular hydrogen is thermodynamically favored. Perhaps the rapid formation of a single molecule chloride precipitate hinders the oxidation reaction kinetically, so that although presumably being exothermic, it does not occur on the ≈100 s timescale of the experiment.

3.6 Conclusion

Hydrated titanium clusters could not be produced with the laser vaporization source using a mixture of He and H_2O as carrier gas. Only clusters of $[TiO(H_2O)_n]^+$ composition were formed. The reaction of these ions with HCl clearly demonstrated that they are hydrated titanium dihydroxide ions, $Ti(OH)_2^+(H_2O)_n$.

Investigation of hydrated vanadium cations $V^+(H_2O)_n$ trapped in an ICR cell reveals an interesting, n-dependent competition between several processes induced by absorption of the black body background infrared radiation. The cluster fragmentation and ligand loss competes with oxidation of the V^+ ions to V^{2+} or V^{3+}, forming VOH^+ and $V(OH)_2^+$ species. This behavior, with two different intracluster redox reactions leading to

two different oxidation states is surely due to the fact that vanadium is a transition metal known to form stable compounds in a variety of oxidation states. In the size range of n≈9-23 vanadium is oxidized to V^{3+}, and reduces water with the development of molecular H_2. In the range n=9-12, also oxidation to V^{2+} and release of H atoms is observed. Clusters with n≥24 and n≤8, on the other hand, exhibit only fragmentation. Upon reaction of large hydrated vanadium cations $V^+(H_2O)_n$ with HCl, oxidation to V^{III}, forming $V(OH)Cl^+$ species, and removal of the upper size limit is observed.

Hydrated metal cations $M^+(H_2O)_n$ containing the heavier metals Cr, Mn, Fe, Co, Ni, Cu, and Zn, fragment by losing successively water molecules if exposed to the black body radiation. In none of these cases, an intracluster reaction leading to the oxidation of the metal ion is observed. In the case of Zn, the oxidation reaction can be induced by HCl and hydrated $ZnCl^+$ cations with Zn in its preferred oxidation state II are formed. In contrast to Mg^+, however, the oxidation reaction only takes place if induced by the strong acid. DFT calculations indicate that only the formation of $ZnCl^+$ is thermodynamically favored whereas the formation of $ZnOH^+$ is endothermic. In the case of Cr, Mn, Fe, Co, Ni, and Cu a single molecule precipitation takes place which seems to hinder the oxidation reaction kinetically although it would presumably be thermodynamically favored.

3.7 References

(1) Achatz, U.; Joos, S.; Berg, C.; Schindler, T.; Beyer ,M.; Albert, G.; Niedner-Schatteburg, G.; Bondybey, V.E. *J. Am. Chem. Soc.* **1998**, *120*, 1876.

(2) Fox, B.S.; Beyer, M.K.; Achatz, U.; Joos, S.; Niedner-Schatteburg, G.; Bondybey, V.E. *J. Phys. Chem. A* **2000**, *104*, 1147.

(3) Achatz, U.; Fox, B.S.; Beyer, M.K.; Bondybey, V.E. *J. Am. Chem. Soc.* **2001**, *123*, 6151.

(4) Gilligan, J.J.; Castleman, A.W. *J. Phys. Chem. A* **2001**, 5601.

(5) Berg, C.; Achatz U.; Beyer M.; Joos, S.; Albert, G.; Schindler, T.; Niedner-Schatteburg, G.; Bondybey, V.E. *Int. J. Mass Spectrom. Ion Proc.* **1997**, *167/168* 723.

(6) Berg, C.; Beyer, M.; Achatz, U.; Joos, S.; Niedner-Schatteburg, G.; Bondybey, V.E. *Chem. Phys.* **1998**, *239*, 379.

(7) Beyer, M. ; Berg, C.; Görlitzer, H.; Schindler, T.; Achatz, U.; Albert, G.; Niedner-Schatteburg, G.; Bondybey, V.E. *J. Am. Chem. Soc.* **1996**, *118*, 7386.

(8) Beyer, M.; Achatz, U.; Berg, C.; Joos, S.; Niedner-Schatteburg, G.; Bondybey, V.E. *J. Phys. Chem. A* **1999**, *103*, 671.

(9) Sanekata, M.; Misaizu, F.; Fuke, K. *J. Chem. Phys.* **1996**, *104*, 9768.

(10) Sanekata M.; Misaizu, F.; Fuke, K.; Iwata, S.; Hashimoto, K. *J. Am. Chem. Soc.* **1995**, *117*, 747.

(11) Misaizu, F.; Sanekata, M.; Fuke, K. *Z. Phys. D* **1993**, *26*, 177.

(12) Fox, B.S.; Balaj, O.P.; Balteanu, I.; Beyer, M.K.; Bondybey, V.E. *J. Am. Chem. Soc.*, in print.

(13) Thölmann, D.; Tonner, D.S.; McMahon, T.B. *J. Phys. Chem.* **1994**, *98*, 2002.

(14) Dunbar, R.C.; McMahon, T.B. *Science* **1998**, *279*, 194.

(15) Sena, M.; Riveros, J.M. *Chem. Eur. J.* **2000**, *6*, 785.

(16) Rodriguez-Cruz, S.E.; Jockusch, R.A.; Williams, E.R. *J. Am. Chem. Soc.* **1999**, *121*, 8898.

(17) Schindler, T.; Berg, C.; Niedner-Schatteburg, G.; Bondybey, V.E. *Chem. Phys. Lett.* **1996**, *250*, 301.

(18) Beyer, M.K.; Fox, B.S.; Reinhard, B.M., *J. Chem. Phys.* **2001**, *115*, 9288.

(19) Buck, U.; Steinbach, C. *J. Phys. Chem. A* **1998**, *102*, 7333.

(20) Mercuri, F.; Mundy, C. J.; Parrinello, M. *J. Phys. Chem. A* **2001**, *105*, 8423.

(21) Mundy, C. J.; Hutter, J.; Parrinello, M. *J. Am. Chem. Soc.* **2000**, *122*, 4837.

(22) Hollemann, A.F.; Wiberg, E. *Lehrbuch der Anorganischen Chemie*, 101. Auflage;Walter de Gruyter: Berlin, 1995.

(23) Berg, C. ; Schindler, T.; Niedner-Schatteburg, G.; Bondybey, V.E. *J. Chem. Phys.* **1995**, *102*, 4870.

(24) *Gaussian 98, Revision A.7*; Frisch, M.J.; Trucks, G.W.; Schlegel, H.B.; Scuseria, G.E.; Robb, M.A.; Cheeseman, J.R.; Zakrzewski, V.G.; Montgomery, J.A., Jr.; Stratmann, R.E.; Burant, J.C.; Dapprich, S.; Millam, J.M.; Daniels, A.D.; Kudin, K.N.; Strain, M.C.;

Farkas, O.; Tomasi, J.; Barone, V.; Cossi, M.; Cammi, R.; Mennucci, B.; Pomelli, C.; Adamo, C.; Clifford, S.; Ochterski, J.; Petersson, G.A.; Ayala, P.Y.; Cui, Q.; Morokuma, K.; Malick, D.K.; Rabuck, A.D.; Raghavachari, K.; Foresman, J.B.; Cioslowski, J.; Ortiz, J.V.; Baboul, A.G.; Stefanov, B.B.; Liu, G.; Liashenko, A.; Piskorz, P.; Komaromi, I.; Gomperts, R.; Martin, R.L.; Fox, D.J.; Keith, T.; Al-Laham, M.A.; Peng, C.Y.; Nanayakkara, A.; Gonzalez, C.; Challacombe, M.; Gill, P.M.W.; Johnson, B.; Chen, W.; Wong, M.W.; Andres, J.L.; Gonzalez, C.; Head-Gordon, M.; Replogle, E.S.; Pople, J.A. Gaussian, Inc.: Pittsburgh, PA, 1998.

(25) Becke, A.D. *Phys. Rev. A* **1988**, *38*, 3098.

(26) Becke, A.D. *J. Chem. Phys.* **1993**, *98*, 1372.

(27) Becke, A.D. *J. Chem. Phys.* **1993**, *98*, 5648.

(28) Lee, C.; Yang, W.; Parr, R.G. *Phys. Rev. B* **1988**, *37*, 785.

(29) Schautz, F.; Flad, H.-J.; Dolg, M. *Theor. Chem. Acc.* **1998**, *99*, 231

(30) Deng, H.; Kerns, P.K.; Guo, B.C.; Bell, R.C.; Castleman, A.W. *Croat. Chem. Acta* **1998**, *71*, 1105.

(31) Dalleska, N.F.; Honma, Kenji; Sunderlin, L.S.; Armentrout, P.B. *J. Am. Chem. Soc.* **1994**, *116*, 3519-3528.*123*, 6151.

(32) Fox, B.S.; Beyer, M.K.; Bondybey, V.E. *J. Phys. Chem. A* **2001**, *105*, 6386.

(33) Clemmer, D.E.; Chen, Y.-M.; Aristov, N.; Armentrout P.B. *J. Phys. Chem.* **1994**, *98*, 7538.

(34) Irigoras, A.; Fowler, J.E.; Ugalde, J.M. *J. Am. Chem. Soc.* **1999**, *121*, 574.

(35) Schindler, T.; Berg, C.; Niedner-Schatteburg, G.; Bondybey, V. E. *Chem. Phys. Lett.* **1994**, *229*, 57.

(36) Ricca, A.; Bauschlicher, C.W., Jr. *J. Phys. Chem.* **1995**, *99*, 9003.

(37) El-Nahas, A.M.; Tajima, N.; Hirao, K. *J. Mol. Struct. (Theochem)* **1999**, *469*, 201.

(38) Schneider, W.F.; Hass, K.C.; Ramprasad, R.; Adams, J.B. *J. Phys. Chem.* **1996**, *100*, 6032.

(39) Feller, D.; Glendening, E.D.; de Jong, W.A. *J. Phys. Chem.* **1999**, *110*, 1475.

(40) Lide, D. R. *CRC Handbook of Chemistry and Physics*; CRC Press: Boca Raton ,1995.

(41) Chen, Y.-M.; Clemmer, D.E.; Armentrout, P.B. *J. Phys. Chem.* **1994**, *98*, 11490.

(42) Moore, C.M. *Atmoic Energy Levels as Derived from the Analyses of Optical Spectra*, Vol. I-II, Nat. Stand. Ref. Data Ser., Nat. Bur. Stand., 1971.

(43) Fox, B. S.; Diplomarbeit, Technische Universität München, 1999.

4 Black Body Fragmentation of Cationic Ammonia Clusters

4.1 Introduction

Molecular clusters bridge the gap between discrete gas phase molecules and bulk condensed phases, and their properties are therefore of considerable interest.[1,2] In recent years, fourier transform ion cyclotron resonance mass spectrometry (FT-ICR) has become a very productive technique with which a large variety of ionic clusters has been investigated. These FT-ICR studies have revealed that while relatively weakly bound clusters with ligands such as argon atoms or molecular nitrogen can be trapped in the ICR cell for many seconds or even minutes, hydrogen bonded cluster ions, in spite of the much stronger bonds, continuously fragment on a millisecond time scale due to the absorption of infrared black body radiation from the apparatus walls.[3-9]

Water is by far the most common solvent, important not only in industry and technology but also in the environment around us. Water molecules are highly polar, they interact strongly with the dissolved solutes, in particular ions, and have a significant effect upon their properties and chemical reactions. The black body fragmentation provides a unique tool for gently removing water ligands from an ionic cluster one by one, and allowing observation of the effects due to loss of the stabilizing solvent from the system under investigation. Individual solvent molecules evaporate in the essentially collision free, high vacuum environment from the hydrated anionic or cationic clusters due to infrared absorption by the water ligands. The rate of the overall energy input, and therefore of the solvent evaporation, is roughly proportional to the number of ligand molecules n.[9-13]

Several recent studies have taken advantage of this effect to explore in a microscopic, molecular detail, a number of different aqueous reactions taking place in the hydrated clusters or nanodroplets.[14-18] The reason why the hydrated clusters fragment, but ions ligated by for instance rare gases, CO or nitrogen do not is that unlike the relatively nonpolar latter ligands, the cluster modes of the hydrogen bonded water network overlap efficiently the room temperature Planck black body emission function.

Water is, however, not unique in this behavior, and one might expect other polar and strongly absorbing systems to behave in a similar way. Another important polar solvent which like water efficiently solvates ions and stabilizes ionic species is ammonia. More importantly, similar to water it has the ability to form strong hydrogen bonds, which in general greatly enhance the transition dipole of infrared transitions. Furthermore, solvating the ions by ammonia also results, similar to hydrated clusters, in the appearance of numerous low frequency intermolecular translational or rotational modes, which ideally overlap the 300 K black body background radiation distribution. Besides similarities, there are also some important differences between the two solvents. For instance, it is also well known that neutral NH_3 forms considerably weaker hydrogen bonds than water as evidenced e.g. by the lower binding energies of the dimers (ammonia <11.72 kJ/mol[19], water dimer: 22.6 ± 2.9 kJ/mol[20-22]).

Even more importantly, a water molecule can form two donor and two acceptor hydrogen bonds, as evidenced by the tetra-coordination which is characteristic both for solid ice and for liquid water and aqueous solutions. In contrast with that, NH_3 could in principle form three donor bonds, but possesses only a single lone pair to form acceptor bonds, making the formation of extended hydrogen bonded networks more difficult. These two differences result in the considerably higher vapor pressure and lower boiling point of liquid NH_3 as compared with water, in spite of the comparable molecular weights of the

two solvents. Due to the fact that ammonia is unable to form more than one acceptor hydrogen bond, one might expect in cationic clusters the single nitrogen lone pair of the first solvation shell ammonia ligands to coordinate the central core ion, making the formation of rings less probable and favoring branched structures, and this in turn makes extensive networks less stable. This view is supported by recent ab initio calculations of $H^+(NH_3)_n$ (n=1-8),[23] which report optimized geometries resembling NH_4^+ ammonium cation core, bound by donor hydrogen bonds to up to four ammonia molecules, with the sixth to eighth ammonia ligands appearing in the second solvation shell. Somewhat different results were recently reported by Bérces et al., who found in the geometries of the $[Cu(NH_3)_n]^{2+}$, n=3-8, ions optimized by static DFT and ab initio molecular dynamics calculations also stationary points with ammonia in bridging position forming two acceptor bonds.[24] Since, however, no vibrational frequencies were apparently calculated, these might represent transition states.

The investigation of the black body radiation induced fragmentation provides useful information about cluster stability, and may also yield some insight into their structure. In this chapter, the results of a first systematic study of the black body fragmentation of ionic ammonia clusters, and of ions solvated by ammonia, and their comparison with the analogous hydrated systems are reported. Specifically solvated Ag^+ is studied, but also $H^+(NH_3)_n$ species are examined, in view of the detailed previous studies of the hydrated $H^+(H_2O)_n$, n=5-65, cluster ions.[9,10]

4.2 Experimental Details

The experiments discussed here were performed on a modified Spectrospin CMS47X mass spectrometer described in detail elsewhere.[25,26] The cluster ions were

generated in a pulsed supersonic expansion source using 10 bar of helium carrier gas seeded with about 30 mbar of either water vapor or ammonia. Metal cations were produced by laser vaporization of a solid silver disk (Chempur, 99.995%+), and the plasma produced by the laser was then entrained in a pulse of the carrier gas. It was cooled by flowing through a confining channel with the clustering and solvation of the ions taking place in the subsequent supersonic expansion into high vacuum. The size and nature of the ions formed was controlled by changing the source parameters, especially laser power and pulse timing. While at lower laser powers the source can be optimized to generate predominantly solvated metal - in the present case silver - cations, by increasing the laser pulse energy and adjusting the delay between the piezoelectric valve trigger and the Q-switch of the Nd:YAG laser, conditions can be found where almost exclusively solvated proton clusters are produced. Laser vaporization thus provides an even more convenient and efficient source of protonated clusters than the discharge source previously used in our laboratory.[9,10] In either case, the cluster ions produced in the source are transferred through several stages of differential pumping into the high-field region of the superconducting magnet and stored inside the ICR cell at a background pressure of about $6x10^{-10}$ mbar. After allowing varying delays for the clusters to fragment or react, the ions remaining in the cell were detected, and the fragmentation products identified by their mass spectra. During all experiments, the vacuum chamber enclosing the ICR cell was cooled by a flow of water through the cooling jacket, resulting in a constant temperature of the apparatus walls of T=291±5 K.

4.3 Computational Details

Computations were carried out on a Pentium III based Linux system using the

Gaussian98[27] program package, employing the three-parameter hybrid Hartree-Fock/Density functional (B3LYP) method described by Becke[28-30] with the Lee-Yang-Parr correlation functional[31] as incorporated in Gaussian98. The 6-31G(d,p) basis set on all atoms was used for the geometry optimizations and frequency calculations, and also zero-point corrections were taken from this level of theory. In most of the optimizations, the structures found by Park[23b] have been used as initial geometries for $H^+(NH_3)_n$, n=1-5, computations. For $H^+(H_2O)_n$, n=4-5, only the solvated H_3O^+ structures, known to be global minima[32-34] were optimized. Single-point energy calculations were performed employing the larger 6-311++G(3df,3pd) basis set on all atoms. The power absorbed by the cluster modes from 298 K black body radiation was calculated from the overlap between the 300 K Planck distribution function and the cluster infrared spectrum and intensities I(ν) taken from the DFT calculations. The power P in kW/mol absorbed at a frequency ν is obtained from the following equation,[35] where ν is in cm^{-1} and I in km/mol:

$$P(\nu, I, T) = \frac{8\pi hc^2\nu^3 I \cdot 10^6}{\exp(100ch\nu / kT) - 1} \qquad (1)$$

No scaling factor for the computed frequencies was used, since the errors resulting from uncertainties in the computed intensities are probably considerably larger than those due to the frequency errors.

With the knowledge of vibrational frequencies of the solvated ions, it is also possible to compute the average internal energies as a function of temperature, which are useful in understanding cluster stability and fragmentation. To estimate the internal energies it was assumed that the clusters behave as ensembles of independent harmonic oscillators, and the expectation values of the energies of each of these oscillators were computed and summed.

4.4 Results and Discussion

4.4.1 Formation of Protonated Cluster $H^+(NH_3)_n$ and $H^+(H_2O)_n$ in the Laser Vaporization Source

With increasing laser pulse energy, the solvated metal ion clusters $Ag^+(NH_3)_n$ and $Ag^+(H_2O)_n$ disappear, and $H^+(NH_3)_n$ and $H^+(H_2O)_n$ become the dominant species in the spectra. In fact, conditions are readily found where the protonated clusters are exclusively observed, while it is comparatively hard to completely eliminate protonated clusters from the solvated metal ion spectra. The explanation for this can be found in the literature. Barnett and Landman[38] review their own computational work[39] and experimental work by Ng et al.[40] and Tomoda and Kimura.[41] In the photoionization of the water dimer, the "oxonium channel" $(H_2O)_2 + h\nu \rightarrow H_3O^+ + OH + e^-$, is favored over the "water channel" $(H_2O)_2 + h\nu \rightarrow H_2O^+ + H_2O + e^-$ by 1.08 eV (calculated) or 1.13 eV (experimentally).[40,41] In the laser vaporization source, ionization of water may not only occur by direct absorption of multiple photons, but also - and more likely so - by collisions with highly excited atoms or ions from the metal plasma. Since the $H_3O^+ + OH$ products are thermochemically favored over $H_2O^+ + H_2O$, individual water cations H_2O^+ will react with other water molecules or clusters to form the protonated species.

Similar arguments apply to the ammonia clusters, with the large body of experimental work reviewed by Park.[23b] From tabulated thermochemistry data,[36] the reaction $NH_3^+ + NH_3 \rightarrow NH_4^+ + NH_2$ is calculated to be exothermic by -58.9 kJ/mol, which illustrates further that in the ion source and in the subsequent evaporative cooling of the clusters during the transfer into the ICR cell, any $(NH_3)_n^+$ species will be converted to $H^+(NH_3)_{n-1}$ by loss of an NH_2 amino radical.

4.4.2 Hydrated Cation Clusters: $Ag^+(H_2O)_n$ and $H^+(H_2O)_n$

First, the aqueous clusters will be briefly discussed since comparison of cations solvated with ammonia with hydrated clusters is one of the major aims of this chapter. As noted above, the fragmentation of hydrated protons, $H^+(H_2O)_n$, has been investigated previously in considerable detail.[9,10] A similar experiment for hydrated silver cations, $Ag^+(H_2O)_n$, is documented in Fig. 1 which shows the initial t=0 cluster distribution and its changes after various time delays. While at t=0 (see Fig. 1a) the distribution exhibits a maximum at n=18 and extends from n=10-28, the shift to smaller sizes at t=3s and 10s is apparent in panels b) and c), and after a reaction time of 40s in Fig. 1d, essentially only the final product $Ag^+(H_2O)_3$ can be seen. This can be compared with the hydrated proton experiments where the final product was $H^+(H_2O)_4$. One can now take advantage of the ability of the FT-ICR technique to mass select a cluster of any desired size n in order to get more detailed information about the fragmentation process. After the mass selection, the reaction delays can be varied, and the intensities of the reactant ion as well as of the products of its fragmentation recorded as a function of time, and the data fitted assuming first order reaction kinetics.

Fragmentation rates of mass selected $Ag^+(H_2O)_n$, n=4-45, obtained in this way are plotted against n in Fig. 2a), where the solid circles give the experimental measurements, and the continuous line represents a linear least square fit of these data. From the diagram it is apparent that the rates increase approximately linearly with the number of ligands n. The data can be well fitted by an expression $k_n=k_f(n-n_0)$ where, in the present case, $k_f=0.18\ s^{-1}$, and $n_0=3.00$. This overall linear n-dependence is in agreement with the earlier observations for hydrated protons, $H^+(H_2O)_n$ (see Fig. 3a), where the analogous fitting

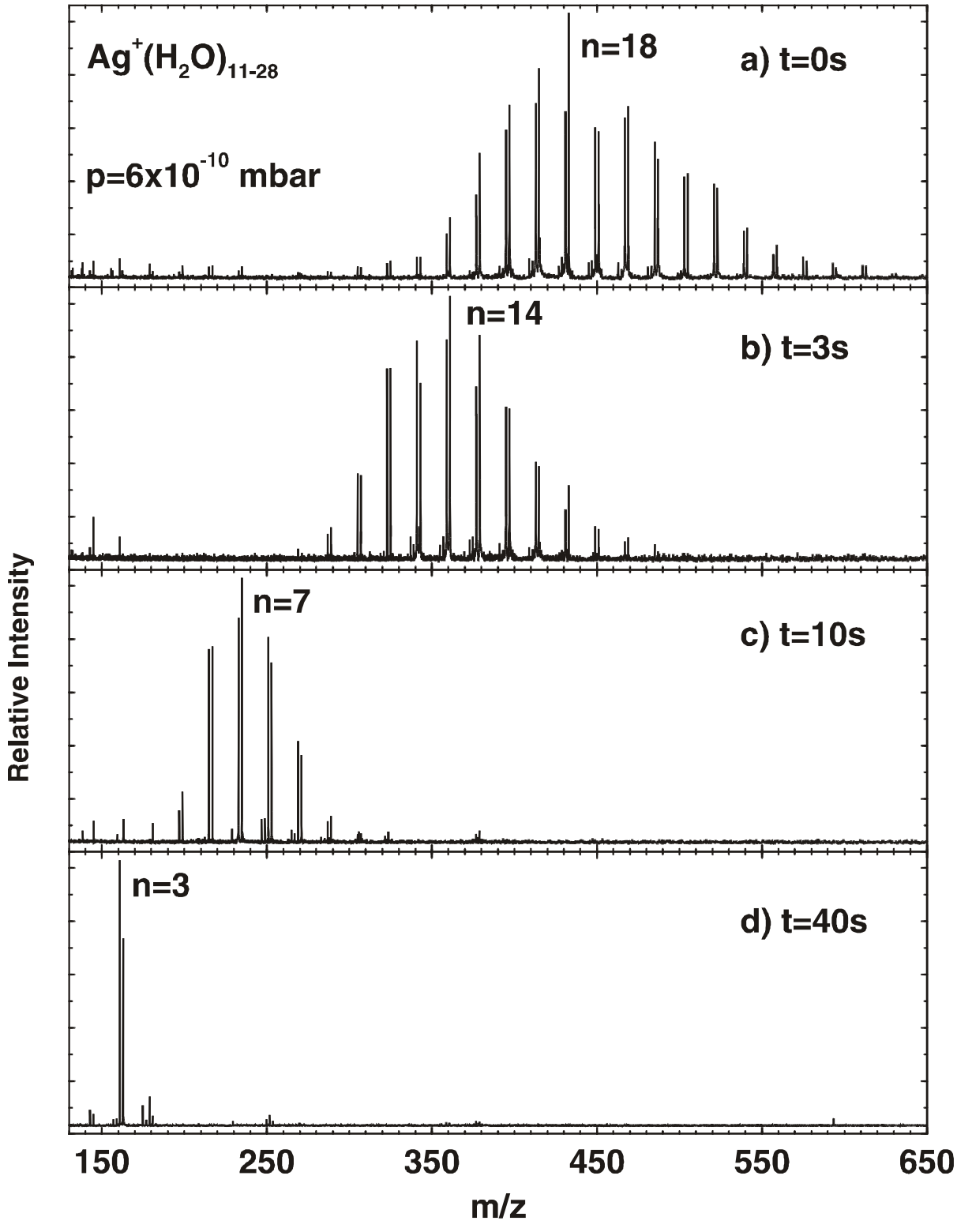

Figure 1: Mass spectra showing the fragmentation of $Ag^+(H_2O)_n$ clusters, n=10-28, after variable reaction delays. At the pressure of about $6x10^{-10}$ mbar in the cell region, the fragmentation is induced by the IR background radiation. The labeled peaks in each panel denote the maximum of the distribution.

procedure for n=5-65 yielded constants k_f=0.20 s^{-1} and n_0=1.39.[9,10] Comparable results, including similar slopes of the rate constant n-dependence, were also found in previous studies of numerous other hydrated ions, including the Mg^+ and Al^+ cations or I^- anions.[11-13]

Table 1: Slopes k_f, standard errors of the slopes and intercepts n_0 obtained by fitting the fragmentation rate constants to an expression $k_n=k_f(n-n_0)$.

cluster ions	slope k_f [s^{-1}]	standard error of slope [s^{-1}]	intercept n_0
$Ag^+(H_2O)_n$	0.18	0.01	3.00
$H^+(H_2O)_n$	0.20[a]	0.01	1.39
$Mg^+(H_2O)_n$	0.17[b]	0.02	2.35
$Al^+(H_2O)_n$	0.16[c]	0.02	1.63
$I^-(H_2O)_n$	0.17[d]	0.01	1.53
$Ag^+(NH_3)_n$	0.17	0.01	2.94
$H^+(NH_3)_n$	0.18	0.02	2.98

[a] Reference 10; [b] Reference 11; [c] Reference 12; [d] Reference 13

Some of the constants obtained in this way for various solvated ions are summarized in Table 1. One can see that independent of the specific nature or charge of the central ion, the slope has for all the hydrated ions an almost identical value of k_f=0.18 s^{-1}. While small differences can be found in the table between the constants obtained for various central ions, one should not try to over-interpret them. Most of the differences are within the experimental error, and furthermore the exact values depend somewhat on the data field, that is on the range of cluster sizes n included in the fit, and these are different for different ions. Obviously, the specific nature and size of the central ion should have some effect upon its fragmentation and therefore on the magnitude of k_f, especially where the range of cluster sizes is relatively narrow. However, the similarity of

the k_f values seen in Table 1 for the hydrates of quite different ions suggests that this effect of the central ion is relatively minor.

4.4.3 Comparison with Clusters Solvated by Ammonia: $Ag^+(NH_3)_n$ and $H^+(NH_3)_n$

As already noted in the experimental part of this chapter, ammonia clusters are formed in the laser vaporization source with almost equal ease as aqueous clusters, and both solvated protons as well as solvated Ag^+ cations have been investigated. Examination of such clusters solvated by ammonia reveals a very similar behavior to that found for the hydrated ions. Like the hydrates, also the ammonia clusters gradually fragment, and the initial cluster size distribution progressively shifts to smaller values of n. One finds again that not all of the ligands are lost, but even after very long delays final products are obtained, which do not seem to fragment further. For the clusters studied here, these are $Ag^+(NH_3)_3$ and $H^+(NH_3)_4$. Like their hydrated counterparts, the investigated ammonia clusters also show a linear dependence of the fragmentation rate on the number of ligand molecules as can be clearly seen in panels b) of Figs. 2 and 3. Linear fitting of the experimental data yields the equations $k_n=0.17(n-2.62)\ s^{-1}$ for $Ag^+(NH_3)_n$ and $k_n=0.18(n-2.97)\ s^{-1}$ for $H^+(NH_3)_n$, respectively, with the constants k_f and n_0 also included in Table 1. Somewhat surprisingly, one finds that also the slopes obtained by fitting the ammonia data seem to agree within the experimental error with those observed for the hydrated ions.

As explained previously for the hydrated ions, the linear dependence of the fragmentation rate can easily be understood. The temperature of the larger, fragmenting clusters, is determined by a competition between radiative heating and evaporative cooling,[9] and one can fairly easily show that they must be relatively cold compared with

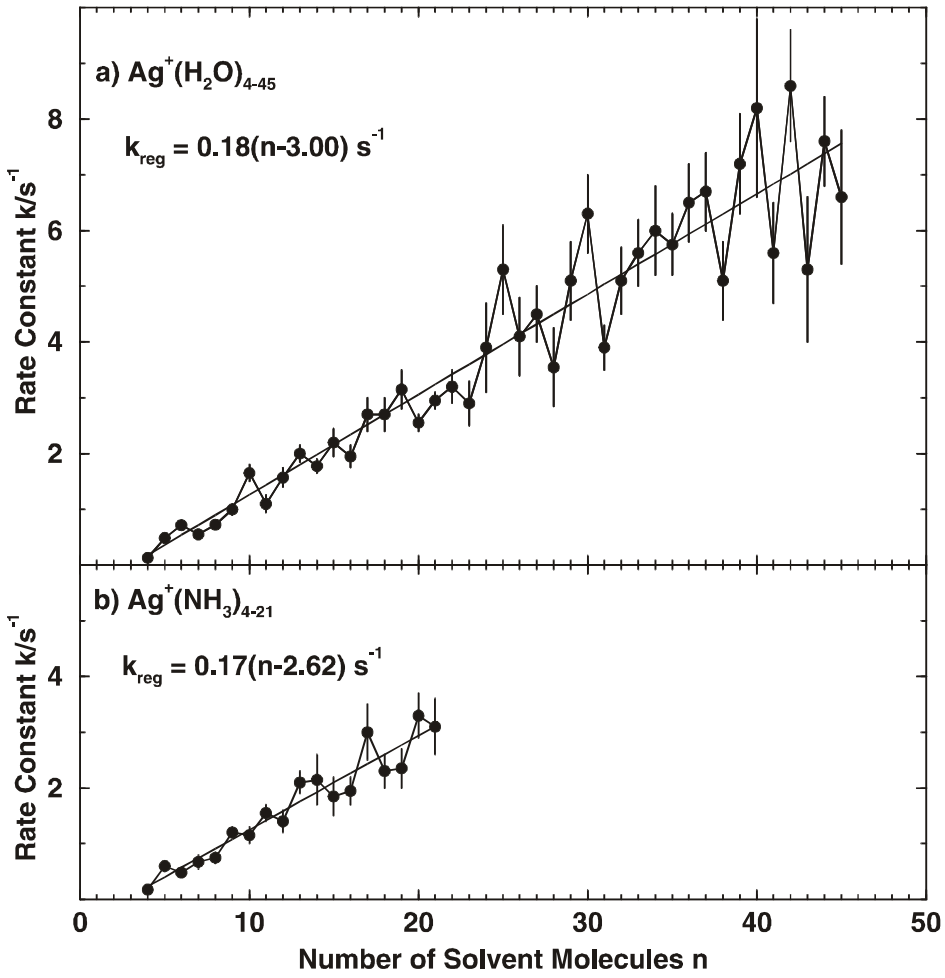

Figure 2: Unimolecular fragmentation rate constants for the black body radiation induced fragmentation of clusters as a function of the number of ligands n. The rate for each size selected cluster was obtained by fitting the initial signal decay, the solid line represents a linear fit to the expression $k_n = k_f (n-n_0)$ [s^{-1}]:
a) $Ag^+(H_2O)_n$, n=4-45, k_f =0.18 s^{-1}, n_0=3.00; b) $Ag^+(NH_3)_n$, n=4-21, k_f=0.17 s^{-1}, n_0=2.62

the ambient walls. For clusters around n=30-50 one can estimate temperatures in the range of 100-150 K,[9] so that the energy loss due to black body emission of the clusters themselves can to a good approximation be neglected. Each time a cluster loses a ligand, an energy comparable to its enthalpy of vaporization is removed, and the cluster effective temperature sinks drastically. Because there are effectively no collisions, before another ligand can evaporate, the cluster has to absorb from the IR black body background at least

enough energy to compensate for this loss, and for the temperature to approach again its original value. The energy is primarily absorbed by the hydrogen bonded ligand network, and therefore the overall rate of the energy absorption, as well as the rate of fragmentation, must be roughly proportional to the number of ligand molecules n. The physical meaning of the inverse of the constant, $1/k_f$, can thus approximately be seen as the time which would be needed by a single ligand molecule in the cluster to absorb from the black body background radiation an energy equivalent to the vaporization enthalpy of the ligand.

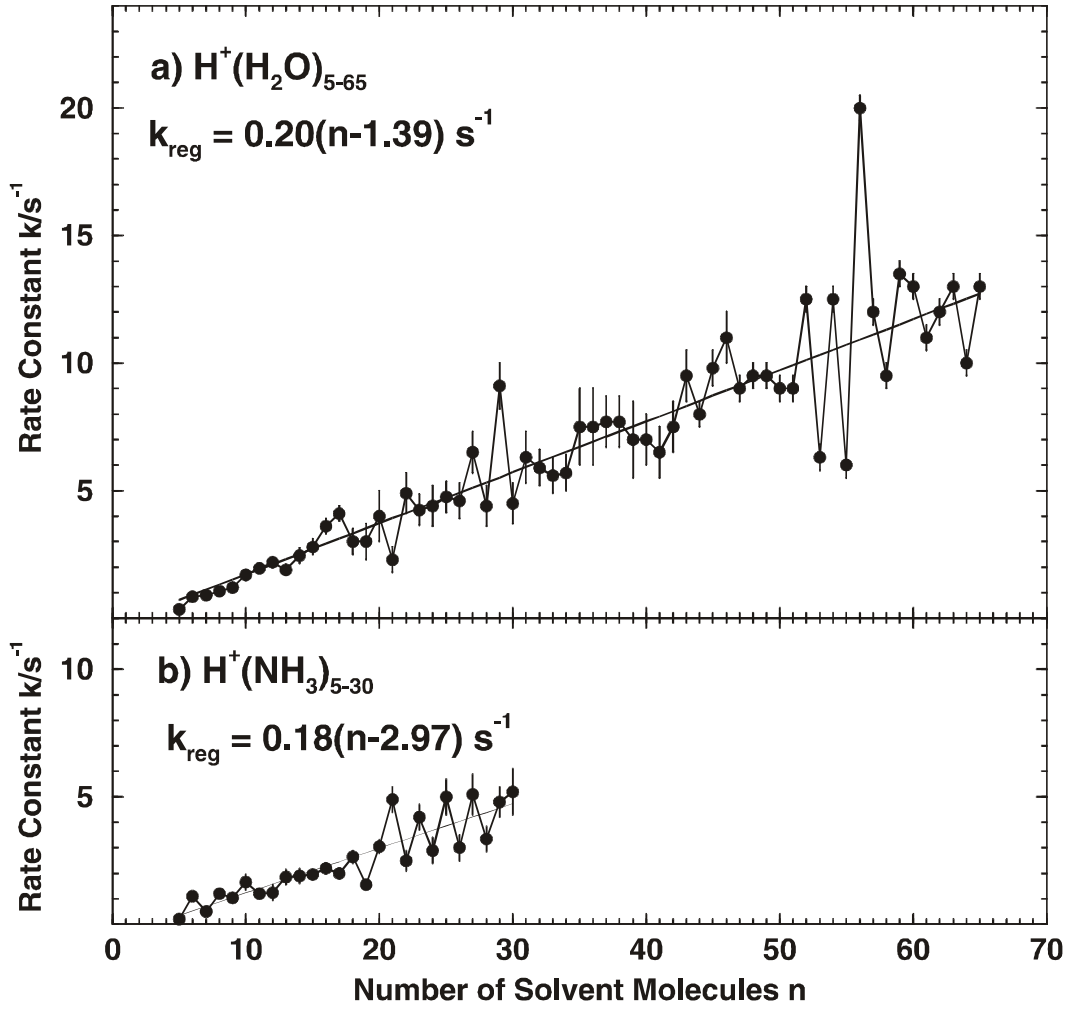

Figure 3: Unimolecular rate constants for the black body radiation induced fragmentation of a) size-selected $H^+(H_2O)_n$ clusters, n=5-65. Linear regression of these rate constants yields a straight line with k_n=0.20(n-1.39) s^{-1}. b) $H^+(NH_3)_n$, n=5-30. The data points can be fitted by the equation k_n=0.18(n-2.97) s^{-1}.

Obviously the energy needed to evaporate a ligand is not the same for all cluster sizes, but must itself be dependent on the value of n. In smaller clusters the ligands are closer to the central ion and feel its charge more strongly, and will therefore be more tightly bound than the surface ligands in larger clusters. Furthermore, often some specific "magic" cluster sizes exhibit higher stability than other nearby cluster sizes, perhaps due to an energetically particularly advantageous closed shell structure. It should also be realized that a ligand will not necessarily immediately evaporate as soon as the energetic threshold is reached. The rate of evaporation will depend on the energy excess above this threshold, and also this dependence itself will, based on statistical RRKM theories, be a function of the density of states, and thus of n, the size of the cluster. These secondary effects are, however, apparently not important enough to mask the basic, linear dependence of the fragmentation rates upon the cluster size n.

According to the above discussion, the constant k_f, that is the slope of the k_n rate against n plot is basically dependent on two factors, the ligand binding energy and the rate of energy absorption, where, in turn, the latter factor should depend on the overlap integral between the ligand absorption spectrum and the Planck black body function at the ambient temperature. Obviously, the k_f constant should show linear dependence on the latter factor, but be inversely proportional to the former one, the energy needed to evaporate one ligand. In other words, the faster the rate of energy absorption, and the lower the ligand binding energy, the faster the cluster will fragment, and vice versa.

The binding energies of hydrated clusters and of clusters solvated with ammonia should, in general, be expected to be different. On the one hand, the proton affinity of ammonia, 854.6 kJ/mol,[36] which will surely be important for the stability of the smallest protonated clusters, is considerably larger than that of water, 691 kJ/mol.[36] On the other hand, however, as already mentioned above, the neutral dimer of ammonia is considerably

weaker bound than that of water. The most relevant properties one should probably use to compare the fragmentation behavior of the larger cluster ions should be the vaporization enthalpies of the two solvents, whose measured values at 298 K are 43.98 kJ/mol for H_2O and 19.86 kJ/mol for NH_3.[37] The larger experimental value found for water again reflects its ability to form two donor and two acceptor hydrogen bonds, which is ideally suited for the formation of extended ligand networks. In spite of this factor of two difference in the vaporization enthalpies, one finds that the two slopes k_f for ammonia and water ligands are almost identical. One has to conclude, that this is most likely fortuitous, and that the factor of two decrease in the binding of ammonia ligands must be almost exactly compensated by their less efficient absorption of the black body radiation.

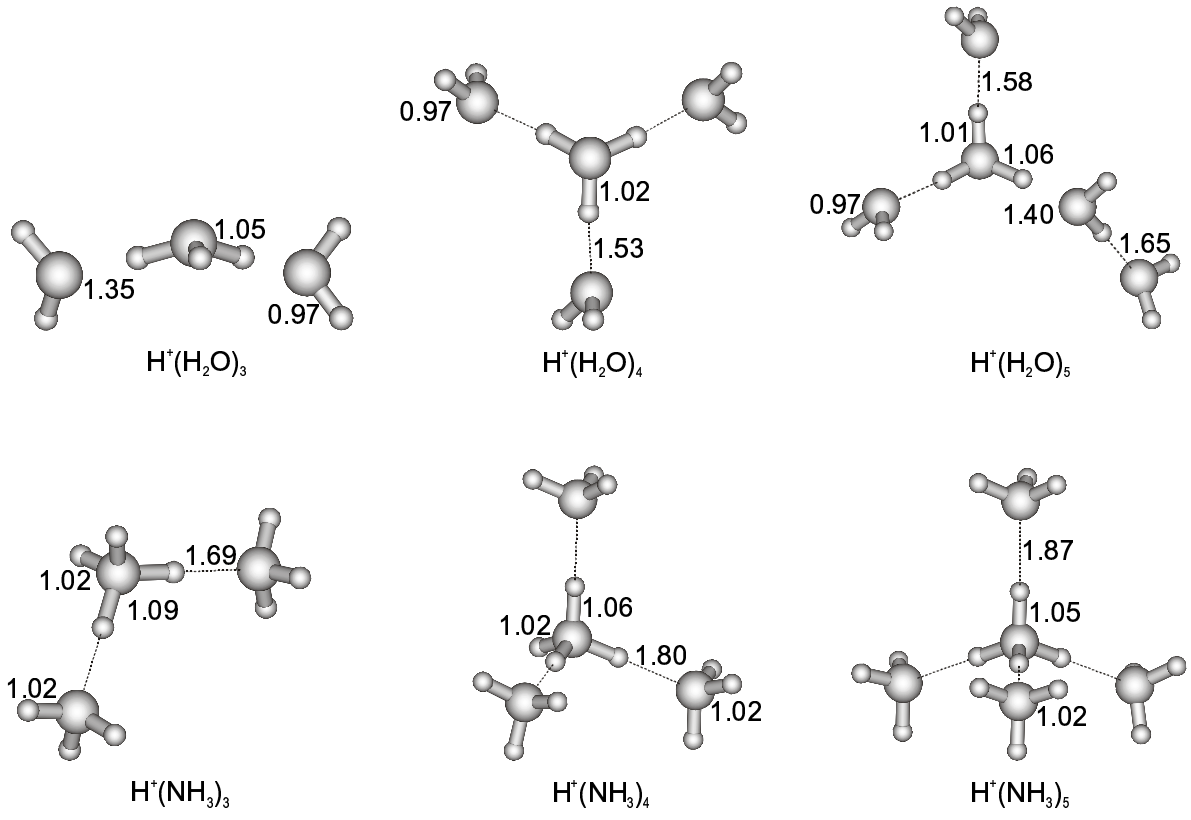

Figure 4: Optimized structures of $H^+(H_2O)_n$, n=2-5, and $H^+(NH_3)_n$, n=2-5. Characteristic distances are indicated in Å.

Since both the vibrational frequencies and IR-intensities have been computed for several of the small solvated ions whose optimized geometries are shown in Fig. 4, the overlap of their spectra with the Planck function, and the rates of energy absorption can also be calculated using Equation 1. Figures 5 and 6 show the computed infrared absorption spectra of $H^+(NH_3)_4$, $H^+(NH_3)_5$, $H^+(H_2O)_4$, and $H^+(H_2O)_5$ superimposed over the 300 K black body function. The dotted line representing the cumulative absorbed power shows very clearly, that while in each case the most intense infrared bands are the OH or NH stretching vibrations, these contribute little to the overall energy absorption from the black body background. This is dominated by the weaker, but lower frequency modes between ≈200-1200 cm^{-1}, which overlap more effectively the Planck function. The figures clearly show that the number of these low frequency modes increases with the cluster size, which leads to a higher rate of energy absorption and thus to the linear dependence of the fragmentation rate constant with n.

Table 2: Experimental and calculated binding energies for $H^+(H_2O)_n$, n=1-5, together with the calculated average internal energy at 300 K and the total absorbed power from 298 K black body radiation.

$H^+(H_2O)_n$	$\Delta H^0_{n-1,n}$ experimental [kJ/mol]	$\Delta H^0_{n-1,n}$ calculated [kJ/mol]	average internal energy [kJ/mol]	total absorbed power [kW/mol]
n=1	-691.0[a]	-680.4	0.2	9.6
n=2	-150.6[b]	-148.4	5.0	38.7
n=3	-93.3[b]	-88.3	12.4	20.3
n=4	-71.1[b]	-70.8	20.7	22.6
n=5	-64.0[b]	-49.6	28.9	26.8

[a] Reference 36; [b] Kebarle, P.; Searles, S.K.; Zolla, A.; Scarborough, J.; Arshadi, M. *J. Am. Chem. Soc.* **1967**, *89*, 6393.

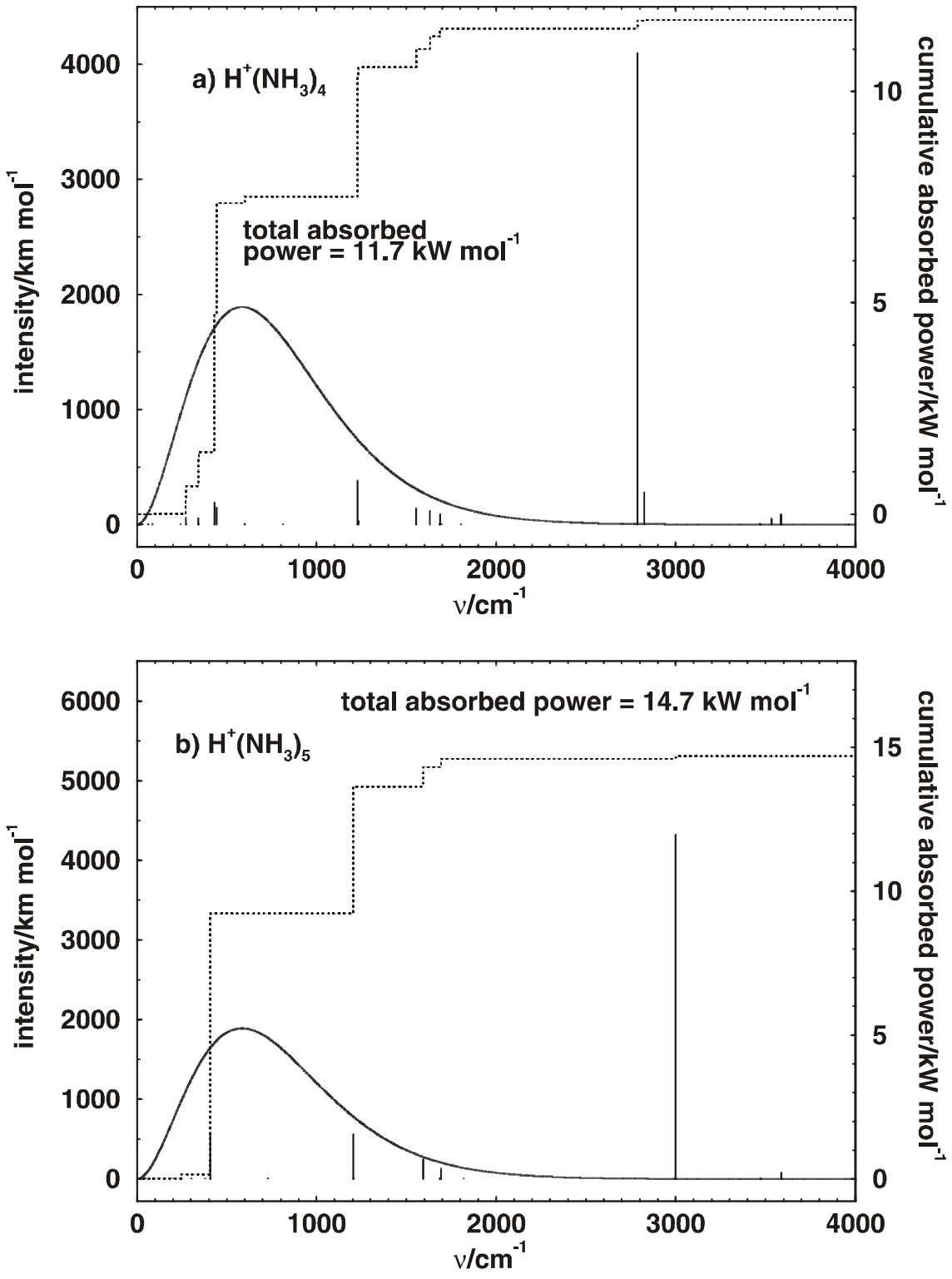

Figure 5: Calculated IR spectrum of a) $H^+(NH_3)_4$ and b) $H^+(NH_3)_5$ superimposed over the 300 K Planck distribution function. Intensities for vibrations within 3 cm^{-1} were summed into one peak. The dotted line represents the cumulative absorbed power in kW/mol.

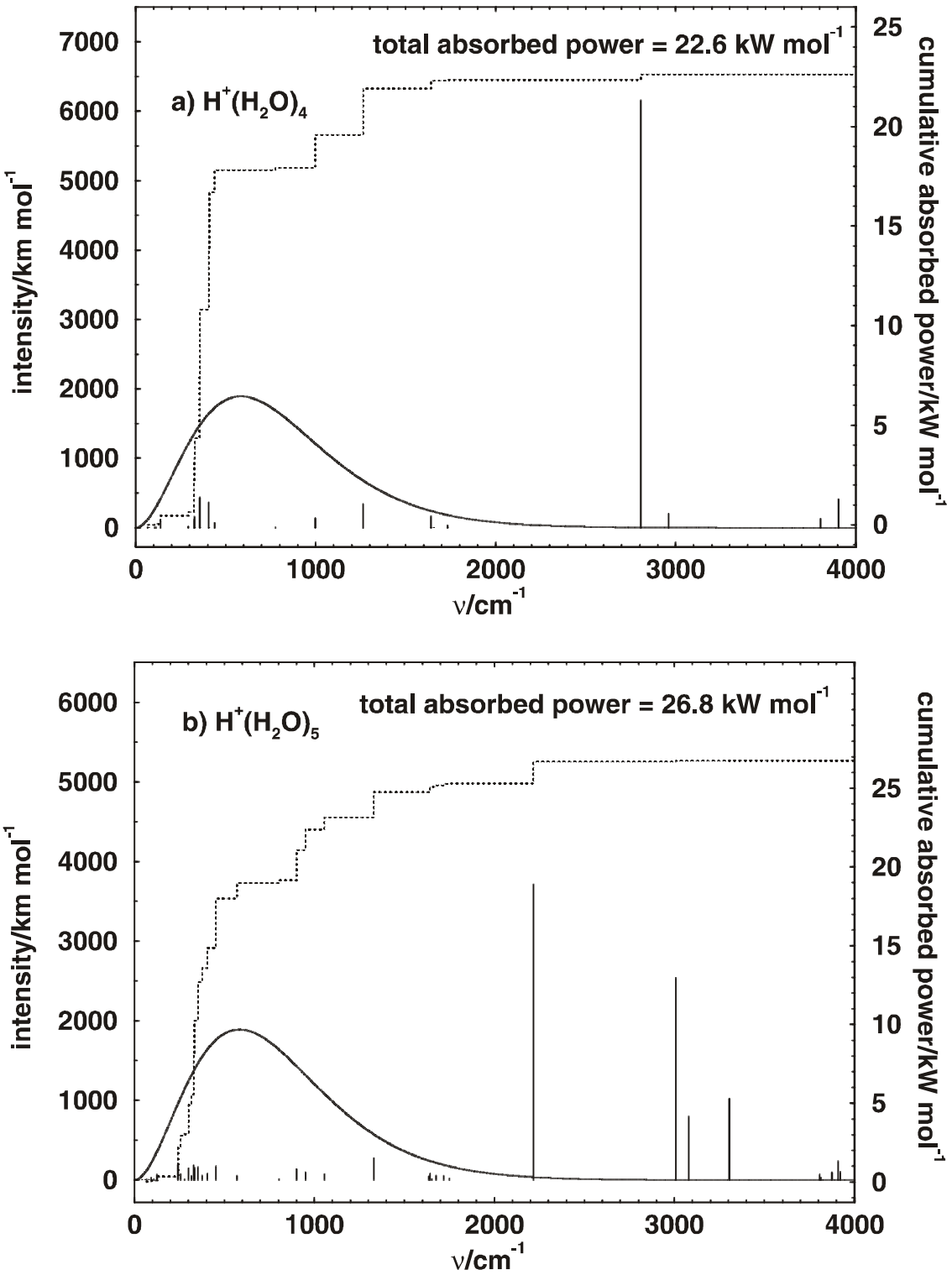

Figure 6: Calculated IR spectrum of a) $H^+(H_2O)_4$ and b) $H^+(H_2O)_5$ superimposed over the 300 K Planck distribution function. Intensities for vibrations within 3 cm^{-1} were summed into one peak. The dotted line represents the cumulative absorbed power in kW/mol.

Table 3: Experimental and calculated binding energies for $H^+(NH_3)_n$, n=1-5, together with the calculated average internal energy at 300 K and the total absorbed power from 298 K black body radiation.

$H^+(NH_3)_n$	$\Delta H^0_{n-1,n}$ experimental [kJ/mol]	$\Delta H^0_{n-1,n}$ calculated [kJ/mol]	average internal energy [kJ/mol]	total absorbed power [kW/mol]
n=1	-853.6[a]	-843.0	0.1	2.0
n=2	-106.3[b]	-113.2	5.7	34.5
n=3	-72.4[b]	-68.7	13.6	9.1
n=4	-59.4[b]	-55.3	23.5	11.7
n=5	-49.4[b]	-44.0	33.9	14.7

[a] Reference 36; [b] Arshadi, M.; Futrell, J.J. *J. Phys. Chem.* **1974**, *78*, 1482.

By comparing the results given in Tables 2 and 3, one can also note that the overall rate of energy absorption of 22.6 kW/mol computed for the water cluster $H^+(H_2O)_4$, is indeed about a factor of two larger than that of the corresponding n=4 ammonia cluster, 11.7 kW/mol, and a similar ratio and stronger binding of the water ligands is found also for n=5. This confirms that, as outlined above, the higher rates of energy absorption by clusters solvated by water almost perfectly compensate their higher binding energies. This then leads to the observed, very similar fragmentation behavior, and similar slopes of the diagrams like Fig. 2 and 3, where the rates k_n are plotted against the number of ligands n, regardless of whether the solvent is water or ammonia. The computation of the rate of energy absorption exemplified in Tables 2 and 3 also confirms the expected, previously discussed approximately linear increase in the energy absorption rates with the number of ligands. It may also be noted that the computed absolute rates of the energy absorption, when compared with the ligand binding enthalpies, are consistent with the measured fragmentation rates, and with the observation that small clusters, e.g. $H^+(H_2O)_5$ fragment on a time scale of many seconds.

4.4.4 Theoretical Investigation of Observed Final Products

In addition to the slope k_f, the fits of the fragmentation behavior are also characterized by a second constant, the intercept n_0. This constant, that is the observation that the fit does not go through the origin is physically simply a reflection of the fact, that the smallest clusters do not fragment at all under the conditions of the experiment. This is due to two important effects. In the first place, while, as already explained above, the larger clusters are quite cold, and their black body infrared emission can be neglected, this is no longer true for the smallest, more stable clusters. The ligands closer to the ionic core of the cluster are more strongly bound than those at the periphery or surface of the larger clusters. Their evaporation requires more energy (see Table 4 and 5), and the cluster temperature has to rise higher before a ligand can evaporate. Eventually, the smallest clusters will reach thermal equilibrium with the apparatus walls, and at this point the rate of energy absorption will be equivalent to the rate of their infrared emission, and the cluster heating will essentially stop.

Table 4: $\Delta H^0_{n-1,n}$ in kJ/mol for the gas phase hydration of H^+ and Ag^+:

$X^+(H_2O)_{n-1} + H_2O \rightarrow X^+(H_2O)_n$ (X=Ag, H)

	n=1	n=2	n=3	n=4	n=5
X=H[a]	-	-150.6	-93.3	-71.1	-64
X=Ag[b]	-139.3	-106.3	-62.8	-62.3	-57.3

[a] Kebarle, P.; Searles, S.K.; Zolla, A.; Scarborough, J.; Arshadi, M. *J. Am. Chem. Soc.* **1967**, *89*, 6393;

[b] Holland, P.M.; Castleman, A.W., Jr. *J. Chem. Phys.* **1982**, *76*, 4195.

Inspection of some of the final products, for instance of the hydrated silver cation clusters shows, however, that this cannnot be the only explanation, and that some other

effects must contribute to the small ion stability. As can be seen in Fig. 1 and Fig. 2a, while $Ag^+(H_2O)_4$ fragments with a non-negligible rate constant ($k=0.13\pm0.02\ s^{-1}$) the next smaller cluster, $Ag^+(H_2O)_3$ does not fragment at all on the time scale of our experiment. Their binding energies which are given in Table 4 differ by only 0.5 kJ/mol, and this small difference can not provide an adequate reason for the observed large difference in the fragmentation rates.

Table 5: $\Delta H^0_{n-1,n}$ in kJ/mol for the gas phase association of NH_3 to H^+ and Ag^+:

$X^+(NH_3)_{n-1} + NH_3 \rightarrow X^+(NH_3)_n$ (X=Ag, H)

	n=1	n=2	n=3	N=4	n=5
X=H[a]	-	-106.3	-72.4	-59.4	-49.4
X=Ag[b]	-139.3	-154.4	-61.1	-54.4	-53.6

[a] Arshadi, M.; Futrell, J.J. *J. Phys. Chem.* **1974**, *78*, 1482; [b] Holland, P.M.; Castleman, A.W., Jr. *J. Chem. Phys.* **1982**, *76*, 4195.

The explanation for this effect can, however be found by examining Tables 2 and 3. These show, besides the experimental and computed binding energies and the rates of the infrared energy absorption, also the average internal energies of the clusters when they reach equilibrium with the apparatus wall, that is at a temperature of approximately 300 K. One can easily see in these tables, that even at room temperature, the energy content of the smallest clusters is very small. This is due not only to the smaller number of degrees of freedom, but more importantly to their relatively rigid structures, and to the absence of low frequency vibrational modes. As the clusters grow, and additional, weaker bound ligands are added to the second or third solvation shell, the number of low frequency modes increases, and the amount of internal energy at 300 K grows drastically. Thus the internal energy of a proton solvated by two or three water molecules is ≈5.0 kJ/mol and

12.4 kJ/mol, respectively, with the corresponding values for two or three ammonia ligands being only slightly larger, 5.7 kJ/mol and 13.6 kJ/mol (see Tables 2 and 3). These values are small compared with the respective binding energies, so that even at 300 K the energetic threshold for ligand loss is very unlikely to be reached. On the other hand, for n=5 the computed internal energies are 28.9 kJ/mol for water and 33.9 kJ/mol for ammonia clusters, which is already comparable with the binding energies. Thus in the above mentioned example of solvated $Ag^+(H_2O)_n$ clusters, the reason for the fragmentation of the n=4 cluster, and lack of it for n=3 is the much larger energy content of the larger ion, rather than the small difference in the binding energies. While similar calculations for ammonia solvated Ag^+ clusters have not been carried out, for the protons solvated by ammonia the computed internal energies at 300 K are 13.6 kJ/mol for n=3, and 23.5 kJ/mol for n=4, a difference of nearly 50%, which can easily explain the different fragmentation behavior.

Although it is still difficult to carry out ab initio computations on larger solvated clusters, it is not difficult to estimate their spectra and the distribution of their vibrational modes. These change systematically with cluster size, and using such estimated spectra one can easily compute the approximate energy content of larger clusters. Such computations of the internal energy as a function of the temperature have been carried out up to n≈100. As an example, for a hydrated cluster with n=55, one predicts at room temperature a value of over 400 kJ/mol. At 150 K, a temperature value which was estimated by extrapolation of bulk water properties for clusters in this size range observed in our experiment,[9] the average computed internal energy is 140 kJ/mol, a value which still exceeds by more than a factor of three the vaporization enthalpy of water. This just confirms what was stated earlier: the larger clusters can be metastable, and survive quite long - on the order of the millisecond to second time scale of our experiment - even though

they have energies quite high above the threshold for fragmentation. In fact the computations indicate that water clusters in this range (near n=55) would have to be cooled to <70K and ammonia species to <40 K to lower their internal energies below the solvent molar vaporization enthalpy.

It would of course be highly desirable to construct a model based on RRK or RRKM theory that produces both the overall linear dependence of k_n on n as well as the insensitivity of the observed fragmentation rate on the identity of the core ion and the solvating molecule. Upon closer inspection of this idea, serious problems become apparent: An RRK based model would produce unrealistic results due to the assumption that all oscillators have the same frequency. In the larger clusters, the internal energy is mainly stored in the low-frequency modes well below 100 cm^{-1}, while the dissociative mode lies at approximately 250 cm^{-1}. Assuming the 250 cm^{-1} for all oscillators would produce at e.g. 100 K an internal energy that is too low by an order of magnitude. Taking a low-frequency mode, however, would make the fragmentation too facile, since an unrealistically low amount of energy would be required. A model that would be truly superior to the semi-quantitative arguments presented here requires extensive numeric modeling based on RRKM theory and the calculated energy absorption rates. This goes well beyond the scope of the present work.

4.4.5 Deviation of Fragmentation Rate from Linearity - Magic Clusters

A closer examination of Figs. 2 and 3 indicates, that while in general the linear relationship between the fragmentation rates and n is reasonably well obeyed, and in some regions the rate constants indeed follow the linear regression fit quite closely, in others considerable fluctuations can be seen, with the deviations of some specific clusters from

the predicted behavior being well outside the error of the experiment. A dramatic example of this behavior are the previously discussed hydrated protons, and the anomalously high stability of the n=55 cluster, with conversely a drastically increased fragmentation rate of the $H^+(H_2O)_{56}$ cluster ion (see Fig. 3a). Similarly, Fig. 2a shows for hydrated Ag^+ that e.g. the n=4-18 and n=33-38 follow well the fit, but in the region between n=41-43, significant deviations can be seen. Also for hydrated Mg^+ and Al^+ cations such regions where significant deviations occur have been observed. For example for $Al^+(H_2O)_n$ such regions were found between n=23-27 and n=36-39 and for $Mg^+(H_2O)_n$ between n=38-41.[11,12] There has been a considerable amount of discussion[12] of whether solvated clusters of this type should be viewed as more or less rigid, solid structures, or as liquid-like, fluxional species. It has been argued that the large local deviations from the overall linear behavior (like e.g. the n=55) suggest the former closer to truth, since in fluxional, liquid structures, many structural isomers would be present, averaging out any effects of local structure. Perhaps one can conversely argue, that in those regions where the deviations from the predicted linear behavior are small, structures are ill-defined, and many isomers are present.

4.5 Conclusion

The results obtained in this chapter show that ionic clusters solvated by ammonia are in the collision-free environment of an ICR cell efficiently fragmented by ambient black body infrared radiation similar to hydrated clusters. Specifically, the fragmentation of size-selected ionized ammonia clusters $Ag^+(NH_3)_n$, n=4-21, and $H^+(NH_3)_n$, n=5-30, has been examined and compared to the corresponding hydrate ions, $Ag^+(H_2O)_n$, n=4-45, as well as to the previously investigated protonated water clusters, $H^+(H_2O)_n$, n=5-65. In all

these cases, as well as in the case of several other hydrated cations as well as anions previously studied, the fragmentation rate constant is linearly dependent on the cluster size n. Slope values obtained by fitting the observed fragmentation rates to the expression $k_n=k_f(n-n_0)$ are found to be essentially identical with $k_f \approx 0.18\ s^{-1}$ not only for all of the hydrated ions studied, but also for ions solvated by ammonia. While the equal values of the k_f constant for all hydrates studied reflect the relative insensitivity of the large ligated clusters to the specific nature and sign of charge of the central ion, the similarity with ions solvated by ammonia is fortuitous, due to accidental cancellation of the effect of the weakened binding in the latter clusters by the less efficient absorption of the black body IR radiation.

4.6 References

(1) Ng, C.-Y.; Baer, T.; Powis, I. (eds.) *Cluster Ions*; Wiley: New York, 1993.

(2) Haberland, H. (ed.) *Clusters of Atoms and Molecules*, Vol. 2; Springer: Berlin, 1994.

(3) Thölmann, D.; Tonner, D.S.; McMahon, T.B. *J. Phys. Chem.* **1994**, *98*, 2002.

(4) Thölmann, D.; Tonner, D.S.; McMahon, T.B. *Chem. Phys. Lett.* **1995**, *233*, 324.

(5) Dunbar, R.C.; McMahon, T.B. *Science* **1998**, *279*, 194.

(6) Rodriguez-Cruz, S.E.; Jockusch, R.A.; Williams, E.R. *J. Am. Chem. Soc.* **1998**, *120*, 5842.

(7) Rodriguez-Cruz, S.E.; Jockusch, R.A.; Williams, E.R. *J. Am. Chem. Soc.* **1999**, *121*, 1986.

(8) Rodriguez-Cruz, S.E.; Jockusch, R.A.; Williams, E.R. *J. Am. Chem. Soc.* **1999**, *121*, 8898.

(9) Schindler, T.; Berg, C.; Niedner-Schatteburg, G.; Bondybey, V.E. *Chem. Phys. Lett.* **1996**, *250*, 301.

(10) Bondybey, V.E.; Schindler, T.; Berg, C.; Beyer, M.; Achatz, U.; Joos, S.; Niedner-Schatteburg G. in: S.S. Xantheas (ed.) *Recent Theoretical and Experimental Advances in Hydrogen-Bonded Clusters*, NATO ASI Series C, Vol. 561, Kluwer: Dordrecht (2000).

(11) Berg, C.; Beyer, M.; Achatz, U.; Joos, S.; Niedner-Schatteburg, G.; Bondybey, V.E. *Chem. Phys.* **1998**, *239*, 379.

(12) Beyer, M.; Achatz, U.; Berg, C.; Joos, S.; Niedner-Schatteburg, G.; Bondybey, V.E. *J. Phys. Chem. A* **1999**, *103*, 671.

(13) Achatz, U.; Joos, S.; Berg, C.; Beyer, M.; Niedner-Schatteburg, G.; Bondybey, V.E. *Chem. Phys. Letters* **1998**, *291*, 459.

(14) Achatz, U.; Joos, S.; Berg, C.; Schindler, T.; Beyer, M.; Albert, G.; Niedner-Schatteburg, G.; Bondybey, V.E. *J. Am. Chem. Soc.* **1998**, *120*, 1876.

(15) Fox, B.S.; Beyer, M.K.; Achatz, U.; Joos, S.; Niedner-Schatteburg, G.; Bondybey, V.E. *J. Phys. Chem. A* **2000**, *104*, 1147.

(16) Schindler, T.; Berg, C.; Niedner-Schatteburg, G.; Bondybey, V.E. *Chem. Phys. Lett.* **1994**, *229*, 57.

(17) Berg, C.; Achatz, U.; Beyer, M.; Joos, S.; Albert, G.; Schindler, T.; Niedner-Schatteburg, G.; Bondybey, V.E. *Int. J. Mass Spectrom. Ion Proc.* **1997**, *167/168*, 723.

(18) Bondybey, V.E.; Beyer, M.; Achatz, U.; Joos, S.; Niedner-Schatteburg, G.; *Israel J. Chem.* **1999**, *39*, 213.

(19) Fraser, G.T.; Nelson, D.D. Jr.; Gerfen, G.J.; Klemperer, W. *J. Chem. Phys.* **1985**, *82*, 2535.

(20) Curtiss, L.A.; Pople, J.A. *J. Mol. Spectrosc.* **1975**, *55*, 1.

(21) Curtiss, L.A.; D.J. Frurip, D.J.; Blander, M. *Chem. Phys. Lett.* **1978**, *54*, 575.

(22) Curtiss, L.A.; D.J. Frurip, D.J.; Blander, M. *J. Chem. Phys.* **1979**, *71*, 2703.

(23) (a) Ichihashi, M.; Yamabe, J.; Murai, K.; Nonose, S.; Hirao, K.; Kondow, T. *J. Phys. Chem.* **1996**, *100*, 10050. (b) Park, J.K. *J. Phys. Chem. A* **2000**, *104*, 5093.

(24) B,rces, A.; Nukada, T.; Margl, P.; Ziegler, T. *J. Phys. Chem. A* **1999**, *103*, 9693.

(25) Berg, C.; Schindler, T.; Niedner-Schatteburg, G.; Bondybey, V.E. *J. Chem. Phys.* **1995**, *102*, 4870.

(26) Beyer, M.; Berg, C.; Görlitzer, H.; Schindler, T.; Achatz, U.; Albert, G.; Niedner-Schatteburg, G.; Bondybey, V.E. *J. Am. Chem. Soc.* **1996**, *118*, 7386.

(27) *Gaussian 98, Revision A.7*; Frisch, M.J.; Trucks, G.W.; Schlegel, H.B.; Scuseria, G.E.; Robb, M.A.; Cheeseman, J.R.; Zakrzewski, V.G.; Montgomery, J.A., Jr.; Stratmann, R.E.; Burant, J.C.; Dapprich, S.; Millam, J.M.; Daniels, A.D.; Kudin, K.N.; Strain, M.C.; Farkas, O.; Tomasi, J.; Barone, V.; Cossi, M.; Cammi, R.; Mennucci, B.; Pomelli, C.; Adamo, C.; Clifford, S.; Ochterski, J.; Petersson, G.A.; Ayala, P.Y.; Cui, Q.; Morokuma,

K.; Malick, D.K.; Rabuck, A.D.; Raghavachari, K.; Foresman, J.B.; Cioslowski, J.; Ortiz, J.V.; Baboul, A.G.; Stefanov, B.B.; Liu, G.; Liashenko, A.; Piskorz, P.; Komaromi, I.; Gomperts, R.; Martin, R.L.; Fox, D.J.; Keith, T.; Al-Laham, M.A.; Peng, C.Y.; Nanayakkara, A.; Gonzalez, C.; Challacombe, M.; Gill, P.M.W.; Johnson, B.; Chen, W.; Wong, M.W.; Andres, J.L.; Gonzalez, C.; Head-Gordon, M.; Replogle, E.S.; Pople, J.A. Gaussian, Inc.: Pittsburgh, PA, 1998.

(28) Becke, A.D. *Phys. Rev. A* **1988**, *38*, 3098.

(29) Becke, A.D. *J. Chem. Phys.* **1993**, *98*, 1372.

(30) Becke, A.D. *J. Chem. Phys.* **1993**, *98*, 5648.

(31) Lee, C.; Yang, W.; Parr, R.G. *Phys. Rev. B* **1988**, *37*, 785.

(32) Lee, E.P.F.; Dyke, J.M. *Mol. Phys.* **1991**, *73*, 375.

(33) (a) Corongiu, G.; Kelterbaum, R.; Kochanski, E. *J. Phys. Chem.* **1995**, *99*, 8038. (b) Kelterbaum, R.; Kochanski, E.; *J. Chem. Phys.* **1995**, *99*, 12493.

(34) Wei, D.Q.; Salahub, D.R. *J. Chem. Phys.* **1997**, *106,* 6086.

(35) Beyer, M.; Savchenkoe, E.V.; Niedner-Schatteburg, G.; Bondybey, V.E. *Low Temp. Phys.* **1999**, *25*, 814.

(36) Mallard, W. G.; Linstrom, P. J.; Eds., NIST Chemistry WebBook, NIST Standard Reference Database Number 69, February 2000. National Institute of Standards and Technology, Gaithersburg MD, 20899 (http://webbook.nist.gov).

(37) Lide, D.R. (Ed.) in Chemical Rubber Company Handbook of Chemistry and Physics, CRC Press, Boca Raton, Florida, USA, 77th edition, 1996.

(38) Barnett, R. N.; Landman, U. *J. Phys. Chem. A* **1997**, *101*, 164.

(39) Barnett, R. N.; Landman, U. *J. Phys. Chem.* **1995**, *99*, 17305.

(40) Ng, C. Y.; Trevor, D. J.; Tiedemann, P. W.; Ceyer, S. T.; Kronebusch, P. L.; Mahan, B. H.; Lee, Y. T. *J. Chem. Phys.* **1977**, *67*, 4235.

(41) Tomoda, S.; Kimura, K. *Chem. Phys.* **1983**, *82*, 215.

5 Coordination Chemistry of Silver Cations

5.1 Introduction

Ammonia is the most common nitrogen-containing donor ligand in aqueous chemistry, especially important in the aqueous chemistry of silver. It is well known that if NH_3 is added to an aqueous solution of a silver salt, the extremely stable linearly coordinated $[Ag(NH_3)_2]^+$ complex ion is formed. Because of its extremely high stability, even an AgCl precipitate can be dissolved simply by the addition of NH_3.

The very stable linearly coordinated silver (I) complexes, AgL_2^+, are well known in both solid and liquid phase, a fact which is often explained by the electronic structure of Ag^+ which allows the formation of two linear orbitals by an sd-hybridization.[1,2] However, it has been demonstrated that in highly concentrated aqueous ammonia solutions a triammine complex $[Ag(NH_3)_3]^+$ forms.[3] Moreover, if a silver salt is dissolved in pure water or liquid ammonia solvents, tetrahedral AgL_4^+ ions are formed.[4-9] These observations seem to be contradictory. Why is the coordination different in pure and mixed solvent systems? Why does sd-hybridization not lead to linear complexes in pure solvents? A promising approach which might provide answers to some of these questions would seem to be the investigation of the silver cation coordination chemistry on a molecular level, in gas phase clusters.

The investigation of ligand exchange reactions is important for the understanding of many chemical phenomena, e.g. the substitution of ligands close to a central ion proceeding in cluster ions in the atmosphere[10,11] or the dynamics of ligand exchange

reactions in solutions of electrolytes.[12] Furthermore, studies of ligand exchange reactions can yield information about their relative binding energies[13-19] or provide new insights into catalytic processes proceeding on metal surfaces.[20,21]

Using the FT-ICR technique with an efficient external ion source one can study solution chemistry in finite clusters and gain a microscopic, molecular scale understanding. In several studies, it was shown that water clusters are very simple model systems for aqueous solutions. It was for instance possible to show that HCl will dissolve ionically in finite clusters just as it does in bulk water,[22,23] redox or neutralization reactions leading to salts can take place,[24-27] organic base or acid catalyzed reactions proceed as they do in bulk[28] and even an analogue to precipitation reactions can be observed.[29] Recently, we have shown[30] that the versatile laser vaporization source developed in our laboratory can, besides hydrated clusters, equally well produce ions solvated by other ligands, including ammonia. In order to gain insight into the coordination chemistry of silver cations in mixed solvent systems, the reactions and ligand exchange of hydrated silver cations $Ag^+(H_2O)_n$ with NH_3 are examined here, as well as the complementary process, the reaction of large ammoniated silver cations $Ag^+(NH_3)_n$ with H_2O. To get a more detailed insight into the structure and energetics of solvated metal cations, the experimental studies were completed by DFT calculations on a number of smaller clusters.

5.2 Computational Details

The computations were carried out on a Pentium III based Linux system using the Gaussian98[31] program package, employing the three-parameter hybrid Hartree-Fock/Density functional (B3LYP) method described by Becke[32-34] with the Lee-Yang-Parr correlation functional[35] as incorporated in Gaussian98. For the geometry optimizations and

frequency calculations, the 6-31G(d,p) basis set was used for H, N, and O, and also thermal corrections were taken from this level of theory. Single-point energy calculations were performed employing the larger Gaussian98 6-311++G(3df,3pd) basis set, treating explicitly all electrons, with two diffuse and four polarization functions on all atoms. For Ag, the pseudo-relativistic effective core basis set of the Stuttgart/Dresden group[36] as implemented in Gaussian98 was used in every case.

5.3 Experimental Details

The experiments discussed here were performed on a modified Spectrospin CMS47X mass spectrometer described in detail elsewhere.[37] The cluster ions were generated in a pulsed supersonic expansion source using 10 bar of helium carrier gas seeded with about 30 mbar of either water vapor or ammonia. Metal cations were produced by laser vaporization of a solid silver disk (Chempur, 99.995%+), using a Nd:YAG laser Continuum Surelite II operating at 10 Hz and a pulse energy of typically 5 mJ. The plasma produced was entrained in a carrier gas pulse and cooled by flowing through a confining channel with the clustering and solvation of the ions taking place in the subsequent supersonic expansion into high vacuum. The cluster ions produced in the source were transferred through several stages of differential pumping into the high-field region of the superconducting magnet and stored inside the ICR cell. The reactant gases, NH_3 and H_2O, were introduced into the ultrahigh vacuum region via a needle valve. The pressure in the cell region after introducing the reactant gas was around 1×10^{-7} mbar corresponding to some ten collisional encounters every second. After accumulating the ions in the ICR cell, the mass spectra of the trapped ions and their products were taken after varying reaction delays.

5.4 Computational Results

5.4.1 Pure Silver-Water Clusters $Ag^+(H_2O)_n$, n=1-4

Various optimized geometries of $Ag^+(H_2O)_n$, n=1-4, are displayed in Fig. 1, together with the key structural parameters. The geometry and bond lengths of $Ag^+(H_2O)$ (**1**) and $Ag^+(H_2O)_2$ (**2**) agree very well with the previous quantum chemical studies by Feller et al.[38] and Widmer-Cooper et al.[39] For the following discussion, the notation suggested by Feller et al.[38] will be used, a tag of the form (m+n) where m equals the number of ligands directly coordinated to the central ion and n equals the number of ligands in the second solvation shell.

For $Ag^+(H_2O)_3$ one (3+0) configuration and two different (2+1) structures were investigated. Starting from the highly symmetric (3+0) structure with three equal Ag-O bond lengths and O-Ag-O angles of 120° the geometry converges fast to the asymmetric, nearly planar structure **3a** shown in Fig. 1. It is interesting to note that while two of the Ag-O bond lengths are nearly identical, the third one is much longer. This, together with the large 144.3° angle between the first two ligands indicates that these try to achieve a linear arrangement. In addition, one can note an interaction between two of the water ligands coordinated at an 89.2° angle. For (2+1) coordination, an open structure (**3b**) and a ring structure (**3c**) were investigated. The open structure contains a linearly coordinated Ag^+ cation. Binding of the second shell water ligand results in a decreased Ag-O bond length due to the additional polarization caused by the hydrogen bond. The ring structure exhibits C_s symmetry, with the comparably long length of the hydrogen bonds indicating that these are rather weak. As can be seen in Table 1, the open, linearly coordinated (2+1)

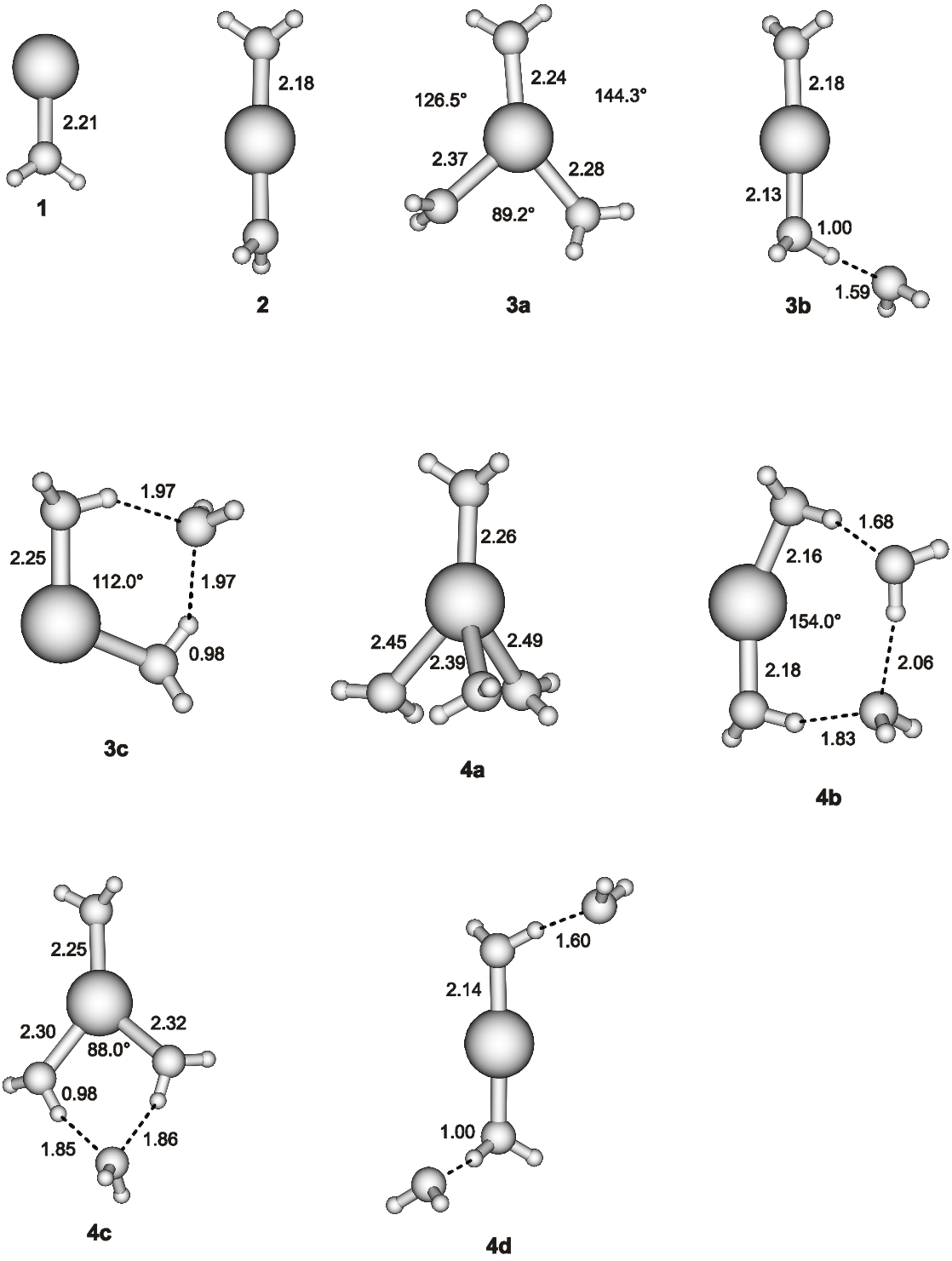

Figure 1: Fully optimized structures of $Ag^{+}(H_2O)_n$, n=1-4, at the B3LYP level of theory. Bond lengths are in angstroms. All O-H bonds, except where otherwise noted, are 0.97 Å.

Table 1: Relative Energies of the isomers of $Ag^+(H_2O)_n$, n=3, 4, calculated at the B3LYP/6-311++(3df,3pd) level of theory referred to the lowest energy structure. Structure numbering refers to Fig. 1.

Structure	3a	3b	3c	4a	4b	4c	4d
ΔH_{298K} [kJ/mol]	7.9	0	32.5	24.9	24.2	10.4	0

structure **3b** is lowest in energy with **3a** being about 7.9 kJ higher. The ring structure **3c** is significantly higher, with a difference of 32.5 kJ/mol, although the additional H-bond might be expected to decrease the energy. The energy difference and the bond lengths of **3b** and **3c** clearly show that the water ligand in the second solvation shell is more strongly bound if the silver cation is linearly coordinated. The energy difference between **3a** and **3b** lies within the accuracy of the method, suggesting that direct coordination of the third water ligand is energetically almost equivalent to placing it in the second solvation shell. However, as structure **3c** shows, this is only valid if the first ligands are linearly coordinated, in which case the silver cation seems to polarize the linearly coordinated water ligands very effectively. Somewhat different results were obtained by Feller et al.[38] They found at the RHF/6-31+G*/ECP+f level of theory that the global minimum is a D_3(3+0) configuration, whereas a C_1(2+1) and a C_s(2+1) structure are both 7.6 kJ/mol higher in energy. At the MP2/ 6-31+G*/ECP+f level of theory the lowest energy structure is a C_2(3+0) configuration and the energy difference to the corresponding (2+1) structure is less than 1 kJ/mol. The lowest energy structure is a transition state with a low frequency mode (-30 cm^{-1}), which Feller et al. attribute to numerical inaccuracies in the ECP gradients. Unfortunately, they did not study a ring configuration. For $Na^+(H_2O)_3$ and $K^+(H_2O)_3$, however, quite different results have been obtained for example by Feller et al.[40] at the MP2 level of theory. In these cases, structures corresponding to **3a** and **3c** are

energetically almost equal (ΔE≈7-8 kJ/mol) while the configuration corresponding to **3b** is higher in energy (ΔE≈12-16 kJ/mol).

The optimized structures obtained for $Ag^+(H_2O)_4$, are displayed in Fig. 1 as **4a-4d**. The fourfold tetrahedrally coordinated configuration converges to the distorted structure **4a** with remarkably long Ag-O bonds. **4c** represents a (3+1) ring structure while **4d** and **4b** are open chain and ring (2+2) structures, respectively. Again, the open chain structure with the silver ion linearly coordinated is the one with lowest energy (see Table 1). Still of comparable energy with a difference of +10.4 kJ/mol is **4c**. The other configurations are more than 20 kJ/mol higher in energy. Thus, the lowest-energy configurations are those obtained by adding an additional water ligand to **3a** and **3b**.

Table 2: Experimental and calculated binding energies of $Ag^+(H_2O)_n$, n=1-4

	$\Delta H_{1,0}$ [kJ/mol]	$\Delta H_{2,1}$ [kJ/mol]	$\Delta H_{3,2}$ [kJ/mol]	$\Delta H_{4,3}$ [kJ/mol]
exp.[a]	-139.3	-106.3	-62.8	-62.3
calc.	-118.3	-116.1	-58.9	-55.6

[a] Reference 45

The incremental binding energies obtained by using the H_{298K} values are summarized and compared with the experimental values in Table 2. This table suggests that the calculated binding energy of the first ligand, $\Delta H_{0,1}$, is underestimated by 21.0 kJ/mol while $\Delta H_{2,1}$ is overestimated by 9.8 kJ/mol. These deviations are probably not caused by too small basis sets, since this usually results in overestimating the binding energies. Quantitatively very similar results were obtained by Widmer-Cooper et al.[39] at both the CCSD(T)/aVDZ(f) and the B3LYP/aVTZ(f) level of theory. The results of Feller et al.[38] show the same tendency. However, if the combined experimental errors and the accuracy of the calculations are taken into account, the values agree reasonably well. The

calculated $\Delta H_{3,2}$ and $\Delta H_{4,3}$ values, on the other hand, agree perfectly well with those determined experimentally. Interestingly, the binding energy of a water ligand in the second solvation shell to a water ligand which is directly coordinated, i.e. for example $\Delta H_{3,2}$=-58.9 kJ/mol, is much higher than the binding energy of the water dimer (22.6 kJ/mol[41-43]) which reflects the strong influence of the polarizing Ag^+ central ion on the hydrogen bond .

5.4.2 Pure Silver-Ammonia-Clusters $Ag^+(NH_3)_n$, n=1-4

Fig. 2 displays various optimized structures of $Ag^+(NH_3)_n$, n=1-4, together with some key geometry parameters. The structures found for $Ag^+(NH_3)$ (**5**) and $Ag^+(NH_3)_2$ (**6**) agree very well with those computed by Widmer-Cooper et al.[39] at the CCSD(T)/aVDZ(f) level of theory. The bond lengths obtained in the present study are 0.1 Å shorter than those obtained by Shoeib et al.[44] at the B3LYP/DZVP level of theory. These differences may be due to the fact that in this study the small DZVP basis set was also used for Ag instead of the SECP basis set[36] used in the other investigations. The (3+0) and (2+1) configurations investigated for $Ag^+(NH_3)_3$ converged to the structures **7a** and **7b**, respectively. **7b** shows like **3b** a shortened Ag-N distance for the NH_3 which has the third ligand attached, again undoubtedly due to the enhanced polarization of the ammonia molecule. Structure **7b** is computed to be lower in energy, but the difference, 2.4 kJ/mol, is probably within the accuracy of the computations. In fact, with the 6-31G(d,p) basis set which was used for the geometry optimization, **7a** becomes the global minimum with a difference of 1.5 kJ/mol. Based on our computations, the two structures must be considered as energetically equal, and within the accuracy of our computation there is little difference between directly

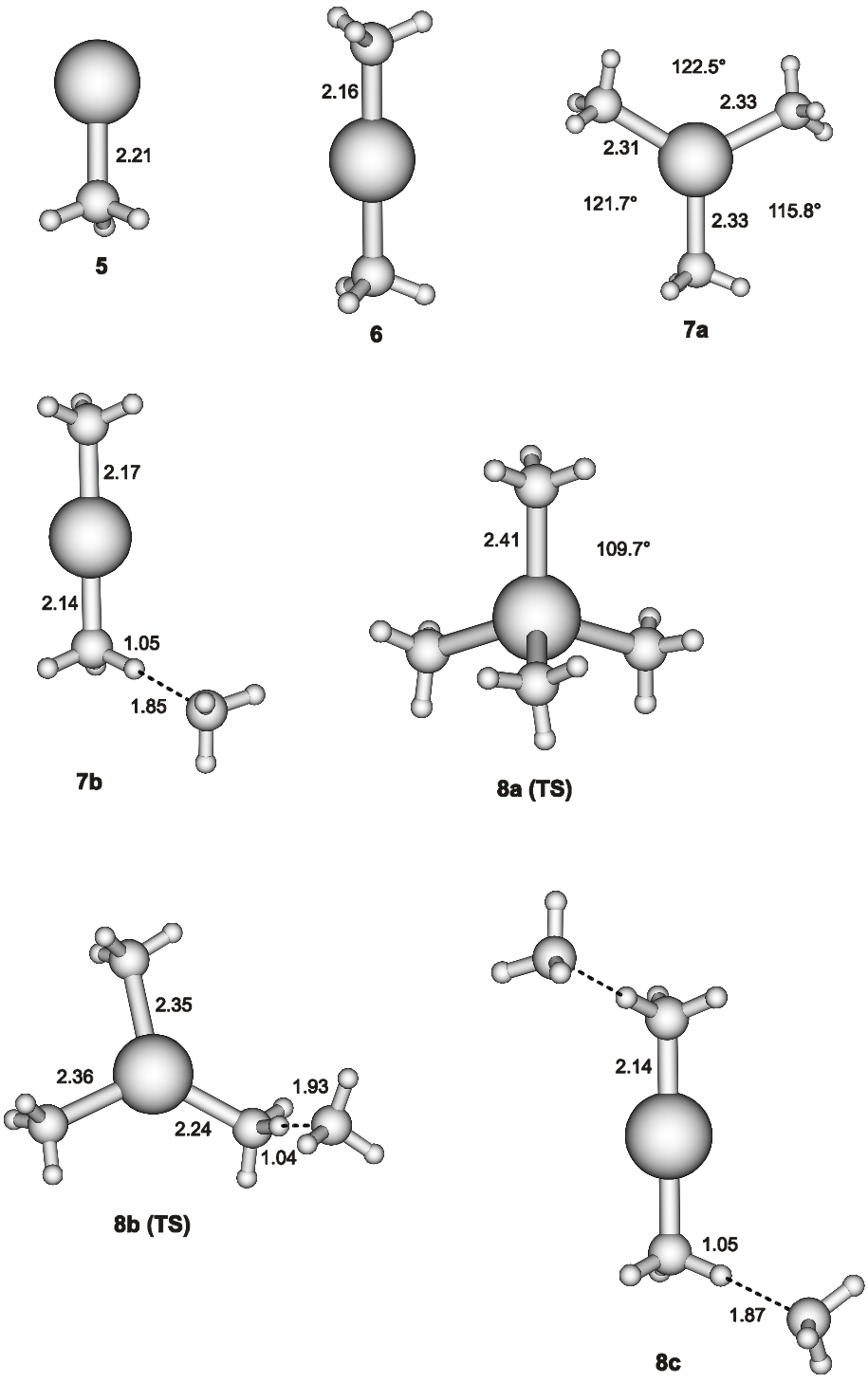

Figure 2: Fully optimized structures of $Ag^{+}(NH_3)_n$, n=1-4, at the B3LYP level of theory. Bond lengths are in angstroms. All N-H bonds, except where otherwise noted, are 1.02 Å. Structures marked with TS are transition states with a low imaginary frequency mode representing internal rotations of the NH_3 groups.

coordinating the third ammonia ligand and placing it into the second solvation shell. This differs from the study of Shoeib et al.[44] who find the **7a** (3+0) configuration to be 17.3 kJ/mol lower in energy. The results of the present study probably again reflect energy lowering of the (2+1) structure due to the strong polarizing effect of the central Ag^+ ion on the hydrogen bonds.

For $Ag^+(NH_3)_4$ three different configurations were considered. The (4+0) structure converged to **4a**, an almost perfect tetrahedron with four comparably long Ag-N bonds. The normal mode analysis produced one low (-28 cm^{-1}) imaginary frequency for this complex, which essentially corresponds to an internal rotation of two of the ammonia ligands. Several attempts to find the minimum with the CalcFC option failed. Since the potential surface is very flat as indicated by the low frequency, the energy difference and the difference in geometry between this transition state and the minimum should be very small and can thus be neglected. The (3+1) structure converged to **8b** which is also a transition state with an even lower imaginary frequency (-7 cm^{-1}). Lowest in energy turned out to be the linear (2+2) configuration **8c**, but again, the energy difference between the structures is found to be small. As can be seen in Table 3, the (2+2) **8c** configuration is found to be the global minimum, but with **8a** and **8b** being only 7.5 and 8.6.kJ/mol, respectively, higher in energy.

Table 3: Relative Energies of the isomers of $Ag^+(NH_3)_n$, n=3, 4, calculated at the B3LYP/6-311++(3df,3pd) level of theory referred to the lowest energy structure. Structure numbering refers to Fig. 2.

Structure	7a	7b	8a	8b	8c
ΔH_{298K} [kJ/mol]	2.4	0	7.5	8.6	0

The calculated binding energies summarized and compared with experimental values in Table 4 exhibit the same trends as the hydrated silver cations. The binding

energy of the first ligand, $\Delta H_{0,1}$ underestimates the experimental value by 21 kJ/mol, while that for the second ligand, $\Delta H_{1,2}$, is overestimated by ≈23 kJ/mol. For the former value the agreement with the experiment is acceptable if one considers the experimental error of about 16 kJ/mol[13] but the latter deviation is well outside the stated ±3.4 kJ/mol accuracy of the experiment.[45] Widmer-Cooper et al.[39] who used in their study much larger basis sets for N and H atoms get a maximum deviation of ≈16 kJ/mol for these energies. The calculated values for the next two incremental binding energies, $\Delta H_{2,3}$ and $\Delta H_{3,4}$ both underestimate slightly the experimental values, with the differences being probably within the combined uncertainties of the experiment and the calculation.

Table 4: Experimental and calculated binding energies of $Ag^+(NH_3)_n$, n=1-4

	$\Delta H_{1,0}$ [kJ/mol]	$\Delta H_{2,1}$ [kJ/mol]	$\Delta H_{3,2}$ [kJ/mol]	$\Delta H_{4,3}$ [kJ/mol]
exp.	-203.8[b]	-154.4[c]	-61.1[c]	-54.4[c]
calc.	-183	-177.3	-45.1	-46.5

[b] Reference 13; [c] Reference 45

5.4.3 Mixed Silver-Water-Ammonia-Clusters $Ag^+(NH_3)_n(H_2O)_m$, n,m=1-4

The optimized geometries obtained for clusters with mixed water and ammonia ligands are presented in Fig. 3. For $Ag^+(NH_3)(H_2O)$, the calculated structure **9** is again a transition state with a low imaginary frequency mode (-22 cm^{-1}) corresponding to an internal rotation of the H_2O group against the NH_3 group. As in the ammonia cluster above, the energy and geometry differences between this structure and the global minimum are negligible. The Ag-O and Ag-N bond lengths are similar to the corresponding distances in the homogeneous $Ag^+(H_2O)_2$ and $Ag^+(NH_3)_2$ clusters. For

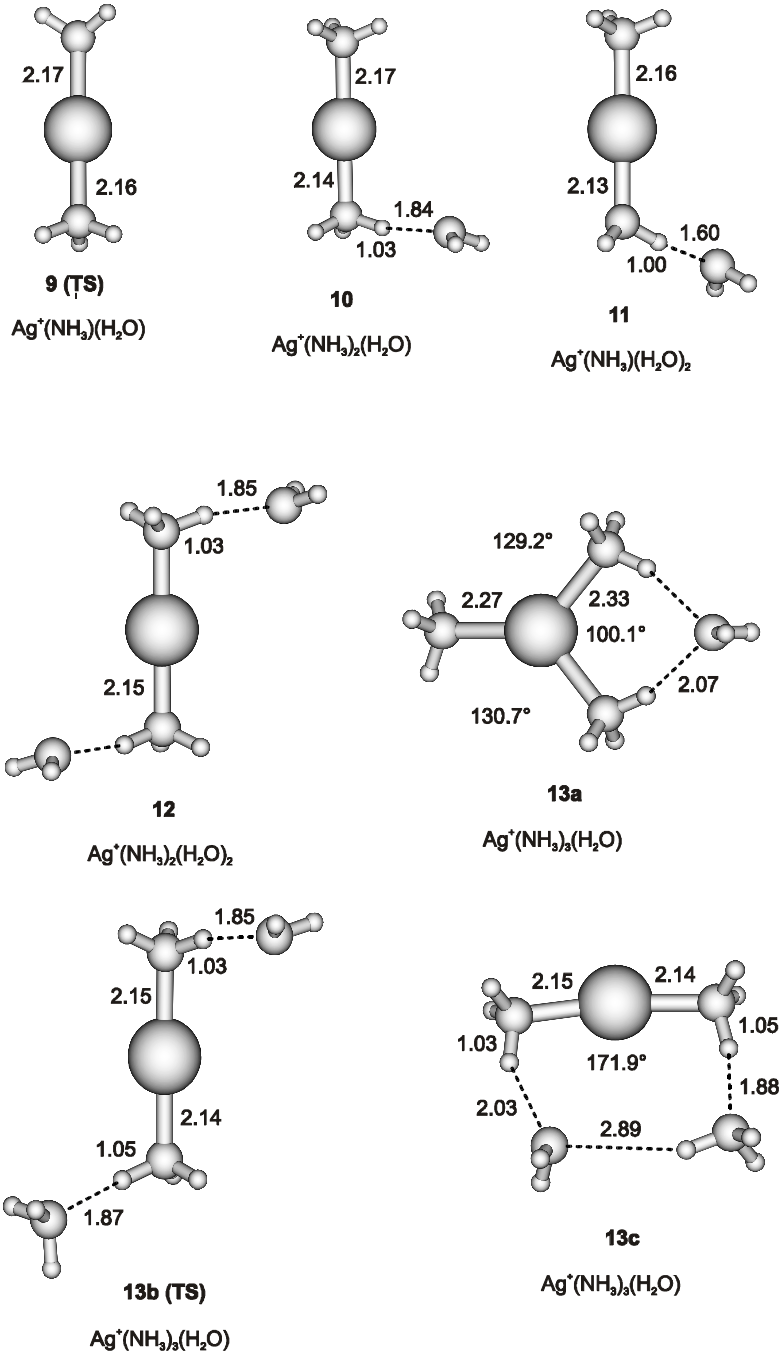

Figure 3: Fully optimized structures of $Ag^+(NH_3)_n(H_2O)_m$, n, m=1-4, at the B3LYP level of theory. Bond lengths are in angstroms. All N-H bonds and O-H bonds, except where otherwise noted, are 1.02 Å and 0.97 Å, respectively. Structures marked with TS are transition states with a low imaginary frequency mode representing an internal rotation of the NH_3 groups.

clusters with more than two ligands no stable (n+0) configurations were found, with all of them converging rapidly to one of the structures shown in the figure. Thus, both $Ag^+(NH_3)_2(H_2O)$ (**10**) and $Ag^+(NH_3)(H_2O)_2$ (**11**) converge to the linear (2+1) type structure, even when starting from a (3+0) configuration. The optimized structure **10** indicates that direct coordination of ammonia to silver is energetically favored, water prefers to be in the hydrogen bonded network around it. As observed for the homogeneous clusters, binding of a ligand in the second coordination shell again shortens the Ag-X bond. Interestingly, the N-H-O hydrogen bond angle in **10** is less than 180°, probably reflecting a weak interaction between the oxygen lone pair and the silver cation. For the same reason, similar slight distortions of the hydrogen bonds are also found in the (2+2) structure (**12**) of $Ag^+(NH_3)_2(H_2O)_2$. Three different structures were found for $Ag^+(NH_3)_3(H_2O)$ with the linear configuration **13b** being the absolute minimum. As can be seen in Table 5, the geometry **13a** is only slightly higher (+4.8 kJ/mol) suggesting that also in the case of mixed complexes the structures with two and three directly coordinated ammonia ligands exhibit comparable stabilities. Interestingly, the structure **13c** is, in spite of having one more hydrogen bond than **13b**, more than 11.7 kJ/mol higher in energy. Apparently, the strong preference for a linear N-Ag-N configuration results in unusually long and weak hydrogen bonds, so that the one additional hydrogen bond can not compensate for the overall increase in the complex energy.

Table 5: Relative Energies of the isomers of $Ag^+(NH_3)_3(H_2O)$ calculated at the B3LYP/6-311++(3df,3pd) level of theory referred to the lowest energy structure. Structure numbering refers to Fig. 3.

Structure	13a	13b	13c
ΔH_{298K} [kJ/mol]	4.8	0	11.7

5.4.4 Discussion of the DFT results

The calculations reveal that clusters with three ligands directly coordinated to the silver cation and those with only two ligands linearly coordinated to the central ion and the third one located in the second solvation shell are energetically almost equal. Accordingly, the coordination chemistry of silver cations is not only dominated by their ability to form two linear hybrid orbitals, but their strong polarizing effect upon the ligands and its effect upon the binding energies of the ligands in the second coordination shell is comparable. Since in the clusters investigated here different isomers are very close in energy, kinetic effects should also be taken into account, and molecular dynamics studies should be interesting and desirable. They could provide information about the "real" geometries of the clusters, although the lower level of theory introduces a different source of errors. High-level Car-Parrinello molecular dynamics simulations would probably be the method of choice.

5.5 Experimental Results and Discussion

5.5.1 Reaction of $Ag^+(NH_3)_n$ with H_2O

The reaction of ammoniated silver cations $Ag^+(NH_3)_n$, n=11-23, with H_2O corresponds to the conditions in aqueous solution in the sense that it proceeds with a large excess of water, so that exchange of ammonia ligands for water, but not of water for ammonia, was possible. To keep the collision rate sufficiently high, a pressure of about $9x10^{-8}$ mbar was maintained in the ICR cell during the experiment. Fig. 4a shows part of a

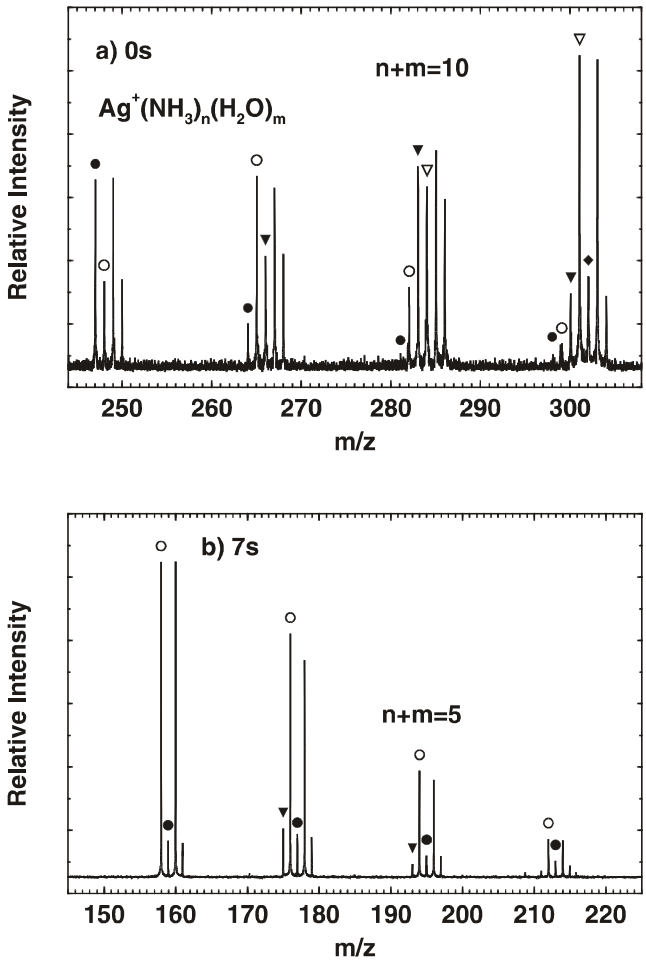

Figure 4: Typical parts of the mass spectrum of the reaction of ammoniated silver cations $Ag^+(NH_3)_n$, n=11-23, with H_2O with a reaction delay of a) 0s and b) 7s. Panel a) shows the remarkably high rate of this reaction. The labeled peaks represent clusters that correspond to a composition $^{107}Ag^+(NH_3)_n(H_2O)_m$, the remaining peaks belong to clusters containing the heavier isotope ^{109}Ag. Clusters $^{107}Ag^+(NH_3)_m(H_2O)_n$ and clusters $^{109}Ag^+(NH_3)_{m+2}(H_2O)_{n-2}$ have very similar masses (Δm=0.03 amu) which are physically resolved but not displayed as two peaks due to the data set size limit of 128 kW. The different cluster species are labeled as follows: ● $Ag^+(NH_3)_n(H_2O)_4$; ○ $Ag^+(NH_3)_n(H_2O)_5$; ▼ $Ag^+(NH_3)_n(H_2O)_6$; ∇ $Ag^+(NH_3)_n(H_2O)_7$; ♦ $Ag^+(NH_3)_n(H_2O)_8$. The most dominant products after 7s can be seen in panel b). These are cluster species of ○ $Ag^+(NH_3)_3(H_2O)_m$ composition. The hydrated silver diammine complex, ● $Ag^+(NH_3)_2(H_2O)_m$, as well as ▼. $Ag^+(NH_3)_4(H_2O)_m$ clusters, are present in lesser amounts.

typical mass spectrum in the range of clusters with 8-11 ligands after a nominal reaction time of 0s. Since the reaction already proceeds while the clusters formed in twenty vaporization cycles are being accumulated in the ICR cell, some products are already present at this "zero" time. The interpretation of the mass spectra is somewhat complicated by the presence of two silver isotopes, $^{107}Ag^+$ and $^{109}Ag^+$ in comparable abundances (51.839 and 48.161 %), as well as by the fact that each exchange of an ammonia ligand for water, i.e. reaction of $Ag^+(NH_3)_n(H_2O)_m$ to $Ag^+(NH_3)_{n-1}(H_2O)_{m+1}$ increases the nominal mass of the cluster by one amu. It should, however, be noted that although for instance the $^{107}Ag^+(NH_3)_m(H_2O)_n$ and $^{109}Ag^+(NH_3)_{m+2}(H_2O)_{n-2}$ clusters differ in mass by only $\Delta m \approx 0.03$ amu, they can in view of the high resolution of the FT-ICR MS easily be resolved but are not displayed due to the data set size limit of 128 kW. As can be seen in Fig. 4a, the reaction takes place remarkably fast, with up to eight water molecules having already been taken up during the cell filling cycle, at a nominal time t=0. Even at this short time, the most abundant products retain only four of the originally present ammonia ligands. Based on the estimated rate, almost every collision must be reactive, with the ligand exchange proceeding according to the following reaction scheme:

$$Ag^+(NH_3)_n(H_2O)_m + H_2O \rightarrow Ag^+(NH_3)_{n-x}(H_2O)_{m+1} + x\ NH_3 \qquad m \geq 0$$

More than one ammonia molecule can be set free, that is x may be larger than one, since in addition to the binding energy also the collision energy can be released as heat in the cluster, and the value will also depend on the size of the cluster. The exact number of ammonia molecules released in a single collision can not be determined accurately, since the ligand exchange proceeds concurrently with collisional and black body radiation induced fragmentation. Due to these processes, the clusters rapidly lose ligands and shrink,

so that after 7s in Fig. 4b the distribution maximum has shifted to n+m = 3. In spite of the long reaction time, and in spite of the fast initial exchange of ammonia for water, the most abundant remaining clusters (marked with hollow circles in the Fig.4b) still retain three ammonia molecules. Much less abundant are clusters $Ag^+(NH_3)_2(H_2O)_m$, that is with only two ammonia ligands remaining, and this does not change appreciably even after longer reaction delays, or in experiments employing a still higher water pressure ($3x10^{-7}$ mbar). The smallest cluster observed in small quantity after a long time is n=2, m=0, and products containing fewer than two ammonia ligands were not observed in any case.

The results thus suggest that the ammonia ligands are easily and efficiently exchanged against water, with the exception of the last three. It also is possible, but apparently energetically not very favorable to exchange one additional ammonia ligand, but then the reaction stops. Since ligand exchange reactions proceed at roughly collision rate as long as they are exothermic, this should indicate that replacing an ammonia by a water ligand is exothermic if more than three ammonia ligands are bound to the cluster. Exchanging an ammonia ligand if only three of them remain would then appear to be slightly endothermic, that is it can happen if collisionally or black body radiation activated, but it is not very favorable. For $Ag^+(NH_3)_2(H_2O)_m$ species, the exchange of an ammonia ligand for water is apparently too endothermic to be activated either by collisions or by black body radiation. In order to verify these conclusions, the enthalpies of several ligand exchange reactions were calculated by using the values obtained in the DFT calculations:

$Ag^+(NH_3)_2 + H_2O \rightarrow Ag^+(NH_3)(H_2O) + NH_3$ $\Delta H = +59.4$ kJ/mol (1)

$Ag^+(NH_3)_2(H_2O) + H_2O \rightarrow Ag^+(NH_3)(H_2O)_2 + NH_3$ $\Delta H = +42.1$ kJ/mol (2)

$Ag^+(NH_3)_3 + H_2O \rightarrow Ag^+(NH_3)_2(H_2O) + NH_3$ $\Delta H = +7.6$ kJ/mol (3)

$Ag^+(NH_3)_3(H_2O) + H_2O \rightarrow Ag^+(NH_3)_2(H_2O)_2 + NH_3$ $\Delta H = +7.3$ kJ/mol (4)

$Ag^+(NH_3)_4 + H_2O \rightarrow Ag^+(NH_3)_3(H_2O) + NH_3$ $\Delta H = +11.9$ kJ/mol (5)

The enthalpies of reactions 1 and 2 clearly confirm that these are too endothermic for an exchange of an ammonia ligand for water to occur under the experimental conditions, if only two NH_3 ligands remain in the cluster, and consistently, no products with less than two ammonia ligands are observed. Again consistent with the experiment, the reactions 3 and 4 show slightly endothermic values, verifying that replacing an ammonia ligand in clusters with three ammonia ligands can be collisionally or black body radiation activated. Somewhat surprisingly, the reaction 5, that is the exchange of an ammonia molecule in a cluster with four NH_3 ligands is found to be more endothermic than the reactions 3 and 4. This might indicate that the investigated structures for the mixed cluster $Ag^+(NH_3)_3(H_2O)$ which can have a lot of isomers did not include the global minimum. A more likely reason, however, is that the reaction is more favorable in an extended hydrogen-bonded network, where the role of water as double acceptor gets more important.

As already mentioned above, this reaction is the gas-phase analogue of the formation of $[Ag(NH_3)_2]^+$ in aqueous solution because both proceed with a large excess of water. The observation that $Ag^+(NH_3)_3(H_2O)_m$ clusters are the dominant products and that additional exchange resulting in $Ag^+(NH_3)_2(H_2O)_m$ appears inefficient seems to be at odds with the bulk solution observations, where the linear $Ag^+(NH_3)_2$ cluster ions seem to dominate. In a bulk liquid, however, the number of collisions is many orders of magnitude

larger than in our experiments, which may make the reaction proceed efficiently to n=2. In addition, the presence of a more extensive hydrogen bonded network may shift the energetics in favor of the $Ag^+(NH_3)_2$ cations.

5.5.2 Reaction of $Ag^+(H_2O)_n$ with NH_3

The complementary reaction of hydrated silver cations with NH_3 has been studied under similar conditions. Fig. 5a shows a section of a typical mass spectrum resulting from the reaction of large hydrated silver cations $Ag^+(H_2O)_n$, n=25-45, with NH_3 after a nominal 0 s delay. As can be seen in Fig. 5a, the reaction again proceeds fast, and first products have already been formed, with up to three ammonia molecules having been taken up during the filling process by some of the clusters. No unreacted $Ag^+(H_2O)_n$ clusters remain after a 1 s delay in Fig. 5b, and clusters with five or even six ammonia ligands are now present. This efficient exchange of water for ammonia is in agreement with the previous investigations on smaller hydrated clusters, $H^+(H_2O)_n$, n=2-11, and $Na^+(H_2O)_n$, n=1-3.[14,46]

While superficially the available data would seem to suggest that for all the hydrated cations a uniformly efficient and rapid ligand exchange is taking place:

$$Ag^+(H_2O)_n(NH_3)_m + NH_3 \rightarrow Ag^+(H_2O)_{n-x}(NH_3)_{m+1} + x\ H_2O \qquad m \geq 0$$

a closer examination of the large cluster reactions reveals a more complex behavior. As can be seen in Fig. 6, at even longer reaction delays the clusters with five ammonia molecules, $Ag^+(NH_3)_5(H_2O)_m$, become dominant, but the uptake of a sixth ligand

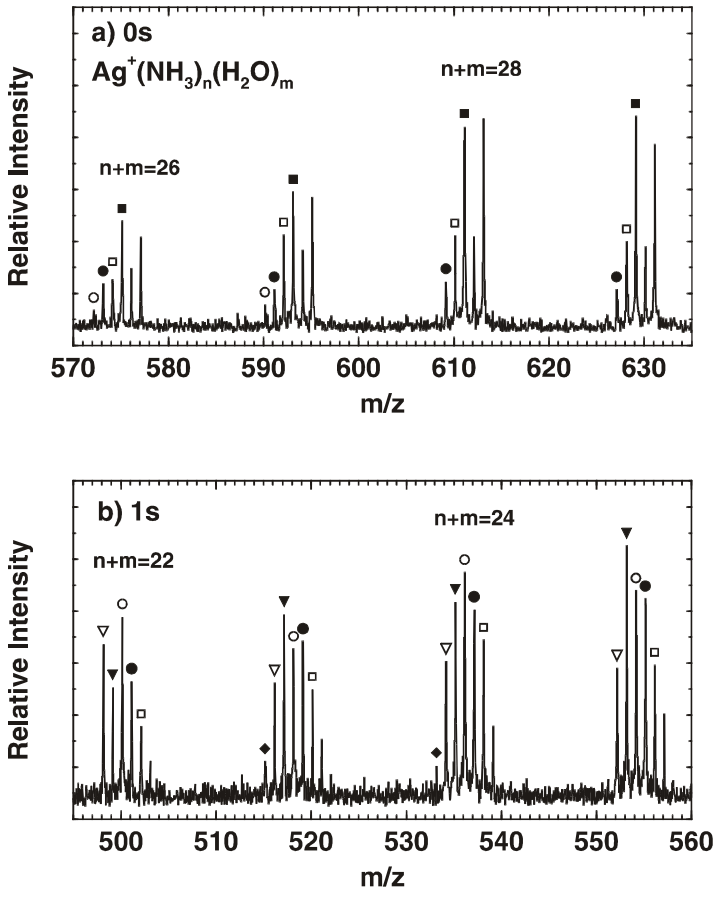

Figure 5: Typical parts of the mass spectrum of the reaction of large hydrated silver cations $Ag^+(H_2O)_n$, n=25-45, with NH_3 with a reaction delay of a) 0s and b) 1s. The clusters are labeled in the following way: ■ $Ag^+(H_2O)_m$, □. $Ag^+(NH_3)(H_2O)_m$, ● $Ag^+(NH_3)_2(H_2O)_m$, ○ $Ag^+(NH_3)_3(H_2O)_m$, ▼ $Ag^+(NH_3)_4(H_2O)_m$, ∇ $Ag^+(NH_3)_5(H_2O)_m$, ♦. $Ag^+(NH_3)_6(H_2O)_m$. The spectra show that up to five ammonia molecules are taken up with high efficiency, a sixth one less efficiently.

is obviously much less efficient, and in no case products with more then six ammonia ligands were observed. To verify that the limit on the number of ammonia ligands that can be taken up is not a function of the cluster size, the experiments were repeated with various initial $Ag^+(H_2O)_n$ distributions. These experiments showed that the rapid exchange of five ligands, but a more hesitant uptake of a sixth one is a common feature of for

instance two experiments with n=25-45 and n=7-15 initial cluster size ranges, respectively, and in neither experiment any uptake of more than six ammonia molecules was observed.

To gain some more insight into these observations and ligand exchange processes, it is instructive to examine the results of our DFT computations compiled in Tables 1-5. Comparison of Tables 2 and 4 immediately reveals an interesting result: while the first two ammonia ligands exhibit appreciably stronger bonds to Ag^+ than water molecules, the situation is reversed in larger clusters. Already the third and fourth ammonia are found to be weaker bound then their water counterparts, a result confirmed also by the experimental results of Holland and Castleman[45] and Deng and Kebarle.[13] While a direct bond to the metal favors ammonia, in a larger solvation shell water with its two electron lone pairs can produce more stable structures than ammonia, which can typically form only a single acceptor hydrogen bond. It is the result of the ability of H_2O to form extended hydrogen bonded networks, which is also reflected in the much higher boiling point and lower vapor pressure of bulk water, when compared with ammonia. If one takes the properties of the two ligands into consideration, it is therefore not surprising that the ligand exchange is initially very efficient, but stops at a certain number of ammonia ligands.

An exception to the observed preference for structures with five ammonia ligands is the $Ag^+(NH_3)_6(H_2O)_2$, n+m=8, cluster ion, which is always more intense than the $Ag^+(NH_3)_5(H_2O)_3$ and $Ag^+(NH_3)_4(H_2O)_4$ species, and also exhibits higher intensities than its n+m=9 and 7 neighbors, $Ag^+(NH_3)_6(H_2O)_3$ and $Ag^+(NH_3)_6(H_2O)$. Clearly, a complex ion with six ammonia and two water ligands appears to be particularly stable. On the other hand, panel a) of Fig. 6 shows that $Ag^+(NH_3)_6(H_2O)_6$ is very weak compared to $Ag^+(NH_3)_6(H_2O)_5$ and $Ag^+(NH_3)_6(H_2O)_7$, suggesting that the structure of this particular composition is especially unfavorable, and it probably fragments efficiently to form either $Ag^+(NH_3)_5(H_2O)_6$ or $Ag^+(NH_3)_6(H_2O)_5$.

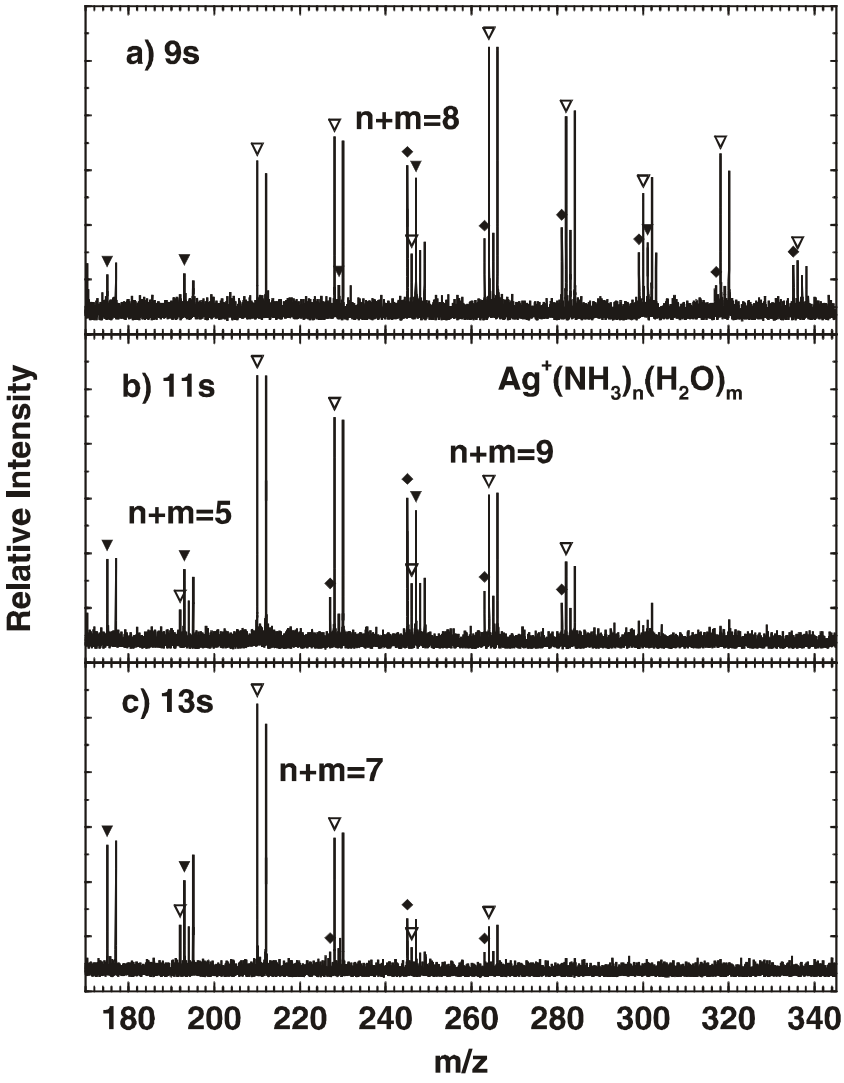

Figure 6: Typical parts of the mass spectrum of the reaction of large hydrated silver cations $Ag^+(H_2O)_n$, n=25-45, with NH_3 with a reaction delay of a) 9s, b) 11s and c) 13s. (Cluster labeling is similar to Figure 5: ▼ $Ag^+(NH_3)_4(H_2O)_m$, ∇ $Ag^+(NH_3)_5(H_2O)_m$, ♦. $Ag^+(NH_3)_6(H_2O)_m$). Even after these longer reaction delays, not more than six ammonia molecules are taken up by the clusters.

The weakly bound nature of a sixth ammonia ligand is also evident by examining the later stages of cluster fragmentation in Fig. 6. The particularly stable $Ag^+(NH_3)_6(H_2O)_2$ cluster ion fragments predominantly by the loss of the sixth ammonia. The very small

amount of $Ag^+(NH_3)_6(H_2O)$ formed fragments in the very next step with a loss of NH_3, so that the sixth ammonia always evaporates before the last water ligand, with the n+m = 6 cluster having a unique composition of $Ag^+(NH_3)_5(H_2O)$. The fact that the sixth ammonia ligand always evaporates before the last water ligand is due to the ability of water to form two acceptor hydrogen bonds, which leads to a higher binding energy. The $Ag^+(NH_3)_5(H_2O)$ cluster fragments preferentially by the loss of an ammonia ligand, but approximately one third of these clusters fragment by losing a water ligand, suggesting that the binding energy of the fifth NH_3 and the last H_2O ligand are comparable. In the next step, both possible fragmentation products, $Ag^+(NH_3)_4(H_2O)$ and $Ag^+(NH_3)_5$, then fragment by forming $Ag^+(NH_3)_4$, indicating that the binding energy of the fifth ammonia ligand in $Ag^+(NH_3)_5$ and the binding energy of the water ligand in $Ag^+(NH_3)_4(H_2O)$ is similar.

In view of the well-known fact that silver salts form in aqueous solutions very stable $[Ag(NH_3)_2]^+$ cations it might at first appear surprising that more than two ammonia ligands can be taken up by the clusters. However, investigations in highly concentrated aqueous ammonia have suggested, that here three NH_3 ligands may be bound to the silver cations.[3] The difference in the FT-ICR study is that here ammonia is present in excess as reaction gas, so that unlike in aqueous solution, the exchange can only proceed in one direction. In order to gain some more insight into the energetics of the ligand exchange reactions, the DFT calculation results were used to obtain the enthalpies of some relevant reactions:

$Ag^+(H_2O) + NH_3 \rightarrow Ag^+(NH_3) + H_2O$ ΔH= -64.7 kJ/mol (6)

$Ag^+(NH_3)(H_2O) + NH_3 \rightarrow Ag^+(NH_3)_2 + H_2O$ ΔH= -59.4 kJ/mol (7)

$Ag^+(NH_3)_2(H_2O) + NH_3 \rightarrow Ag^+(NH_3)_3 + H_2O$ ΔH= -7.6 kJ/mol (8)

$Ag^+(NH_3)_2(H_2O)_2 + NH_3 \rightarrow Ag^+(NH_3)_3(H_2O) + H_2O$ ΔH= -7.3 kJ/mol (9)

$Ag^+(NH_3)_3(H_2O) + NH_3 \rightarrow Ag^+(NH_3)_4 + H_2O$ ΔH= -11.9 kJ/mol (10)

The results are clearly in good agreement with the experimental observations. The reactions 6 and 7 show that taking up the first and second NH_3 molecule is a strongly exothermic process, and will probably lead to evaporation of more than one water molecule. The exchanges of a third and fourth ligand are found to be also exothermic by a much smaller amount but probably outside the uncertainty of the computations. Unfortunately, the computations for larger clusters are getting progressively more tedious and time consuming due to the drastically increasing number of isomers, and with n+m=4 ions the limit was reached of what is feasible with the available computing time. It would, of course be very interesting to extend the calculations to still larger species. Based on the experimental results, one might expect also the exchange of the fifth ligand to be exothermic. The reluctance of the clusters to accept a sixth one probably indicates that this step is slightly endothermic, and occurs as a result of thermal or collisional activation. Also computations of species which appear to be particularly stable, such as $Ag^+(NH_3)_6(H_2O)_2$ or $Ag^+(NH_3)_5(H_2O)$ would surely be of interest.

5.6 Conclusion

The reaction of the gas phase $Ag^+(NH_3)_{10\text{-}26}$ cluster ions with water vapour is the analogue to the well known formation of the diammine silver complex $[Ag(NH_3)_2]^+$ in

aqueous solutions, since both proceed in a large excess of H_2O. In the gas phase, the dominant products are species with three remaining NH_3 ligands, $Ag^+(NH_3)_3(H_2O)_m$, but at longer times cluster ions with only two ammonia ligands are also present. The reluctance of the third ammonia to be exchanged may be due to a slight change of the relative energies of the solvated ions in the cluster and in bulk solutions, or may reflect a high activation barrier for the exchange process which is overcome in the large number of collisions in the bulk. Overall, the gas phase reaction is analogous to the bulk aqueous solutions, where depending on the ammonia concentration either $Ag^+(NH_3)_2$ or $Ag^+(NH_3)_3$ seems to prevail.

In the complementary process, the reaction of hydrated silver cations $Ag^+(H_2O)_{25\text{-}45}$ with NH_3, again a ligand exchange reaction takes place, with first five ammonia molecules being very efficiently exchanged for water, and with a sixth one being taken up much more reluctantly. This rapid exchange confirms the results of the DFT computations indicating that the NH_3 ligands are more strongly bound to the cation as long as they are in its immediate proximity. The limit of six NH_3 ligands, and the lack of exchange of more remote ligands simply reflects the weaker interactions between NH_3 molecules, the much higher volatility of ammonia, and its reduced ability to form extended hydrogen bonded networks when compared with water.

The experiments show that in mixed clusters the first and second ammonia ligand, however, are much more strongly bound than water because they cannot be exchanged. The third ammonia ligand is also more strongly bound since it can only be replaced by water if the clusters are additionally activated by collisions or black body radiation. The binding energy of the fifth and fourth ammonia ligand is comparable to the binding energy of the respective water ligands because ligand exchange proceeds efficiently in both directions. The sixth NH_3 ligand, however, is much more weakly bound than a water

ligand. It is taken up very reluctantly even in the reaction with 100 % excess of NH_3 and very quickly replaced by water in the complementary reaction. This gradual transition of the relative water/ammonia binding energies is responsible for the observed coordination numbers.

The accompanying DFT calculations of small hydrated silver cations, $Ag^+(H_2O)_n$, n=1-4, ammoniated silver cations, $Ag^+(NH_3)_n$, n=1-4, and silver cations solvated by mixed ligands, $Ag(NH_3)_n(H_2O)_m$, n,m=1-4, clearly show that the coordination chemistry of silver is characterized by subtle differences in the binding energies between the first and second solvation shell. Cooperative effects in the surrounding solvent have to be taken into account to fully describe the observed effects. Thus, the coordination chemistry of silver cations is much more complex than the simple textbook picture of linear, twofold coordination would suggest.

5.7 References

(1) Cotton, F.A.; Wilkinson, G. *Advanced Inorganic Chemistry*; John Wiley & Sons: New York, 1988, p.941.

(2) Orgel, L.E. *J. Chem. Soc.* **1958**, *90*, 4186-4190.

(3) Bjerrum, J. *Acta Chem. Scand. A* **1986,** *40*, 392-395.

(4) Yamaguchi, T.; Lindqvist, O.; Boyce, J.B.; Claeson, T. *Acta Chem. Scand.* **1984**, *A38*, 423-428.

(5) Sandström, M.; Nielson, G.W.; Johansson, G.; Yamaguchi, T. *J. Phys. C: Solid State Phys.* **1985**, *18*, L1115-L1121.

(6) Yamaguchi, T.; Johansson, G.; Holmberg, B.; Maeda, M. Ohtaki, H. *Acta Chem. Scand.* **1984**, *A38*, 437-451.

(7) Maeda, M.; Maegawa, Y.; Yamaguchi, T.; Ohtaki, H. *Bull. Chem. Soc. Jpn.* **1979**, *52*, 2545-2550.

(8) Yamaguchi, T.; Wakita, H.; Nomura, M. *J. Chem. Soc., Chem. Commun.* **1988**, 433-434.

(9) Tsutsui, Y.; Sugimoto, K.-I.; Wasada, H. ;Inada, Y.; Funahashi, S. *J. Phys. Chem. A* **1997**, *101*, 2900-2905.

(10) Ferguson, E.E.; Fehsenfeld, F.C.; Albritton, D.L. *Gas Phase Ion Chemistry*, edited by Bowers, M.T. (Academic, New Yotk, 1979), Vol. 1, pp. 45-82.

(11) Zhang, X.; Mereand, E.L.; Castleman, Jr., A.W. *J. Phys. Chem.* **1994**, *98*, 3554-3557.

(12) Malenkov, G.G.; Dyakonova, L.P. *Dokl. Acad. Nauk SSSR* **1980,** *251*, 1433-1436.

(13) Deng, H.; Kebarle, P. *J. Phys. Chem* **1998,** *102*, 571-579.

(14) Yang, X.; Castleman, Jr., A.W. *J. Chem. Phys.* **1990**, *93*, 2405-2412.

(15) Achatz, U.; Beyer, M.; Joos, S.; Fox, B.S.; Niedner-Schatteburg, G.; Bondybey, V.E. *J. Phys. Chem. A* **1999**, *103*, 8200-8206.

(16) Capron, L.; Feng, W.Y.; Lifshitz, C.; Tjelta, B.L.; Armentrout, P.B. *J. Phys. Chem.* **1996**, *100*, 16571-16576.

(17) Gapeev, A.; Yang, C.-N.; Klippenstein, S.J.; Dunbar, R.C. *J. Phys. Chem. A* **2000**, *104*, 3246-3256.

(18) Nielsen, S.B.; Masella, M.; Kebarle, P. *J. Phys. Chem. A* **1999**, *103*, 9891-9898.

(19) Haynes, C.L.; Armentrout, P.B. *Chem. Phys. Lett.* **1996**, *249*, 64-70.

(20) Beyer, M.; Berg, C.; Albert, G.; Achatz, U.; Joss, S.; Niedner-Schatteburg, G.; Bondybey, V.E. *J. Am. Chem. Soc.* **1997**, *119*, 1466.

(21) Dieterle, M., Harvey, JN., Heinemann, C., Schwarz, J., Schröder, D., Schwarz, H. *Chem. Phys. Lett.* **1997**, *277*, 399-405.

(22) Schindler, T.; Berg, C.; Niedner-Schatteburg ,G.; Bondybey, V.E. *Chem. Phys. Lett.* **1994**, *229*, 57-64.

(23) Schindler, T.; Berg, C.; Niedner-Schatteburg ,G.; Bondybey, V.E. *J. Phys. Chem.* **1995**, *99*, 12434-12443.

(24) Beyer, M.; Berg, C.; Görlitzer, H.W.; Schindler, T.; Achatz, U.; Albert, G.; Niedner-Schatteburg, G.; Bondybey, V.E. *J. Am. Chem. Soc.* **1996**, *118*, 7386-7389.

(25) Berg, C.; Beyer, M.; Achatz, U.; Joos, S.; Niedner-Schatteburg, G.; Bondybey, V.E. *Chem. Phys.* **1998** ,*239*, 379-392.

(26) Berg, C.; Achatz, U.; Beyer, M.; Joos, S.; Albert, G.; Schindler, T.; Niedner-Schatteburg, G.; Bondybey, V.E. *Int. J. Mass Spectrom. Ion Processes* **1997**, *176/168*, 723-734.

(27) Beyer, M.; Achatz, U.; Berg, C.; Joos, S.; Niedner-Schatteburg, G.; Bondybey, V.E. *J. Phys. Chem. A* **1999**, *103*, 671-678.

(28) Achatz, U.; Joos, S. ;Berg, C.; Schindler, T.; Beyer, M.; Albert, G.; Niedner-Schatteburg, G.; Bondybey, V.E. *J. Am. Chem. Soc.* **1998**, *120*, 1876-1882.

(29) Fox, B.S.; Beyer, M.K.; Achatz, U.; Joos, S.; Niedner-Schatteburg, G.; Bondybey, V.E. *J. Phys. Chem. A* **2000**, *104*, 1147-1151.

(30) Fox, B.S.; Beyer, M.K.; Bondybey, V.E. *J. Phys. Chem. A* **2001**, *105*, 6386-6392.

(31) Gaussian 98, Revision A.7, M. J. Frisch, G. W. Trucks, H. B. Schlegel, G. E. Scuseria, M. A. Robb, J. R. Cheeseman, V. G. Zakrzewski, J. A. Montgomery, Jr., R. E. Stratmann, J. C. Burant, S. Dapprich, J. M. Millam, A. D. Daniels, K. N. Kudin, M. C. Strain, O. Farkas, J. Tomasi, V. Barone, M. Cossi, R. Cammi, B. Mennucci, C. Pomelli, C. Adamo, S. Clifford, J. Ochterski, G. A. Petersson, P. Y. Ayala, Q. Cui, K. Morokuma, D. K. Malick, A. D. Rabuck, K. Raghavachari, J. B. Foresman, J. Cioslowski, J. V. Ortiz, A. G. Baboul, B. B. Stefanov, G. Liu, A. Liashenko, P. Piskorz, I. Komaromi, R. Gomperts, R. L. Martin, D. J. Fox, T. Keith, M. A. Al-Laham, C. Y. Peng, A. Nanayakkara, C. Gonzalez, M. Challacombe, P. M. W. Gill, B. Johnson, W. Chen, M. W. Wong, J. L. Andres, C. Gonzalez, M. Head-Gordon, E. S. Replogle, and J. A. Pople, Gaussian, Inc., Pittsburgh PA, 1998.

(32) A.D. Becke, Phys. Rev. A 38 (1988) 3098-3100.

(33) A.D. Becke, J. Chem. Phys. 98 (1993) 1372-1377.

(34) A.D. Becke, J. Chem. Phys. 98 (1993) 5648-5652.

(35) C. Lee, W. Yang, R.G. Parr, Phys. Rev. B 37 (1988) 785-789.

(36). Andrae, D.; Haeussermann, U.; Dolg, M.; Stoll, H.; Preuss, H. *Theor. Chim. Acta* **1990**, *77*, 123-141.

(37) Berg, C.; Schindler, T.; Niedner-Schatteburg, G.; Bondybey, V.E. *J. Chem. Phys.* **1995**, *102*, 4870-4874.

(38) Feller, D.; Glendening, E. D.; de Jong, W. A. *J. Chem. Phys.* **1999**, *110*, 1475-1491.

(39) Widmer-Cooper, A. N.; Lindoy, L. F.; Reimers, J. R. *J. Phys. Chem. A* **2001**, *105*, 6567-6574.

(40) Feller, D.; Glendening, E. D.; Woon, D. E.; Feyereisen, M. W. *J. Chem. Phys.* **1995**, *103*, 3526-3542.

(41) Curtiss, L.A.; Pople, J.A. *J. Mol. Spectrosc.* **1975**, *55*, 1-14.

(42) Curtiss, L.A.; D.J. Frurip, D.J.; Blander, M. *Chem. Phys. Lett.* **1978**, *54*, 575-578.

(43) Curtiss, L.A.; D.J. Frurip, D.J.; Blander, M. *J. Chem. Phys.* **1979**, *71*, 2703-2711.

(44) Shoeib, T.; Milburn, R. K.; Koyanagi, G. K.; Lavrov, V. V.; Bohme, D. K.; Siu, K. W. M.; Hopkinson, A. C. *Int .J. Mass Spectrom.* **2000**, *201*, 87-100.

(45) Holland, P.M.; Castleman, A.W., Jr. *J. Chem. Phys.* **1982**, *76*, 4195-4205.

(46) Viggiano, A.A.; Dale, F.; Paulson, J.F. *J. Chem. Phys.* **1988**, *88*, 2469-2477.

6 Summary

The investigation of solvated ions offers the unique possibility to study their chemistry on a molecular level without cooperative effects since only one ion interacts with the solvent and with single reactant molecules. Therefore, e.g. metal ions in unusual oxidation states which are in solution instable due to disproportionation reactions can be stabilized for at least several seconds. In the scope of this thesis, hydrated first-row transition metal cations, $M^+(H_2O)_n$, M = V, Cr, Mn, Fe, Co, Ni, and Cu, together with Zn, were examined for the first time. Only vanadium ions are oxidized under the influence of black body radiation. Zn^+ as well as V^+ ions are oxidized by HCl whereas the heavier transition metal cations form single molecule precipitates.

Black body fragmentation is a very useful tool to gently remove solvent molecules from the ions and offers thus the extraordinary possibility to study the ion's chemistry depending on the number of solvent molecules. This phenomen was studied in detail experimentally and theoretically by comparing ammoniated ions with their hydrated analogues, and a more quantitative understanding of the process was reached.

A new approach was employed to study coordination chemistry of ions in mixed solvent systems. The ions were first ligated by up to 50 molecules of one solvent and then reacted with 100 % excess of a second solvent. Like this, one can simulate the conditions for complex formation reactions in solutions, where the solvent is present in almost 100 % excess over the ligand. In this way, the coordination chemistry of silver cations was examined in the water/ammonia solvent system. The experiments were again complemented by DFT calculations.

The results of each chapter can be summarized in the following way:

✯ Using the versatile laser vaporization source developed in our laboratory, metal ions in unusual oxidation states can be introduced into water clusters. Previous studies demonstrated that black body fragmentation of hydrated monovalent main group metals results in oxidation of the metal to its prefered oxidation state accompanied by the loss of atomic or molecular hydrogen. These processes can be accelerated by reaction of the cluster with strong acids. In the scope of this thesis, hydrated monovalent transition metals were investigated since they are known to occur in a number of oxidation states and are also able to easiliy change their oxidation state.

Hydrated vanadium cations $V^+(H_2O)_n$, n=5-30, were stored in the collision-free environment of an FT-ICR mass spectrometer and their reactions due to absorption of black body radiation were studied. Besides the loss of water ligands, the clusters show two different intracluster redox reactions, whose branching ratios are strongly size-dependent. Oxidation to the +II state results in $V(OH)^+(H_2O)_n$ ions, and a concurrent release of atomic hydrogen. Alternatively $V(OH)_2^+(H_2O)_n$ clusters can form leaving vanadium in the +III state, common in aqueous solutions, and simultaneously molecular H_2 evaporates from the cluster. This behavior reflects the properties of transition metals, and the ability of vanadium to form stable compounds in a variety of oxidation states, and differs from the previously studied intracluster reactions involving the hydrated monovalent main group metals Mg^+ and Al^+ which only react to their preferred oxidation state, $MgOH^+$ and $Al(OH)_2^+$, respectively. In reactions of large hydrated vanadium cations, $V^+(H_2O)_n$ with HCl acceleration of the molecular hydrogen formation and removal of the upper size limit was observed.

Hydrated metal cations $M^+(H_2O)_n$ containing the heavier metals Cr, Mn, Fe, Co,

Ni, Cu, and Zn were also produced and stored in the collision-free environment of the FT-ICR cell. They fragment by subsequent loss of water molecules. No intracluster reaction leading to oxidation of the metal ion was observed. The strong acid hydrogen chloride only oxidizes the Zn cation, yielding $ZnCl^+(H_2O)_n$ clusters similar to the reaction products of hydrated Mg^+ ions. In contrast to Mg^+, however, the oxidation reaction only takes place if induced by the strong acid. DFT calculations indicate that only the formation of $ZnCl^+$ is thermodynamically favored whereas the formation of $ZnOH^+$ is endothermic. Cr, Mn, Fe, Co, Ni, and Cu retain their unusual +I oxidation state, and the binary metal chlorides M(I)Cl precipitate. The solubility appears to increase in the MnCl, FeCl, AgCl, CrCl, CuCl, CoCl, NiCl order. Perhaps the single molecule precipitation hinders the oxidation reaction kinetically although it would presumably be thermodynamically favored.

✯ To get insight into the differences of the two important solvents water and ammonia the first systematic study of the black body radiation induced fragmentation of size-selected ionic ammonia clusters was carried out and compared with that of the corresponding hydrates. Specifically, the Ag^+ and H^+ cation clusters were studied, with the fragmentation rate constants of the ions solvated with ammonia being found to exhibit the same overall linear dependence on the number of ligands n, which was previously observed for the corresponding hydrates as well as for a number of other hydrated ions. To facilitate the interpretation of the experimental observations, DFT calculations of the cluster structures and of their harmonic frequencies and intensities were carried out. For the first time, the total absorbed power from 298 K black body radiation was quantified for $H^+(NH_3)_n$, n=1-5, and $H^+(H_2O)_n$, n=1-5. The observed fragmentation rate constants exhibit an excellent agreement with the computed rates of energy absorption from the black body infrared radiation background.

✯ While in pure solvents Ag^+ is found to be tetrahedrally coordinated, in the presence of ligands such as ammonia, it forms linear complexes, usually explained by the ion's tendency towards sd-hybridization. To explore this disparity, the reaction of ammoniated silver cations $Ag^+(NH_3)_n$, n=11-23, with H_2O as well as the complementary process, the reaction of $Ag^+(H_2O)_n$, n=25-45, with NH_3 were investigated. In both cases, ligand exchange reactions take place, leading to clusters with a limited number of NH_3 ligands. The former reaction proceeds very rapidly until only three NH_3 ligands are left, followed by a much slower loss of an additional ligand to form $Ag^+(NH_3)_2(H_2O)_m$ clusters. In the complementary process, the reaction of $Ag^+(H_2O)_n$ with NH_3, five ammonia ligands are very rapidly taken up by the clusters, with a much less efficient uptake of a sixth one. The accompanying DFT calculations reveal a delicate balance between competing effects where not only the preference of Ag^+ for sd-hybridization, but also its ability to polarize the ligands and affect thus the strength of their hydrogen bonding, as well as the ability of the solvent to form extended hydrogen bonded networks, are important.

These results can give rise to a number of novel experimental and theoretical studies, which in the future further elucidate the principles of ion solvation:

❑ The reactions of hydrated transition metal cations with HCl have opened up the new experimental field of aqueous transition metal(I) chemistry. Other strongly oxidizing reactants which do not lead to the formation of insoluble compounds can be reacted with the clusters to clarify if the metal cations can be oxidized and what oxidation states the ions will prefer under these conditions. Possible reactive gases are SO_3 or HNO_3.

❑ Reactions of metal cations in unusual oxidation states can be studied in different solvent systems, e.g. alcohols, to get a more detailed insight into the role of the solvent in

these processes.

- Temperature resolved studies may yield valuable information on the activation of of atomic and molecular hydrogen formation. For this purpose, a temperature cooled ICR cell will be installed soon in Garching. In addition, electronic spectroscopy can determine the electronic state of the vanadium ion in $V^+(H_2O)_n$.
- Electronic spectroscopy or DFT calculations can also be used to determine the electronic state of the heavier transition metal ions dependent on the number of solvent molecules.
- Molecular dynamics studies are highly desirable for the mixed $Ag^+(NH_3)_2(H_2O)_m$ clusters to take kinetic effects into account.

A List of Publications

1. **The Platinum Hydrido-Methyl Complex: A Frozen Reaction Intermediate?**
U. Achatz, M. Beyer, S. Joos, B. S. Fox, G. Niedner-Schatteburg,
and V. E. Bondybey
J. Phys. Chem. A **1999**, *103*, 8200-8206.

2. **Methane Activation by Platinum Cluster Ions in the Gas Phase: Effects of Cluster Charge on the Pt_4 Tetramer**
U. Achatz, C. Berg, S. Joos, B. S. Fox, M. Beyer, G. Niedner-Schatteburg,
and V. E. Bondybey
Chem. Phys. Lett. **2000**, *320*, 53-58.

3. **Precipitation Reactions in Water Clusters**
B. S. Fox, M. K. Beyer, U. Achatz, S. Joos, G. Niedner-Schatteburg,
and V. E. Bondybey
J. Phys. Chem. A **2000**, *104*, 1147-1151.

4. **Black Body Fragmentation of Cationic Ammonia Clusters**
B. S. Fox, M. K. Beyer, and V. E. Bondybey
J. Phys. Chem. A **2001**, *105*, 6386-6392.

5. **Hypoiodous Acid as Guest Molecule in Protonated Water Clusters: A Combined FT-ICR/DFT Study of $I(H_2O)_n^+$**
U. Achatz, B. S. Fox, M. K. Beyer, and V. E. Bondybey
J. Am. Chem. Soc. **2001**, *123*, 6151-6156.

6. **Wet Electrons and How to Dry Them**
M. K. Beyer, B. S. Fox, B. M. Reinhard, and V. E. Bondybey
J. Chem. Phys. **2001**, *115*, 9288-9297.

7. **Single Molecule Precipitation of Transition Metal(I) Chlorides in Water Clusters**
B. S. Fox, O. P. Balaj, I. Balteanu, M. K. Beyer, and V. E. Bondybey
J. Am. Chem. Soc. **2002**, *124*, 172-173.

8. **Coordination Chemistry of Silver Cations**
B. S. Fox, M. K. Beyer, and V. E. Bondybey
submitted to *J. Am. Chem. Soc.*

9. **Black Body Radiation Induced Hydrogen Formation in Hydrated Vanadium Cations $V^+(H_2O)_n$**
B. S. Fox, I. Balteanu, O. P. Balaj, H. Liu, M. K. Beyer, and V. E. Bondybey
submitted to *Phys. Chem. Chem. Phys.*

10. **Reactions of hydrated aluminum ions with methanol and formic acid**
O. P .Balaj, E. P. F. Lee, I. Balteanu, B. S. Fox, M. K. Beyer, J. M. Dyke,
and V. E. Bondybey
submitted to *Int. J. Mass Spectrom.*

11. **Black Body Fragmentation of Hydrated Zinc Cations $Zn^+(H_2O)_n$ and their reaction with HCl**
B. S. Fox, I. Balteanu, O. P. Balaj, M. K. Beyer, and V. E. Bondybey
in preparation.

12. **Uptake and reaction of N_2O_5 on NaCl and synthetic sea salt**
M. E. Gebel, B. S. Fox, and B. J. Finlayson-Pitts
in preparation.

B National and International Presentations

1. **"Fällungsreaktionen in größenselektierten Wasserclustern - ein Vergleich der Systeme AgCl und NaCl"**
   B. S. Fox, M. K. Beyer, U. Achatz, S. Joos, G. Niedner-Schatteburg, and V. E. Bondybey
   63. Frühjahrstagung der Deutschen Physikalischen Gesellschaft, March 15-19, 1999, Heidelberg, Germany, Talk.

2. **"Precipitation Reactions in Water Clusters"**
   B. S. Fox, M. K. Beyer, U. Achatz, S. Joos, G. Niedner-Schatteburg, and V. E. Bondybey
   DFG-Kolloquium Schwerpunktprogramm Molekulare Cluster, May 25-29, 1999, Niederpöcking, Germany, Poster.

3. **"Precipitation Reactions in Water Clusters"**
   B. S. Fox, M. K. Beyer, U. Achatz, S. Joos, G. Niedner-Schatteburg, and V. E. Bondybey
   European Fourier Transform Mass Spectrometry Workshop, September 16-18, 1999, Warwick, UK, Talk.

4. **"Coordination Chemistry of Silver Cations"**
   B. S. Fox, M. K. Beyer, U. Achatz, S. Joos, G. Niedner-Schatteburg, and V. E. Bondybey
   48th ASMS Conference on Mass Spectrometry and Allied Topics, June 11-15, 2000, Long Beach, USA, Talk.

5. **"Nanodroplets as Aqueous Reaction Media"**
   B. S. Fox, U. Achatz, M. K. Beyer, V. E. Bondybey
   34. DGMS-Diskussionstagung, March 4-7, 2001, München, Germany, Poster.

6. **"Blackbody Fragmentation of Cationic Ammonia Clusters"**
   B. S. Fox, M. K. Beyer, V. E. Bondybey
   European Conference on Atomic and Molecular Physics/DPG Conference, April 2-6, 2001, Berlin, Germany, Talk.

Acknowledgement

All those who have contributed to this work I want to cordially thank. My deep gratitude goes to my supervisor Prof. Dr. Vladimir E. Bondybey whose ideas, overwhelming knowledge and critical advice are the sound fundament of this work. His group provides an extremely creative, inspiring and international working environment.

I want to thank Dr. Martin Beyer, the head of the Garching ICR group, for helpful discussions and advices, which cover the whole range from technical details to the fundamentals of gas phase ion chemistry.

Without the collaboration and fruitful discussions with the other active members of the ICR crew, Iulia Balteanu, Petru Balaj, Matthias Stecher, and, recently, Haichuan Liu, the former members, Dr. Christian Berg, Dr. Uwe Achatz, Stefan Joos, and Prof. Dr. Gereon Niedner-Schatteburg, this work would have been much more difficult and much less enjoyable. Special thanks to the “Dragas” for giving me insights into the Romanian language and culture. Matthias’ work is invaluable to the whole group since he is on the way to replace Infraserv.

I cordially thank Sabine Kullick, who is not only our secretary but heart and soul of the group, for her help in doing all kinds of paperwork. I also thank Peter Kämmerer and our former "Hacker" Andreas Lammers for their assistance in fights with different computer systems and Dr. Edmund Cmiel for his help in bureaucratic things.

During my research visit at the University of California, Irvine, I had the pleasure to be guest in the group of Prof. Dr. Barbara J. Finlayson-Pitts. The brief, but intense collaboration with her and her coworker Dr. Michael Gebel was delighting and fruitful. Stacey Tibbett, Administrative Staff Supervisor, and Aimee Alwood, Personell Analyst, did a great job with all the paperwork which was necessary for this stay, and I am greatly

indebted to them.

I want to thank the other members of the Bondybey group, Dr. Dieter Kraus, (soon Dr.) Bernhard Urban, Marcin Frankowski, Dr. Alice Smith-Gicklhorn, the former member Dr. Martin Lorenz, and our "permanent visitor" Dr. Elena Savchenko for their ever cooperative attitude. Special thanks to Marcin for teaching us how to call different kinds of “budding whateverowe”.

The electronics and machine workshops provide us continously with excellent work and invaluable troubleshooting and I want to cordially thank them.

I want to thank my "13-Days-Students", Paul Mazac, Martin Paulus, Sandra Pröckl, Wolfgang Kleist, Alexander Schriewer, Andreas Brandl, and Melanie Zimmermann for their help in the laboratory as well as Martin Weimer who did his case study for the "Vertiefungsfach Theoretische Chemie und Spektroskopie" in our group.

Financial support by the Deutsche Forschungsgemeinschaft and the Fonds der Chemischen Industrie is gratefully acknowledged.

The deepest "thank you" is reserved for my parents. They supported me in every way until I learned to stand on my own feet.